Synthesis of chiral rotaxanes: Controlling the molecular chirality of bis-catechol spiroborate through threading

Kion Takada, Rin Usui, Takumi Takizawa, Masaya Naito, Yusuke Okada, Nagao Kobayashi, Shinobu Miyagawa and Yuji Tokunaga

TOC

Experimental

XRD structure determination

A crystal suitable for XRD was analyzed using a Rigaku R-AXIS RAPID diffractometer and graphite-monochromated $Mo_{K\alpha}$ radiation (λ = 0.71075 Å). The structure of (*P*,*S*)-**3a** was solved using direct methods and refined by applying the full-matrix least-squares method. In subsequent refinement, the function $\Sigma\omega(F_o^2 - F_c^2)^2$ was minimized, where F_o and F_c are the observed and calculated structure factor amplitudes, respectively. The positions of non-hydrogen atoms were determined from difference Fourier electron density maps and were refined anisotropically. All calculations were performed using the Rigaku CrystalStructure crystallographic software package; illustrations were generated in the ORTEP style. Details of the structural determinations are provided in Figures 3, S10 and Table S1. CCDC 2502226 contains the supplementary crystallographic data for this paper.

Materials and General Methods

Compounds **1** [S1] and **2c** [S2] were prepared according to literature procedure. DMF and CH_2Cl_2 were dried over 4 Å molecular sieves. Other solvents and commercially available chemicals were used as received. ^1H and ^{13}C NMR spectra were recorded using JEOL ECX-500II, ECZ-500, and ECA-600II spectrometers, with tetramethylsilane (TMS) in $CDCl_3$, and with DMSO-d_5 (2.49 ppm for ^1H NMR) and DMSO-d_6 (39.5 ppm for ^{13}C NMR) as internal references. Mass spectra were recorded using JEOL JMS-S-3000. Infrared spectra were recorded using a JASCO FT/IR-4100 spectrometer. Circular dichroism spectra were recorded using a JASCO J-725 spectrometer. UV-Vis absorption spectra were recorded using a Hitachi U-3900 spectrometer. All reactions were performed under a positive atmosphere of dry N_2. All solvents were removed through rotary evaporation under reduced pressure. For reactions that require heating used an oil bath as the heat source. Silica gel column chromatography was performed using Kanto Chemical silica gel 60 N. Thin layer chromatography (TLC) was performed using Merck Kieselgel $60PF_{254}$.

Synthesis

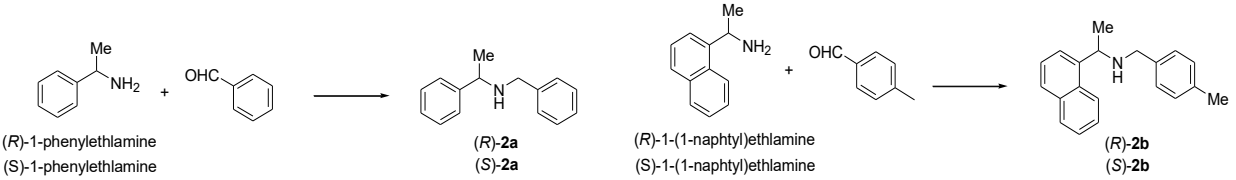

Scheme S1.

Synthesis of crude product of amines **2**

A suspension of the corresponding amine (1 equiv.), the aldehyde (1 equiv.), Na_2SO_4 (1 equiv.), and K_2CO_3 (0.11 equiv.) in anhydrous toluene and CH_2Cl_2 (1/1) was stirred for 1 d. After filtration, the filtrate was concentrated. The corresponding residue (imine) was dissolved in MeOH and $NaBH_4$ (1 equiv.) was added portionwise at room temperature, and the mixture was then refluxed for 18 h. 10% HCl aq. was added to the reaction mixture at 0 ºC, and the mixture was neutralized with 10% Na_2CO_3 aq. After removal of MeOH, the residual aqueous mixture was extracted with CH_2Cl_2 three times. Combined organic layer was washed with sat. NaCl aq., dried (Na_2SO_4), and concentrated to yield the corresponding crude amines (see below for purification).

(*S*)-*N*-Benzyl-1-phenylethylamine **2a**

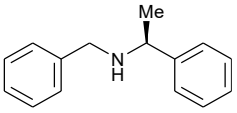

The crude product, obtained from (*S*)-1-phenylethylamine (1.54 g, 12.7 mmol) and benzaldehyde (1.29 mL, 12.7 mmol), was purified by silica gel column chromatography (eluent: hexane:ethyl acetate = 7:1), and the product in diisopropyl ether (16 mL) was treated with 5.2 N HCl in dioxane (2 equiv.) to give the corresponding HCl salt as a solid, which was washed with diisopropyl ether. The HCl salt was dissolved in CH_2Cl_2 and washed with 10% Na_2CO_3 and sat. NaCl aq., dried (Na_2SO_4), and concentrated to yield (*S*)-amine **2a** (2.37 g, 88%) as a pale brown oil.

^{1}H NMR (500 MHz, $CDCl_3$) δ 7.37–7.22 (m, 10H), 3.81 (q, J = 6.7 Hz, 1H), 3.66 (d, J = 13.2 Hz, 1H), 3.59 (d, J = 13.2 Hz, 1H), 1.36 (d, J = 6.7 Hz, 3H).
The ^{1}H NMR was identical to that reported previously.[S3]

(*R*)-*N*-Benzyl-1-phenylethylamine **2a**

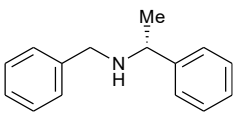

(*R*)-Amine **2a** (2.37 g, 88%) was obtained from (*R*)-1-phenylethylamine (1.58 g, 13.0 mmol) and benzaldehyde (1.35 mL, 13.3 mmol) as a pale brown oil.

(*S*)-*N*-Toluyl-1-(naphthyl)ethylamine **2b**

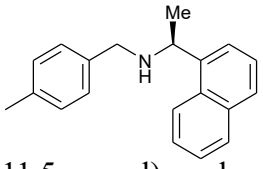

The crude product, obtained from (*S*)-1-(naphthyl)ethylamine (1.98 g, 11.5 mmol) and *p*-tolualdehyde (1.40 mL, 11.9 mmol), was purified by silica gel column chromatography (eluent: hexane:ethyl acetate = 5:1) to yield (*S*)-amine **2b** (2.89 g, 91%) as a pale brown oil.

$[\alpha]_D^{18}$ −14.1° (*c* = 0.10, CH_3CN)
IR (NaCl, ν_{max}) cm^{-1}: 3327, 3047, 2970, 2867, 2824, 1595, 1513, 1442, 1394, 1368, 1174, 1117, 1021, 800, 778, 685.
^1H NMR (500 MHz, $CDCl_3$) δ 8.11 (d, *J* = 7.7 Hz, 1H), 7.81 (dd, *J* = 7.2 and 2.2 Hz, 1H), 7.73 (d, *J* = 7.1 Hz, 1H), 7.70 (d, *J* = 8.2 Hz, 1H), 7.47–7.39 (m, 3H), 7.17–7.13 (m, 2H), 7.09–7.06 (m, 2H), 4.63 (q, *J* = 6.6 Hz, 1H), 3.69 (d, *J* = 13.0 Hz, 1H), 3.61 (d, *J* = 13.0 Hz, 1H), 2.29 (s, 3H), 1.46 (d, *J* = 6.6 Hz, 3H).
^{13}C NMR (125 MHz, $CDCl_3$) δ 141.0, 137.5, 136.3, 133.9, 131.3, 128.9, 128.3, 128.0, 127.1, 125.7, 125.6, 125.2, 122.9, 122.8, 52.8, 51.5, 23.6, 21.0.
MS (MALDI-TOF): *m*/*z* calcd for $C_{20}H_{22}N^+$ $[M+1]^+$: 276.1747; found: 276.1744.

(*R*)-*N*-Toluyl-1-(naphthyl)ethylamine **2b**

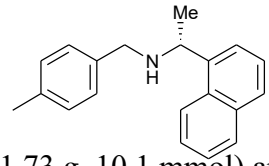

(*R*)-Amine **2b** (1.91 g, 68%) was obtained from (*R*)-1-(naphthyl)ethylamine (1.73 g, 10.1 mmol) and *p*-tolualdehyde (1.20 mL, 10.2 mmol) as a pale brown oil.

$[\alpha]_D^{18}$ +15.0° (*c* = 0.10, CH_3CN)
MS (MALDI-TOF): *m*/*z* calcd for $C_{20}H_{22}N^+$ $[M+1]^+$: 276.1747; found: 276.1743.

Synthesis of pseudo[2]rotaxanes **3**

(*S*)-Pseudo[2]rotaxane **3a**

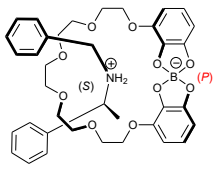

Reaction in CH_3CN

A suspension of bis-catechol **1** (30.1 mg, 66.2 μmol), $B(OH)_3$ (4.11 mg, 66.5 μmol), and (*S*)-amine **2a** in CH_3CN (6.60 mL) was heated at 50 °C for 26 h. After concentration, the residue was dissolved in $CHCl_3$ (6.60 mL), and the reaction mixture was stirred at room temperature for 3 d. After the

chloroform was removed, EtOH/$CHCl_3$ (3 mL/0.1 mL) was added to the residue, and the suspension was stored in a refrigerator for 1 d. The precipitate was collected by filtration and washed with ether to afford (*S*)-pseudo[2]rotaxane **3a** (31.0 mg, 69%) as a white solid.

Reaction in $CHCl_3$

A suspension of bis-catechol **1** (100 mg, 220 μmol), $B(OH)_3$ (14.2 mg, 230 μmol), and (*S*)-amine **2a** in $CHCl_3$ (22.0 mL) was heated at 50 °C for 3 days. After heating, the mixture was left at room temperature for 2 d. After the chloroform was removed, EtOH/$CHCl_3$ (3 mL/0.1 mL) was added to the residue, and the suspension was stored in a refrigerator for 1 d. The precipitate was collected by filtration and washed with ether to afford (*S*)-pseudo[2]rotaxane **3a** (124 mg, 84%) as a white solid.

$[\alpha]_D^{21}$ +42.4° (*c* = 0.10, CH_3CN)
IR (KBr, ν_{max}) cm^{-1}: 3436, 3065, 3037, 2904, 2877, 1624, 1497, 1469, 1354, 1293, 1252, 1229, 1085, 1058, 1033, 956, 912, 878, 847, 762, 716, 700.
^1H NMR (600 MHz, $CDCl_3$, 5 °C) δ: 9.56–9.38 (1H, m), 7.59 (2H, d, *J* = 7.5 Hz), 7.39 (2H, d, *J* = 7.3 Hz), 7.36 (2H, t, *J* = 7.5 Hz), 7.30 (1H, t, *J* = 7.5 Hz), 7.16–7.05 (1H, m), 7.01 (1H, t, *J* = 7.3 Hz), 6.92 (2H, t, *J* = 7.3 Hz), 6.55 (1H, t, *J* = 8.3 Hz), 6.52 (1H, dd, *J* = 8.3 and 1.1 Hz), 6.51 (1H, dd, *J* = 8.3 and 1.1 Hz), 6.46 (1H, t, *J* = 8.3 Hz), 6.31 (1H, dd, *J* = 8.3 and 1.1 Hz), 5.73 (1H, dd, *J* = 8.3 and 1.1 Hz), 4.97 (1H, td, *J* = 11.4 and 3.5 Hz), 4.85 (1H, ddd, *J* = 11.2, 5.9, and 2.3 Hz), 4.61 (1H, t, *J* = 11.4 Hz), 4.47 (1H, dq, *J* = 8.9 and 7.1 Hz), 4.85 (1H, ddd, *J* = 11.2, 6.4, and 2.5 Hz), 3.98–3.89 (2H, m), 3.87–3.82 (1H, m), 3.79–3.54 (9H, m), 3.43–3.39 (1H, m), 3.08 (1H, dd, *J* = 10.3, and 9.3 Hz), 3.01–2.97 (1H, m), 2.97–2.91 (2H, m), 3.08 (1H, t, *J* = 10.3 Hz), 1.33 (3H, d, *J* = 7.1 Hz).
^{13}C NMR (150 MHz, $CDCl_3$, 5 °C) δ: 152.6, 152.0, 142.1, 141.6, 139. 3, 139.0, 136.9, 131.3, 130. 5, 128.64, 128.58, 128.4, 127.6, 118.4, 117.7, 105.6, 104.3, 103.8, 101.1, 72.3, 72.0, 71.7, 71.3, 70.82, 70.81, 70.7, 70.3, 67.2, 65.5, 59.9, 50.4, 18.5.
MS (MALDI-TOF): *m*/*z* calcd for $C_{37}H_{44}BNO_{10}^+$ $[M]^+$: 673.3111; found: 673.3167.
Mp: 147–148 °C (CH_3CN).

(*R*)-Pseudo[2]rotaxane **3a**

(*R*)-pseudo[2]Rotaxane **3a** (35.3 mg, 77%) was obtained from bis-catechol **1** (30.9 mg, 68.0 μmol), $B(OH)_3$ (4.19 mg, 67.8 μmol), and (*R*)-amine **2a** (28.0 μL, 134 μmol) as a white solid.

$[\alpha]_D^{21}$ −39.5° (*c* = 0.10, CH_3CN)
MS (MALDI-TOF): *m*/*z* calcd for $C_{37}H_{44}BNO_{10}^+$ $[M]^+$: 673.3102; found: 673.3167.
Mp: 143–144 °C (CH_3CN).

(*S*)-Pseudo[2]rotaxane **3b**

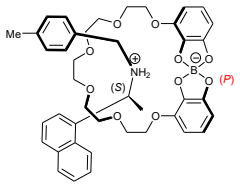

Reaction in CH_3CN

The borate-forming reaction was performed as described above using bis-catechol **1** (20.1 mg, 44.2 μmol), $B(OH)_3$ (2.78 mg, 45.0 μmol), and (*S*)-amine **2b** (18.3 mg, 62.6 μmol). The crude product was washed with Et_2O/CH_3CN (3 mL/0.3 mL) and Et_2O to afford (*S*)-pseudo[2]rotaxane **3b** (23.6 mg, 72%) as a white solid.

Reaction in $CHCl_3$

The borate-forming reaction was performed as described above using bis-catechol **1** (100 mg, 220 μmol), $B(OH)_3$ (14.4 mg, 233 μmol), and (*S*)-amine **2b** (72.7 mg, 264 μmol). The crude product was washed with $Et_2O/CHCl_3$ (3 mL/0.1 mL) and Et_2O to afford (*S*)-pseudo[2]rotaxane **3b** (149 mg, 92%) as a white solid.

$[\alpha]_D^{21}$ +27.9° (*c* = 0.10, CH_3CN)

IR (KBr, ν_{max}) cm^{-1}: 3479, 3042, 2878, 1623, 1496, 1469, 1355, 1292, 1252, 1227, 1167, 1101, 1052, 1034, 954, 909, 880, 852, 779, 715.

^1H NMR (600 MHz, $CDCl_3$, 5 °C) δ: 9.94–9.71 (1H, m), 8.19 (1H, d, *J* = 7.7 Hz), 7.92 (1H, d, *J* = 7.9 Hz), 7.85 (1H, dd, *J* = 8.3 and 1.7 Hz), 7.78 (1H, d, *J* = 7.7 Hz), 7.53 (1H, t, *J* = 7.7 Hz), 7.51–7.46 (2H, m), 7.40 (1H, d, *J* = 7.9 Hz), 7.25–7.15 (1H, m), 6.72 (1H, d, *J* = 7.9 Hz), 6.52 (1H, dd, *J* = 8.0 and 1.0 Hz), 6.48 (1H, t, *J* = 8.0 Hz), 6.47 (1H, t, *J* = 8.0 Hz), 6.44 (1H, dd, *J* = 8.0 and 1.0 Hz), 6.27 (1H, dd, *J* = 8.0 and 1.0 Hz), 5.71 (1H, dd, *J* = 8.0 and 1.0 Hz), 5.57–5.47 (1H, m), 5.09 (1H, td, *J* = 11.3 and 3.1 Hz), 4.76 (1H, ddd, *J* = 11.2, 5.7, and 2.4 Hz), 4.66 (1H, t, *J* = 11.3 Hz), 4.22 (1H, ddd, *J* = 11.2, 6.6, and 2.6 Hz), 3.93 (1H, dd, *J* = 10.6 and 8.3 Hz), 3.91–3.87 (1H, m), 3.83 (1H, ddd, *J* = 10.6, 6.6, and 2.4 Hz), 3.81–3.73 (2H, m), 3.73–3.64 (5H, m), 3.60 (1H, t, *J* = 10.1 Hz), 3.52 (1H, dd, *J* = 11.0 and 4.8 Hz), 3.19 (1H, t, *J* = 10.2 Hz), 3.09 (1H, t, *J* = 10.4 Hz), 3.01–2.92 (2H, m), 2.66 (1H, d, *J* = 10.8 Hz), 2.14 (3H, s), 1.98 (1H, t, *J* = 10.8 Hz), 1.41 (3H, d, *J* = 6.6 Hz).

^{13}C NMR (150 MHz, $CDCl_3$, 5 °C) δ: 152.6, 152.3, 142.1, 141.7, 139.4, 138.4, 137.0, 136.1, 133.4, 130.5, 129.3, 129.0, 128.4, 128.3, 128.2, 126.2, 126.1, 125.7, 124.5, 122.5, 118.1, 117.6, 105.1, 104.5, 103. 9, 101.1, 72.4, 71.9, 71.6, 71.5, 70.9, 70.7, 70.5, 70.1, 67.1, 65.6, 55.2, 50.7, 21.1, 18.7.

MS (MALDI-TOF): *m/z* calcd for $C_{42}H_{48}BNO_{10}^+$ $[M]^+$: 737.3480; found: 737.3453.

Mp: 155–157 °C ($CHCl_3/Et_2O$).

(*R*)-Pseudo[2]rotaxane **3b**

(*R*)-Pseudo[2]rotaxane **3b** (35.3 mg, 77%) was obtained from bis-catechol **1** (30.9 mg, 68.0 μmol), $B(OH)_3$ (4.19 mg, 67.8 μmol), and (*R*)-amine **2b** (28.0 μL, 134 μmol) as a white solid.

$[\alpha]_D^{21}$ −28.2° (*c* = 0.10, CH_3CN)

MS (MALDI-TOF): *m*/*z* calcd for $C_{42}H_{48}BNO_{10}^{+}$ $[M]^+$: 738.3480; found: 738.3429.

Mp: 157 °C ($CHCl_3$/Et_2O).

References

S1) T. Takizawa, K. Ohtani, M. Naito, S. Miyagawa, Y. Tokunaga, Rotaxane Formation from Borate Ion-Containing Crown Ether and Ammonium Ion: Enhancement of Their Association through Ion-Pairing. *Org. Lett.,* 2024, **26**, 8211–8215.

S2) S. Guizzetti, M. Benaglia, S. Rossi, Highly Stereoselective Metal-Free Catalytic Reduction of Imines: An Easy Entry to Enantiomerically Pure Amines and Natural and Unnatural α-Amino Esters. *Org. Lett*., 2009, **11**, 2928–2931.

S3) C. Guerin, V. Bellosta, G. Guillamot, J. Cossy, Mild Nonepimerizing *N*-Alkylation of Amines by Alcohols without Transition Metals. *Org. Lett*., 2011, **13**, 3534–3537.

Selective formation of (*S*)-pseudo[2]rotaxane **3a** under thermodynamic conditions.

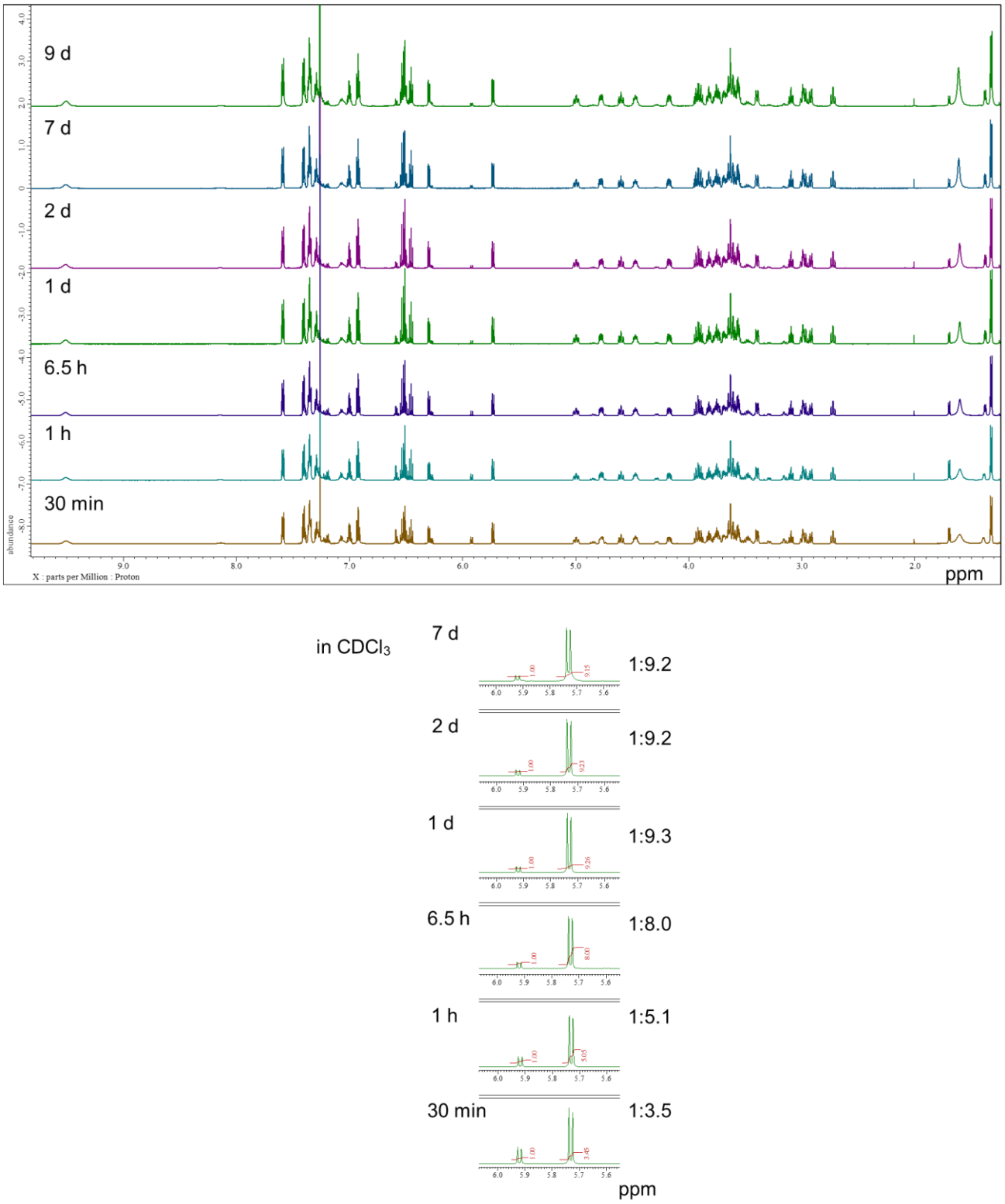

Figure S1a. Selective formation of (*S*)-pseudo[2]rotaxane **3a** in $CDCl_3$ under thermodynamic conditions.

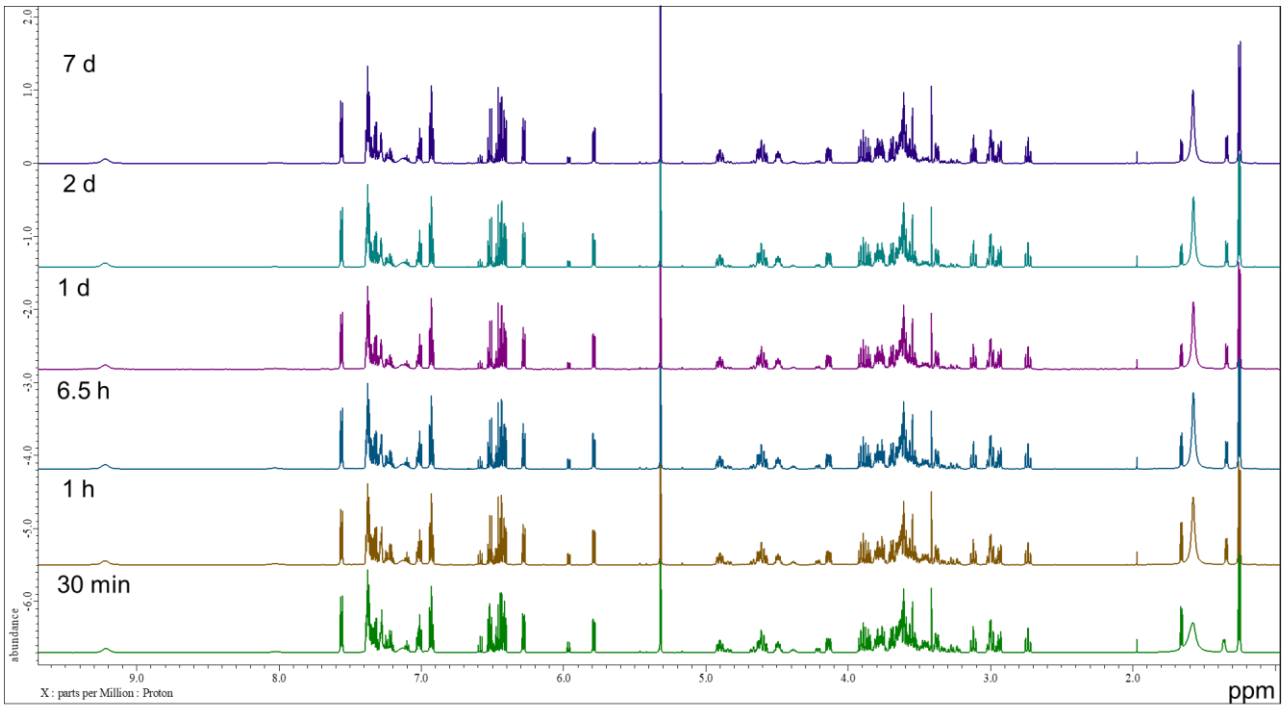

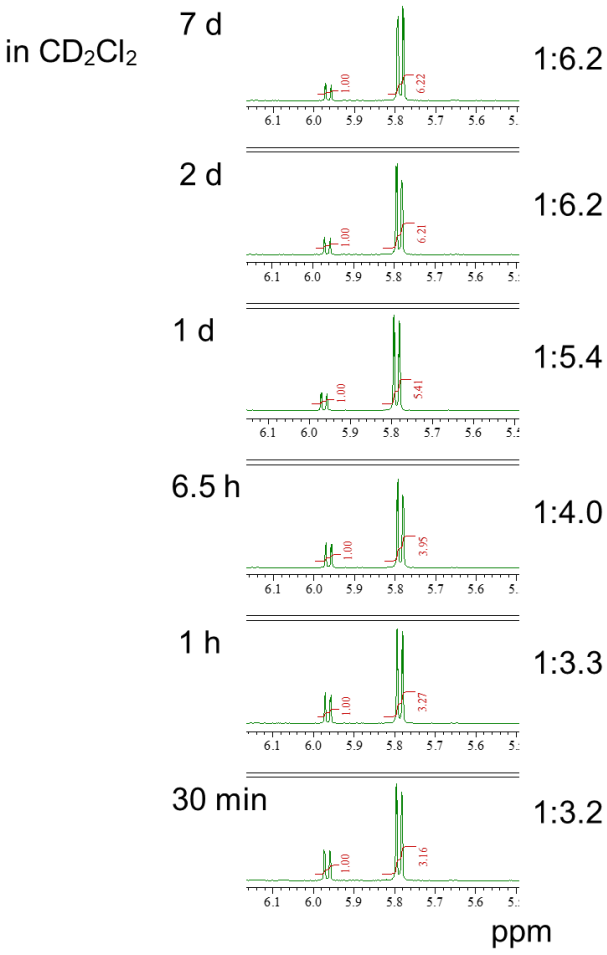

Figure S1b. Selective formation of (*S*)-pseudo[2]rotaxane **3a** in CD_2Cl_2 under thermodynamic conditions.

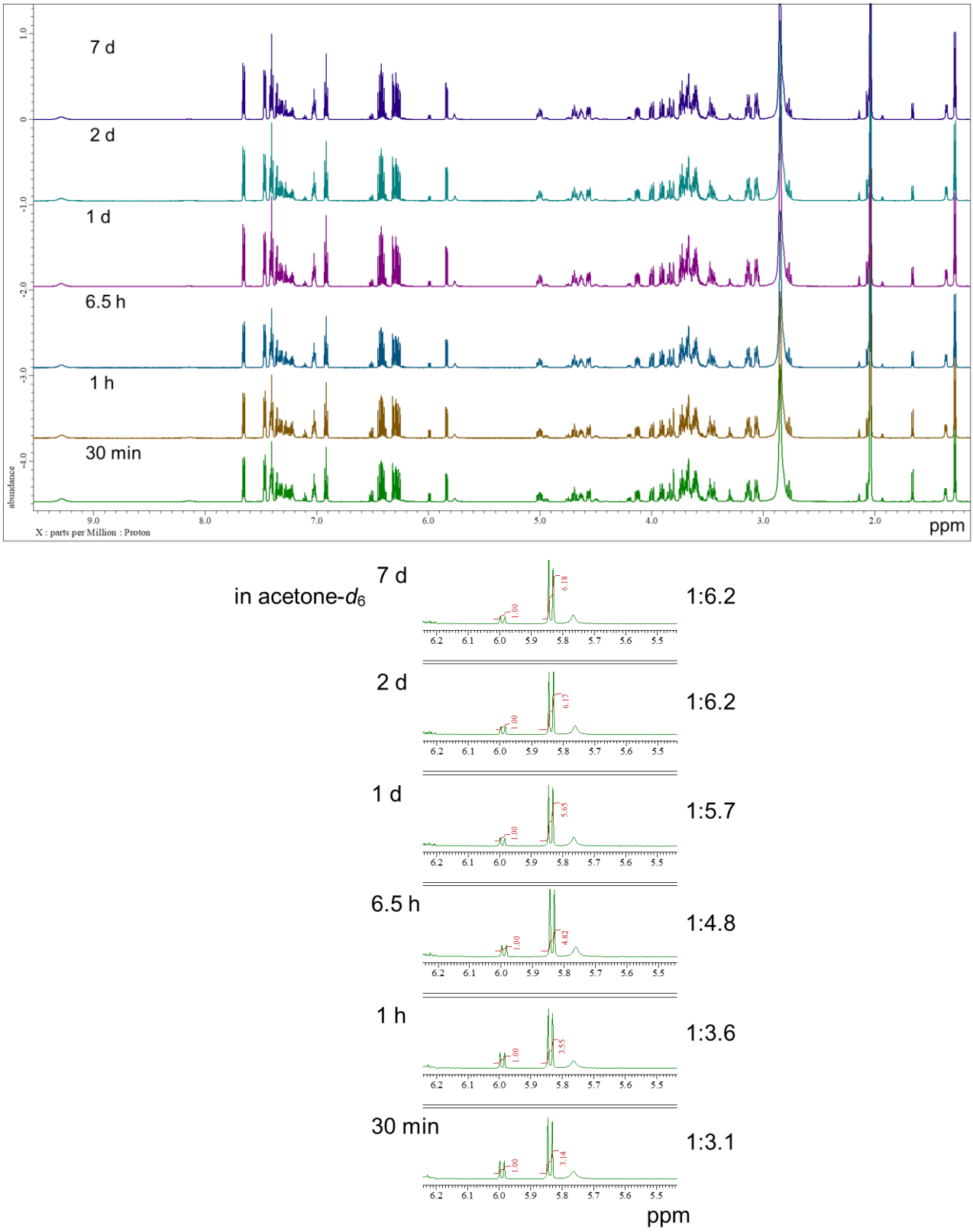

Figure S1c. Selective formation of (*S*)-pseudo[2]rotaxane **3a** in acetone-d_6 under thermodynamic conditions.

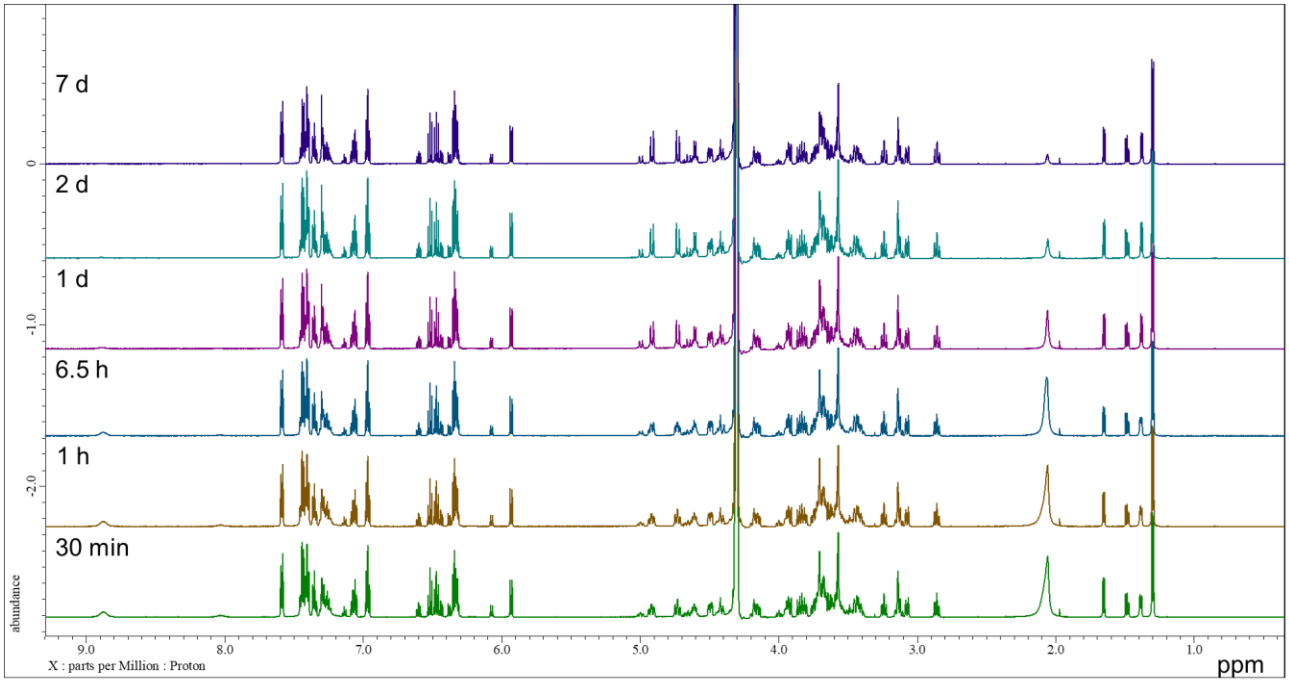

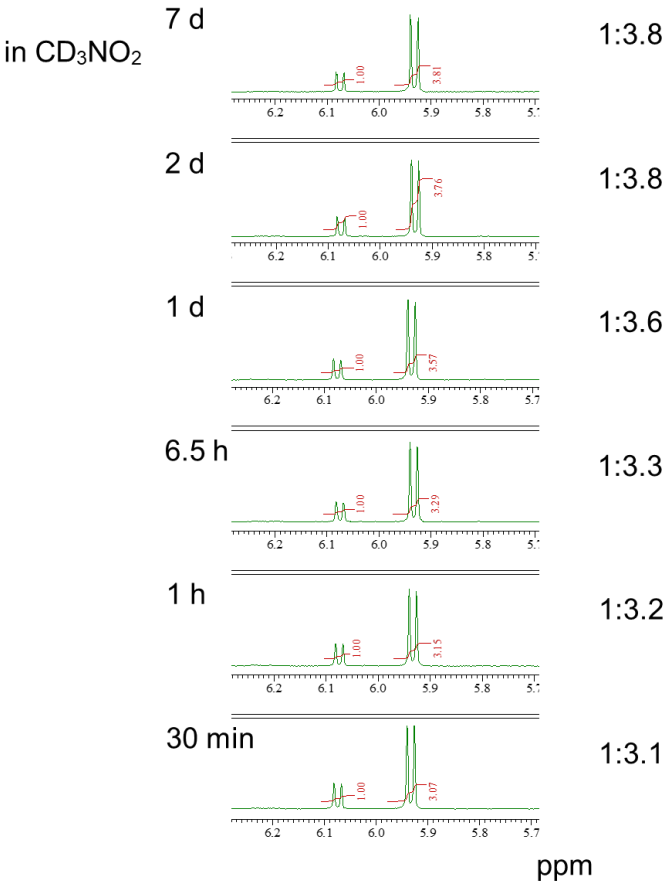

Figure S1d. Selective formation of (*S*)-pseudo[2]rotaxane **3a** in CD_3NO_2 under thermodynamic conditions.

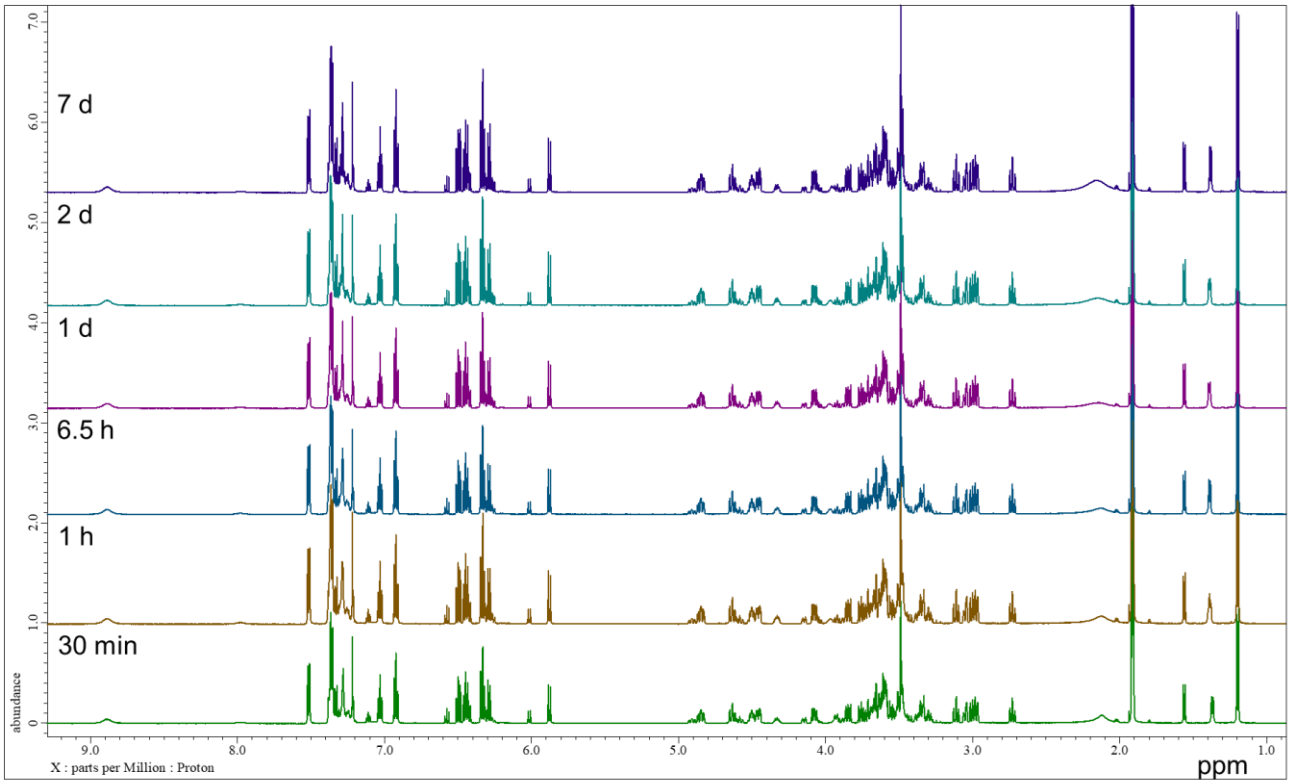

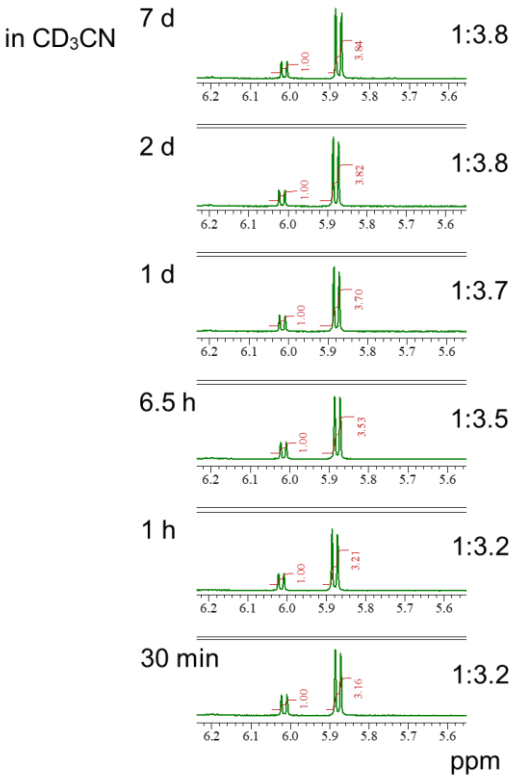

Figure S1e. Selective formation of (*S*)-pseudo[2]rotaxane **3a** in CD_3CN under thermodynamic conditions.

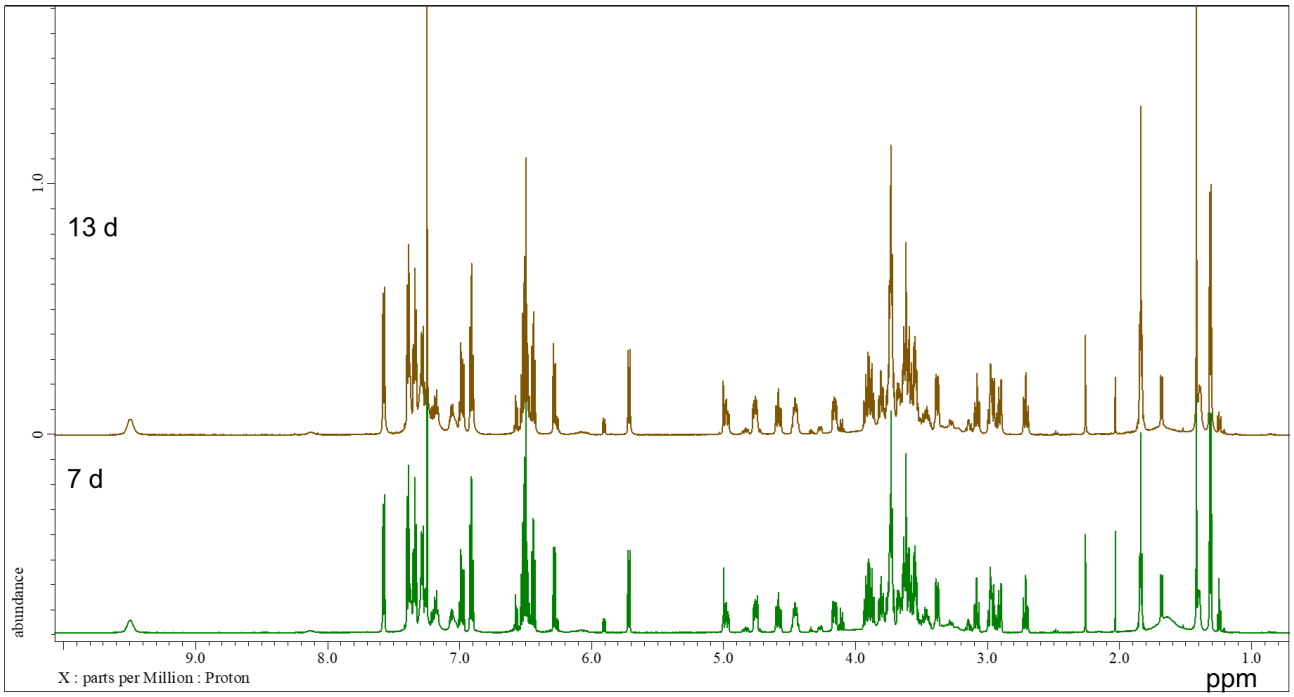

After removal of the solvent, $CDCl_3$ was used for ^1H NMR analysis.

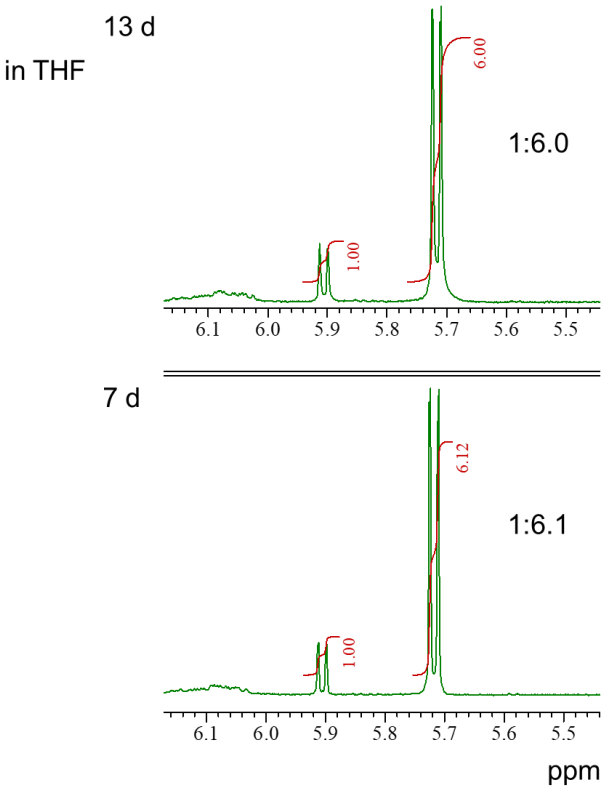

Figure S1f. Selective formation of (*S*)-pseudo[2]rotaxane **3a** in THF under thermodynamic conditions.

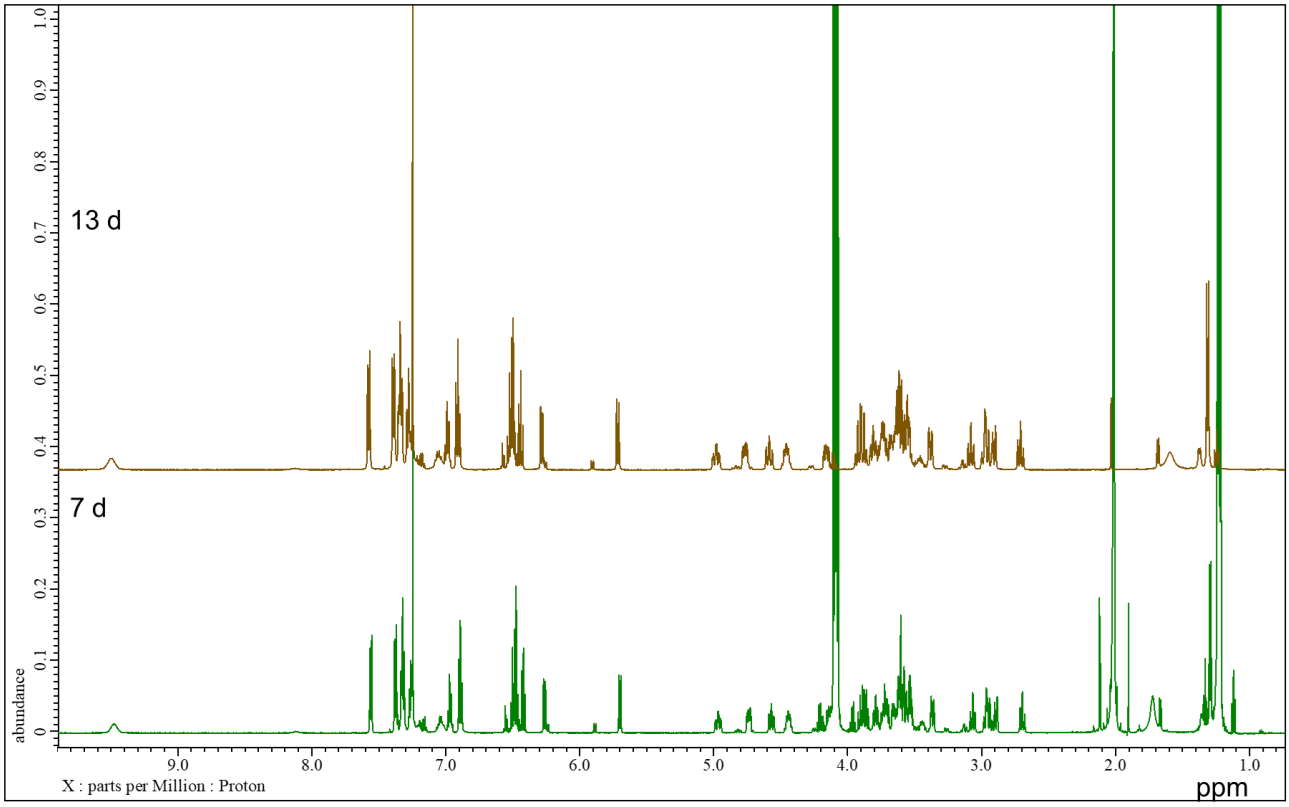

After removal of the solvent, $CDCl_3$ was used for ^1H NMR analysis.

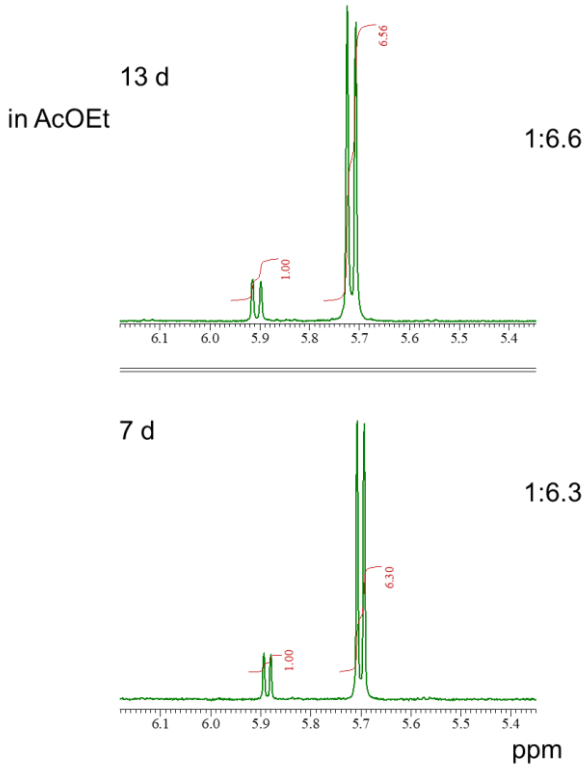

Figure S1g. Selective formation of (*S*)-pseudo[2]rotaxane **3a** in AcOEt under thermodynamic conditions.

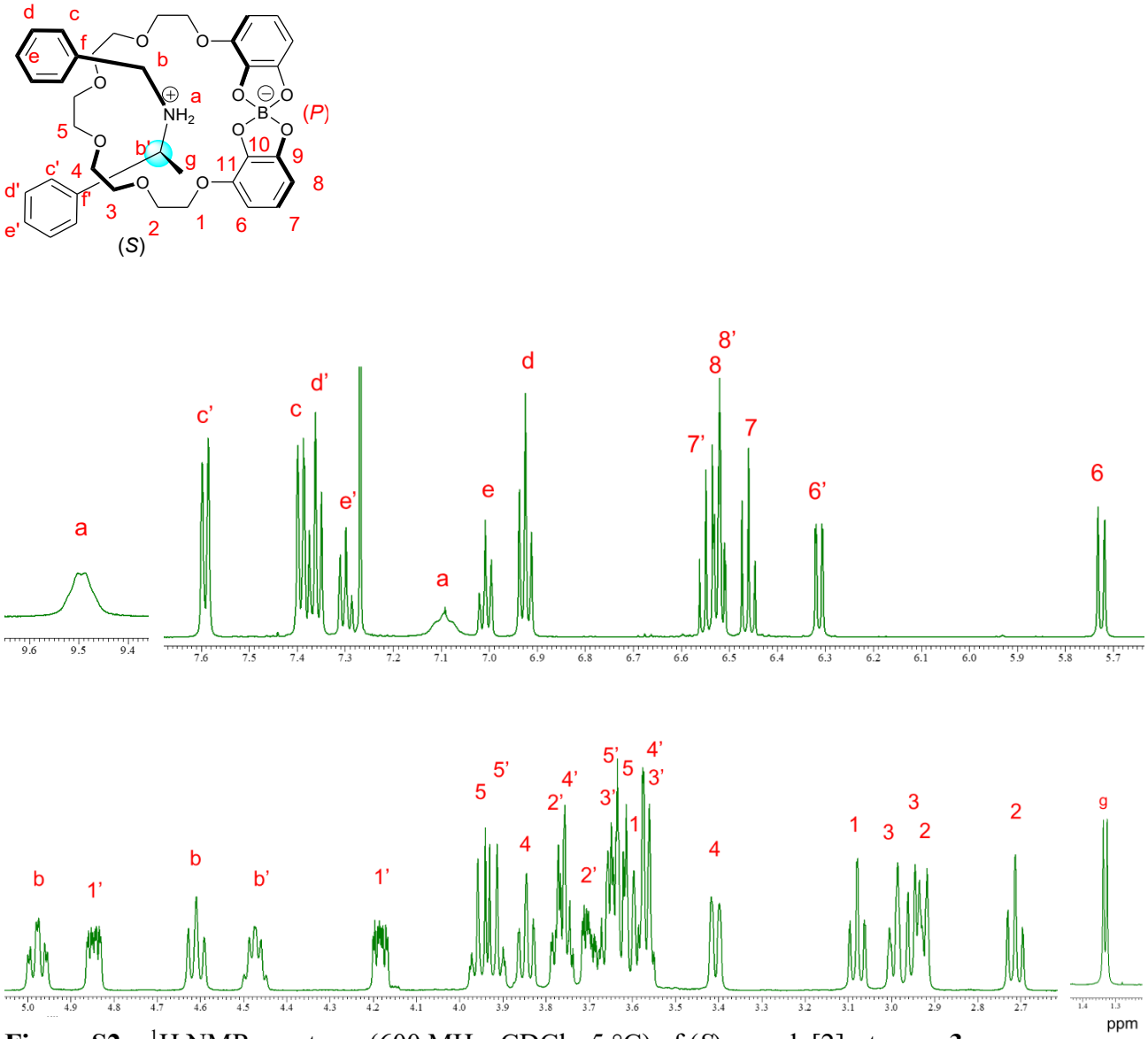

Figure S2a. ^{1}H NMR spectrum (600 MHz, $CDCl_3$, 5 °C) of (*S*)-pseudo[2]rotaxane **3a**.

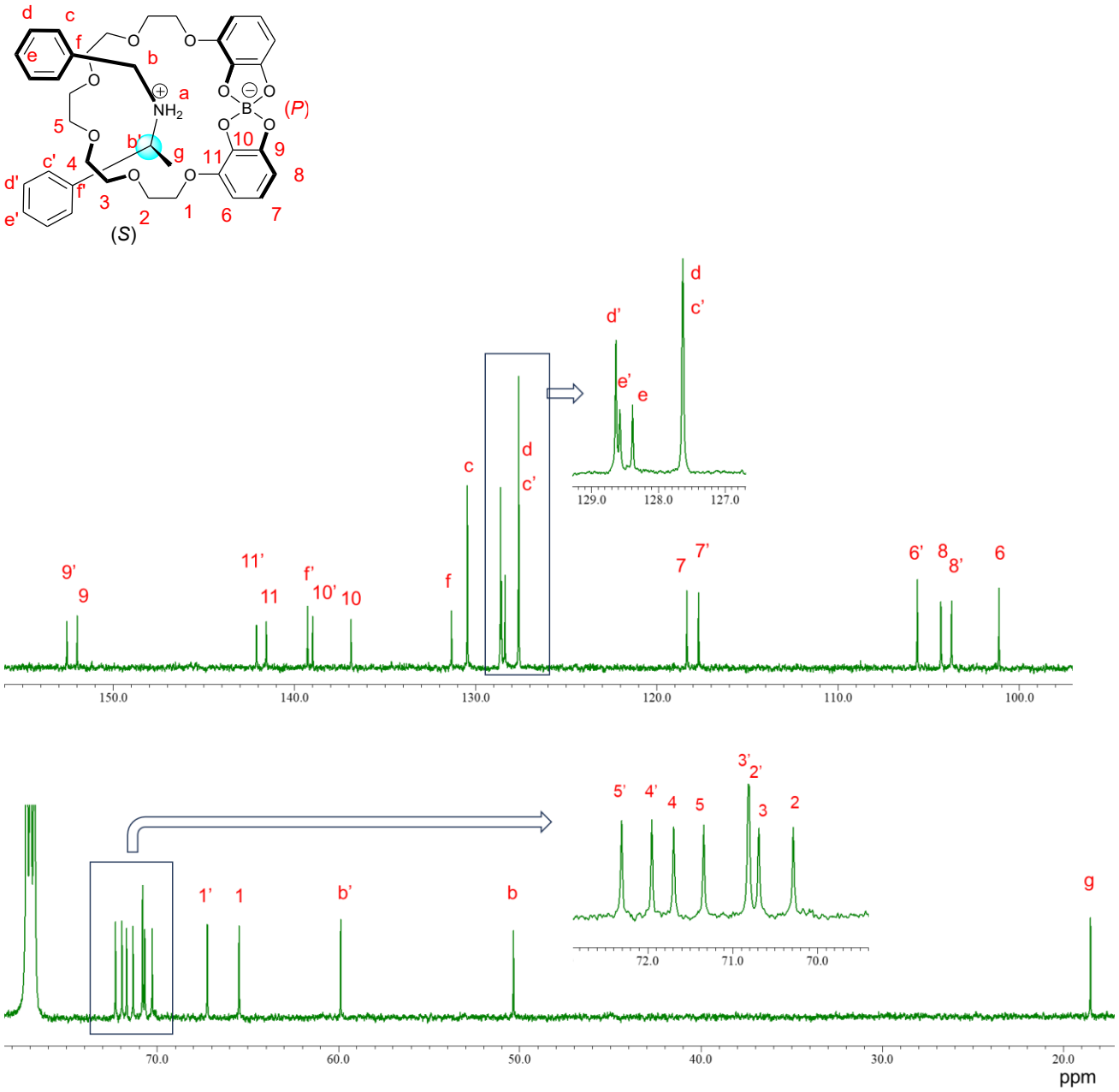

Figure S2b. ^{13}C NMR spectrum (150 MHz, $CDCl_3$, 5 °C) of (*S*)-pseudo[2]rotaxane **3a**.

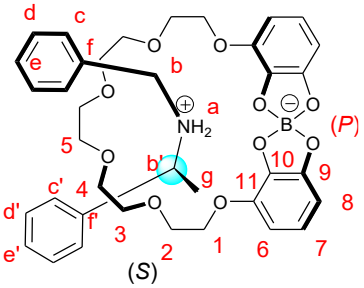
d
c
f
e
b
a
NH2
(P)
5
b'
g
10
9
c'
4
11
8
d'
f'
3
2
1
6
7
e'
(S)

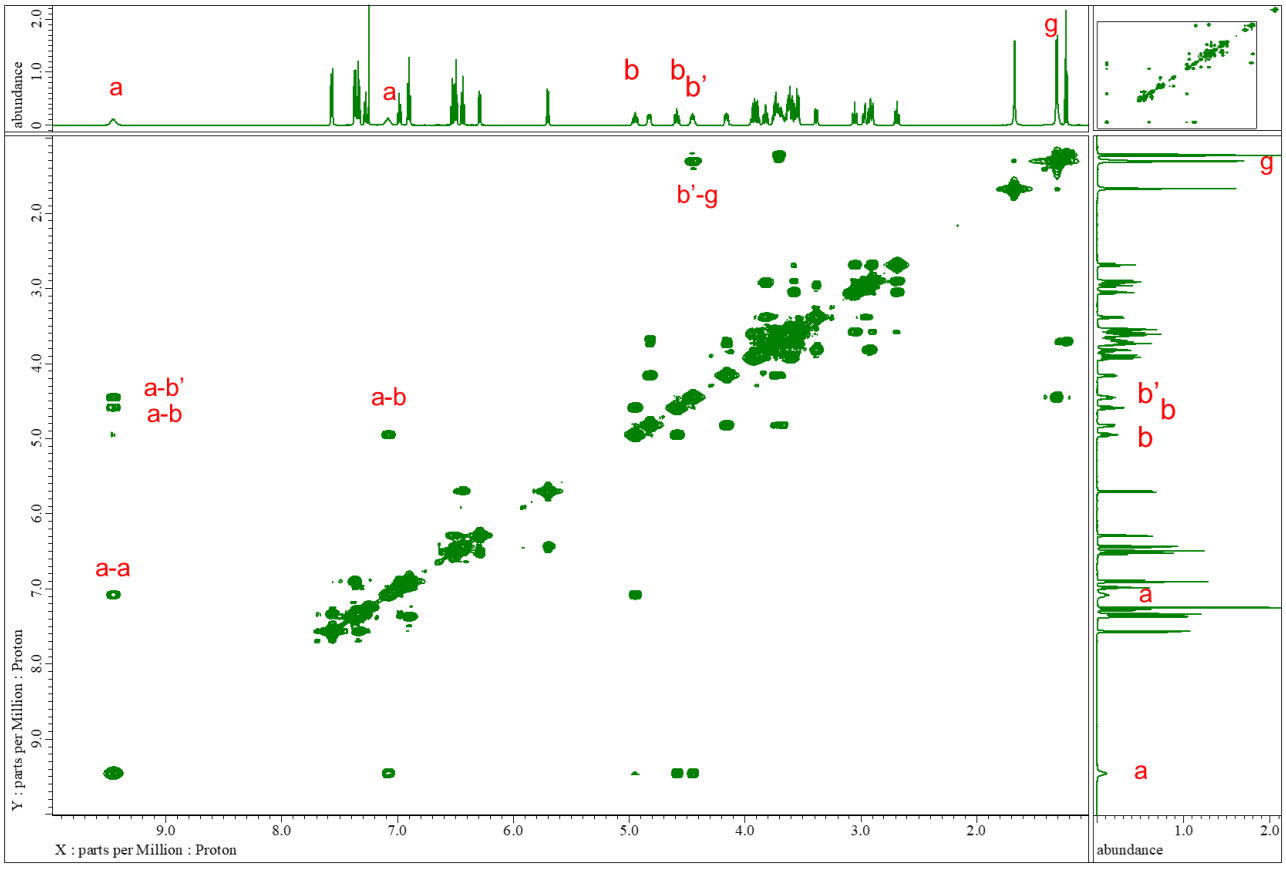
abundance
a
a
b
b
b'
g
b'-g
a-b'
a-b
a-b
a-a
g
b'
b
b
a
a
Y : parts per Million : Proton
X : parts per Million : Proton
abundance

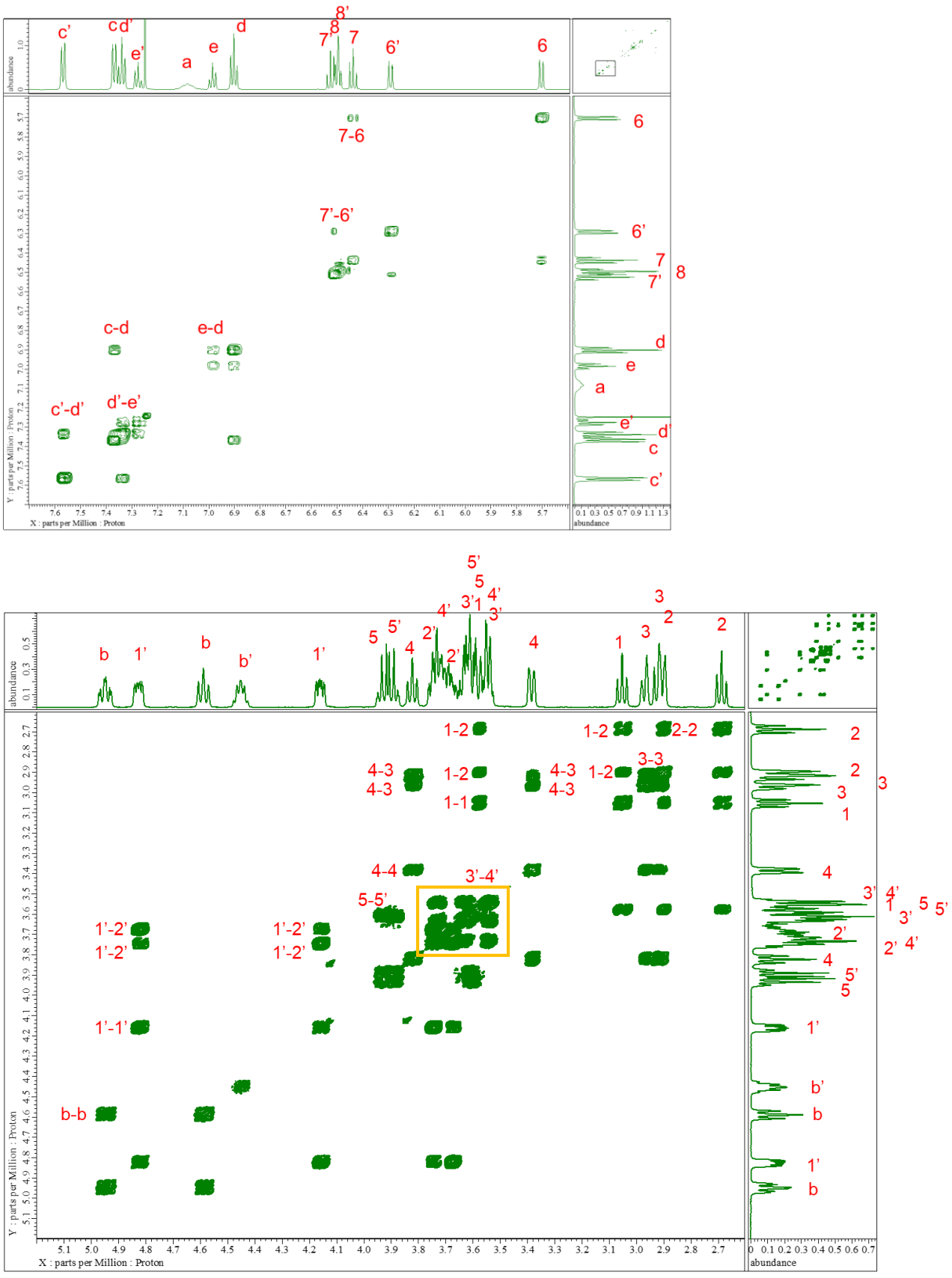

Figure S3a. COSY spectrum (600 MHz, $CDCl_3$, 5 °C) of (*S*)-pseudo[2]rotaxane **3a**.

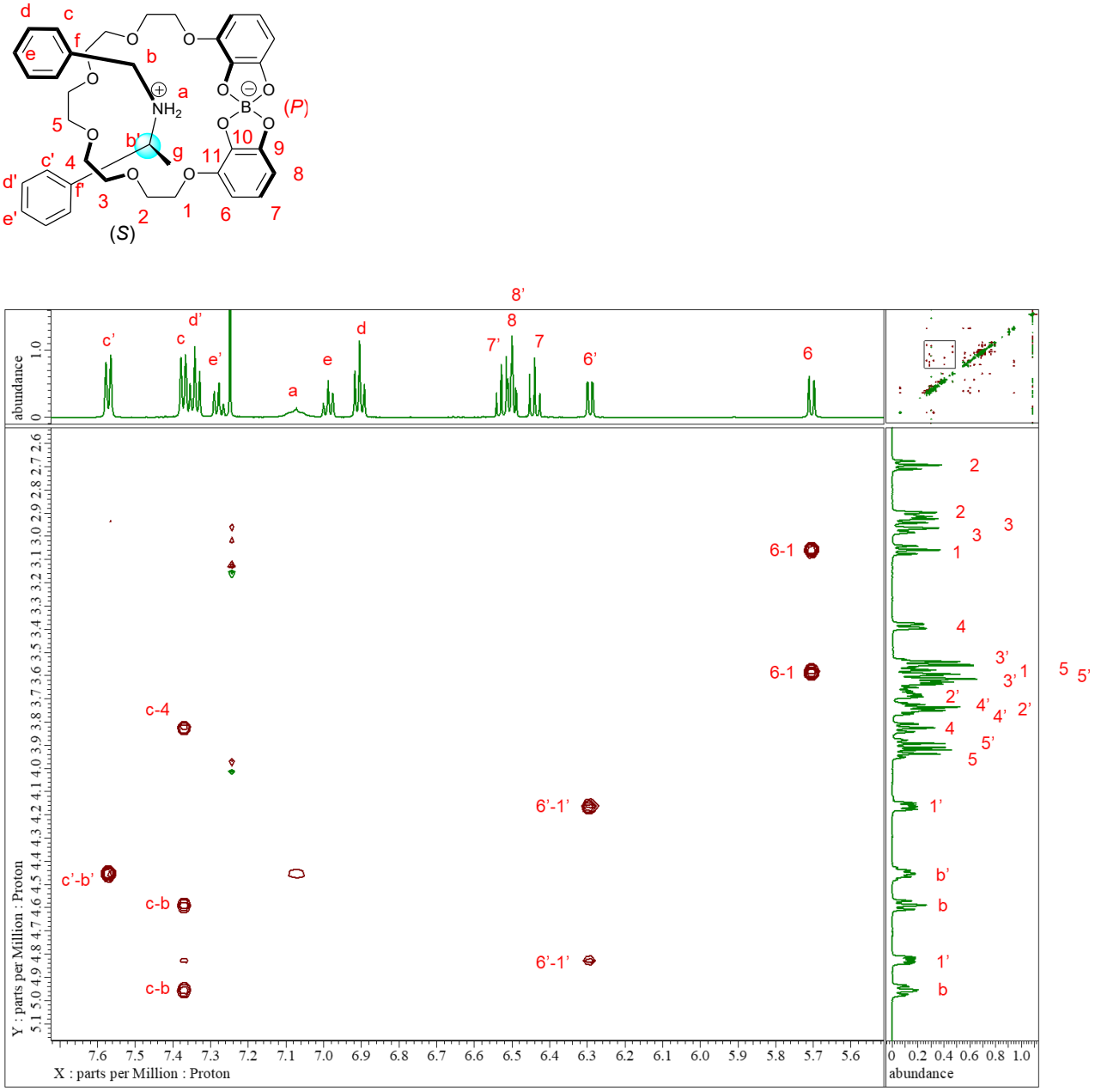

Figure S3b. ROESY spectrum (600 MHz, $CDCl_3$, 5 °C) of (*S*)-pseudo[2]rotaxane **3a**.

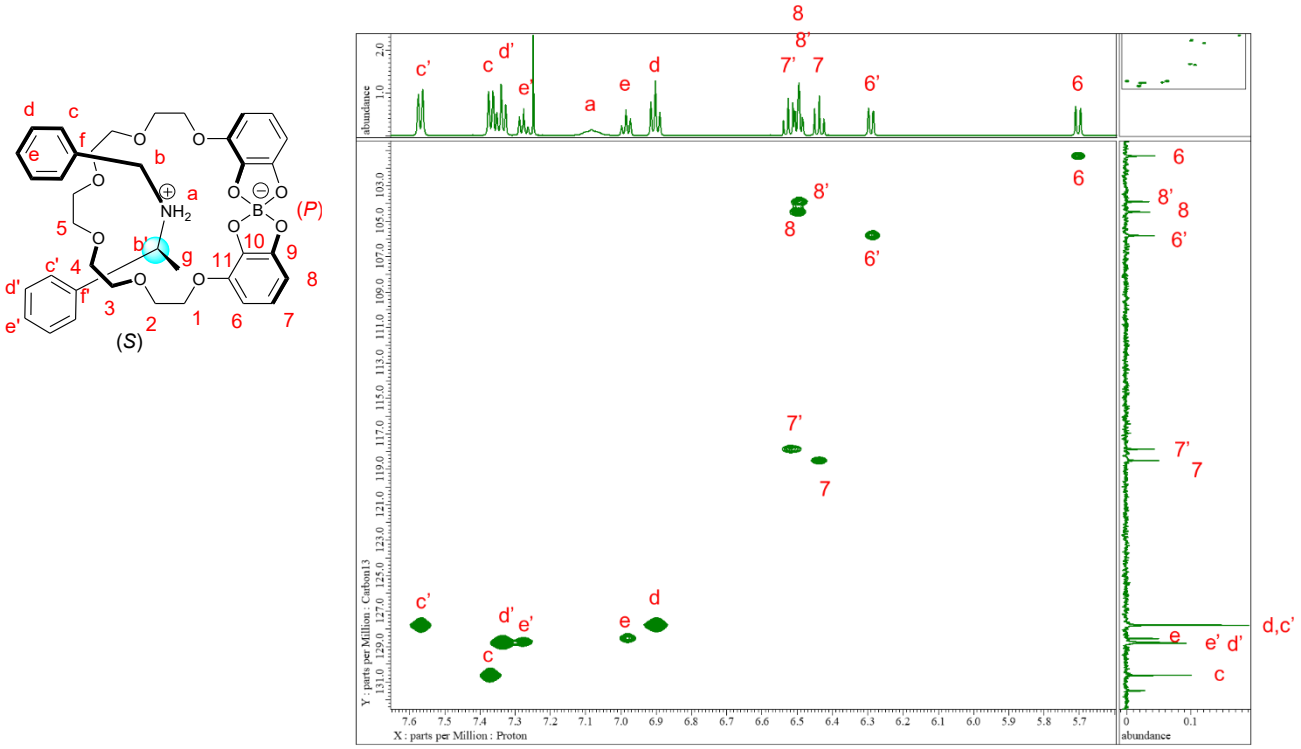
(P)
(S)
X : parts per Million : Proton
Y : parts per Million : Carbon13
abundance

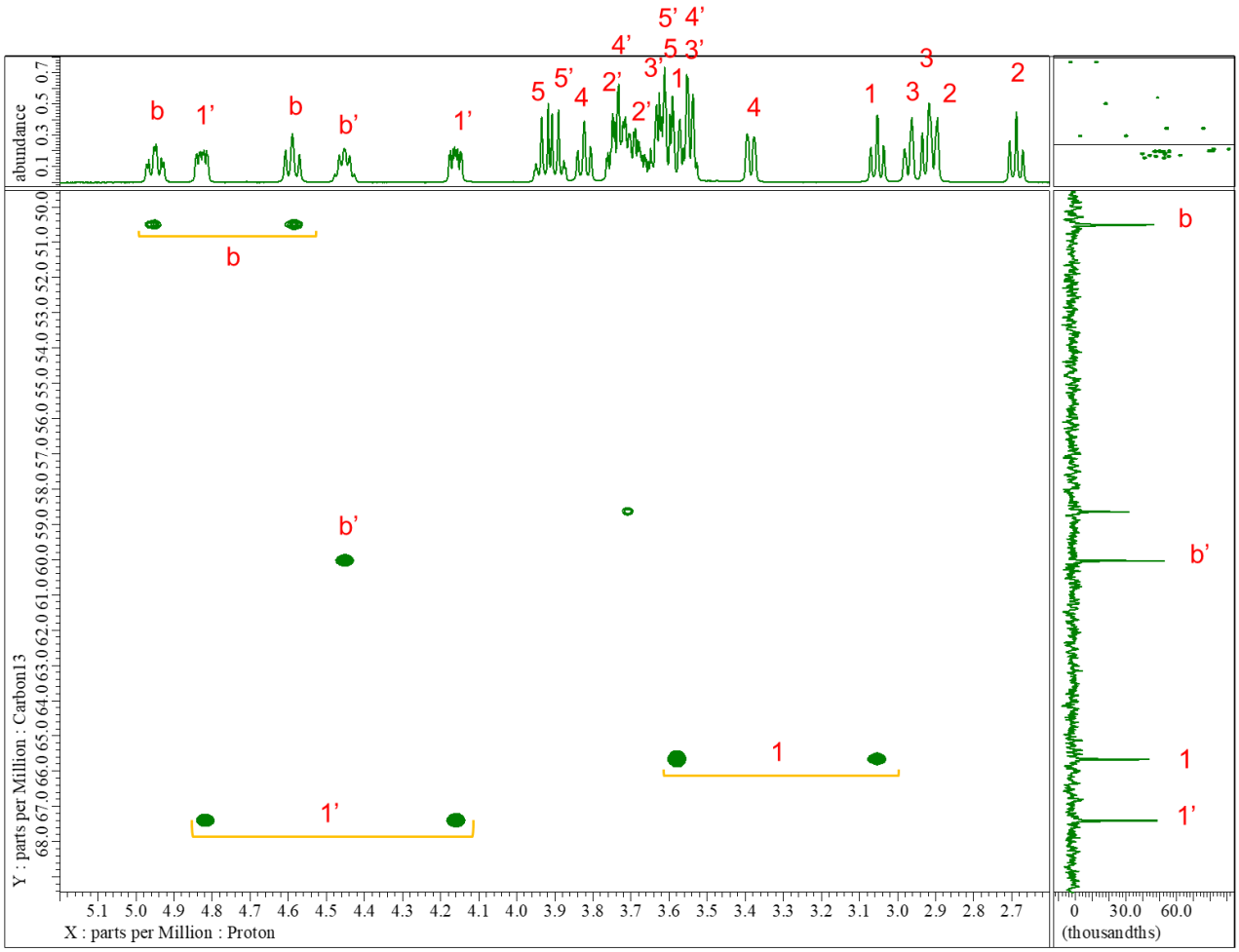
X : parts per Million : Proton
Y : parts per Million : Carbon13
abundance
(thousandths)

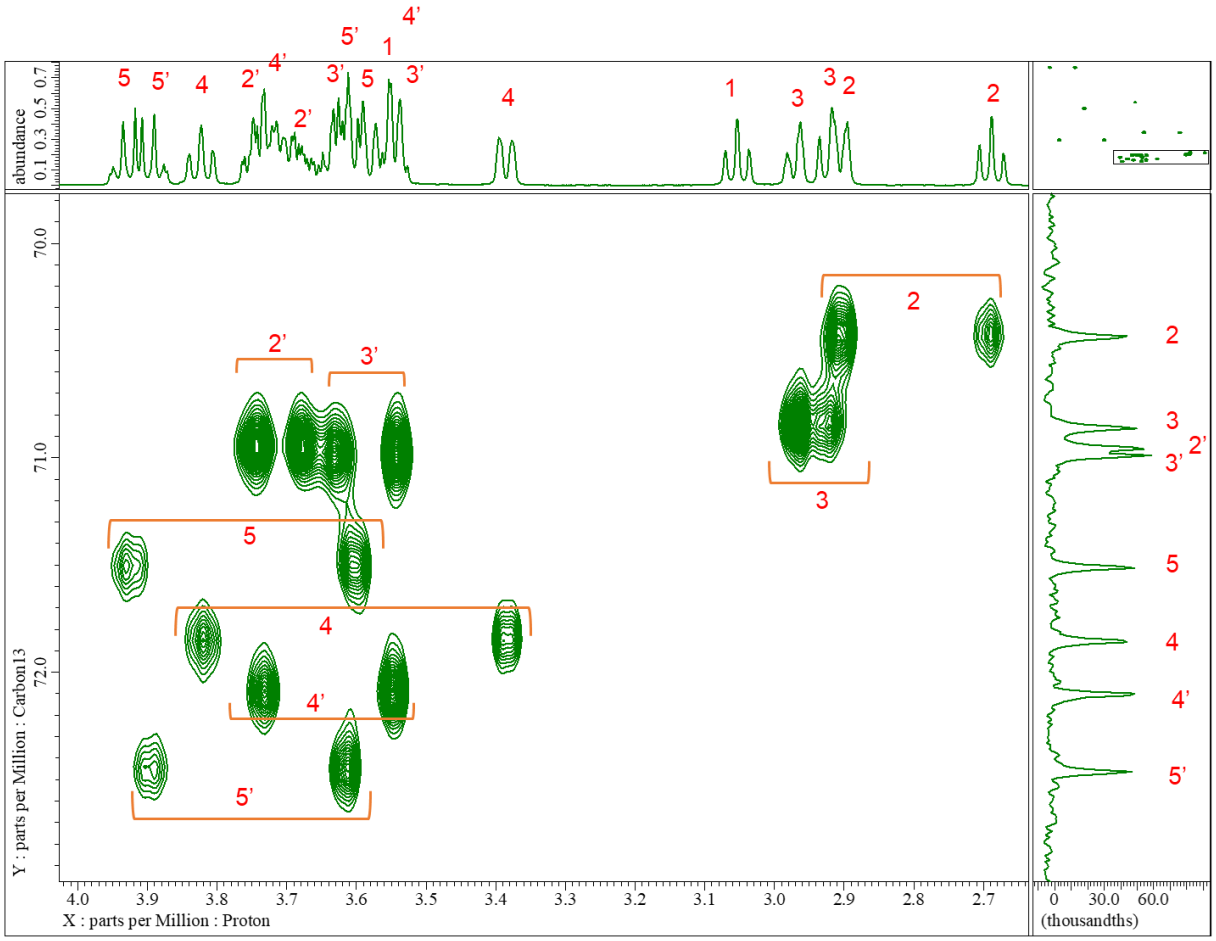

Figure S3c. HSQC spectrum (600 MHz, $CDCl_3$, 5 °C) of (*S*)-pseudo[2]rotaxane **3a**.

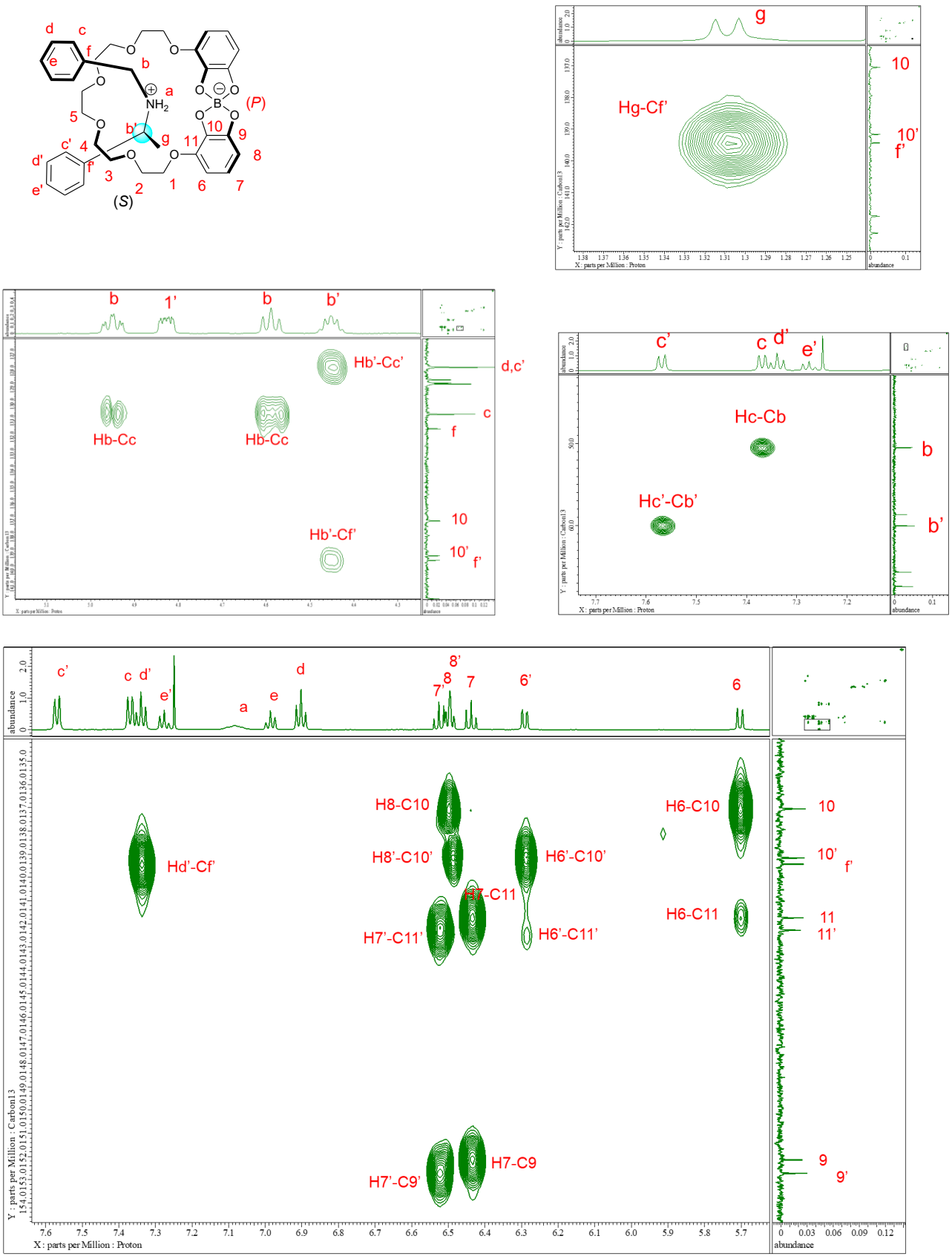

Figure S3d. HMBC spectrum (600 MHz, $CDCl_3$, 5 °C) of (*S*)-pseudo[2]rotaxane **3a**.

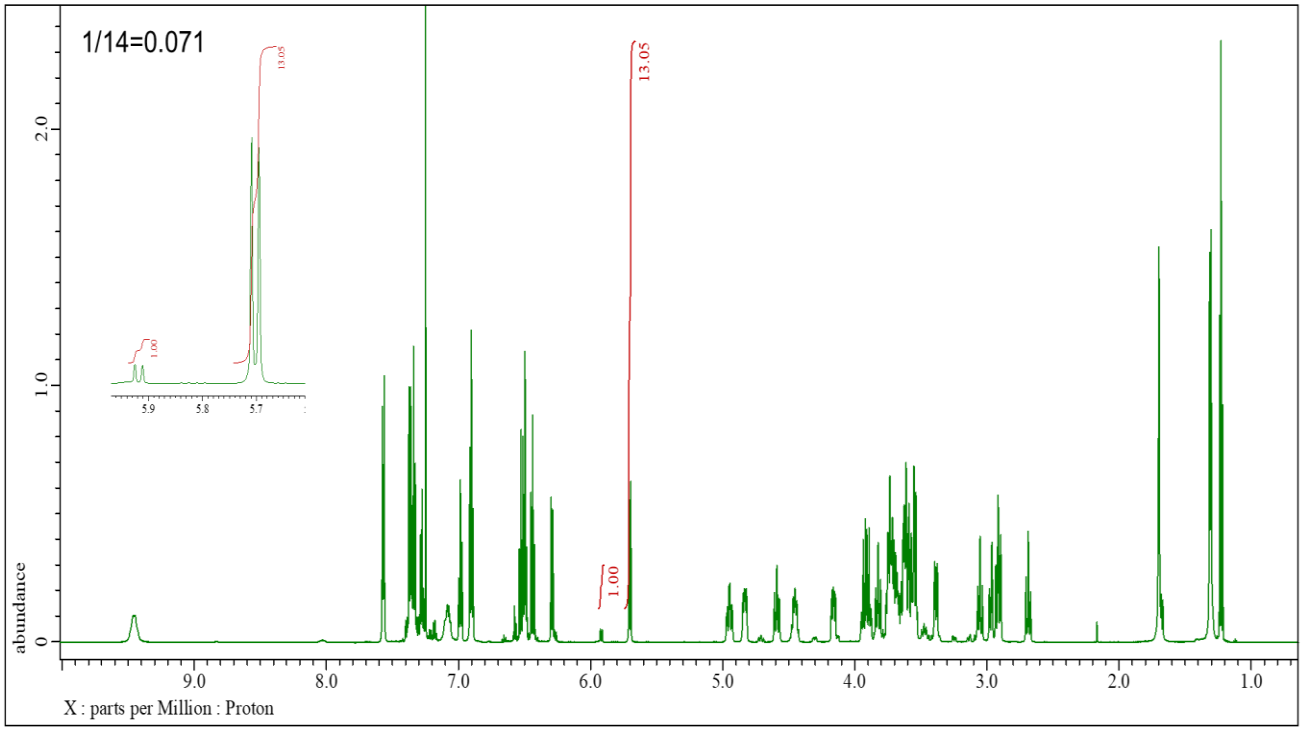

Figure S3e. ^{1}H NMR spectrum (600 MHz, $CDCl_3$, 5 °C) of (*S*)-pseudo[2]rotaxane **3a** after 2D NMR experiments (in $CDCl_3$ at 5 °C after 2.5 d)

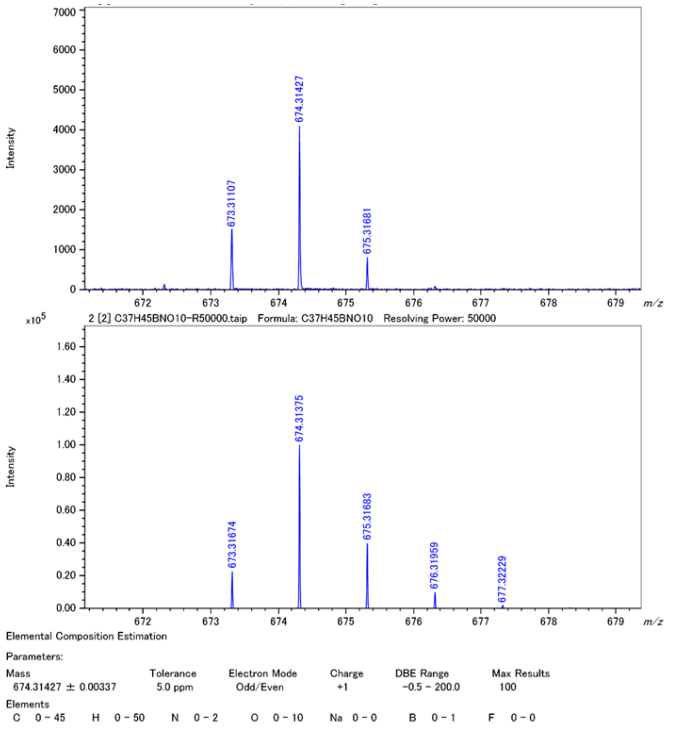

Figure S4a. Mass spectra of (*S*)-pseudo[2]rotaxane **3a**.

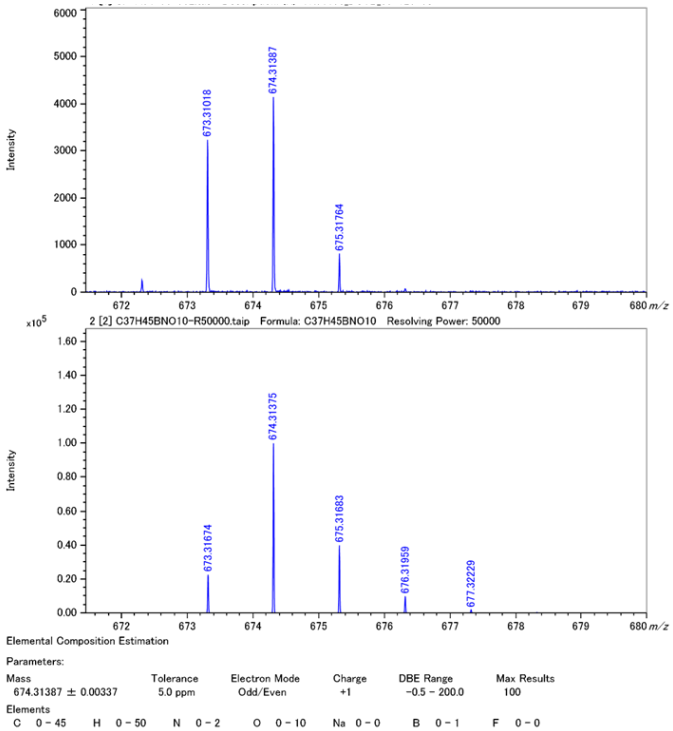

Figure S4b. Mass spectra of (*R*)-pseudo[2]rotaxane **3a**.

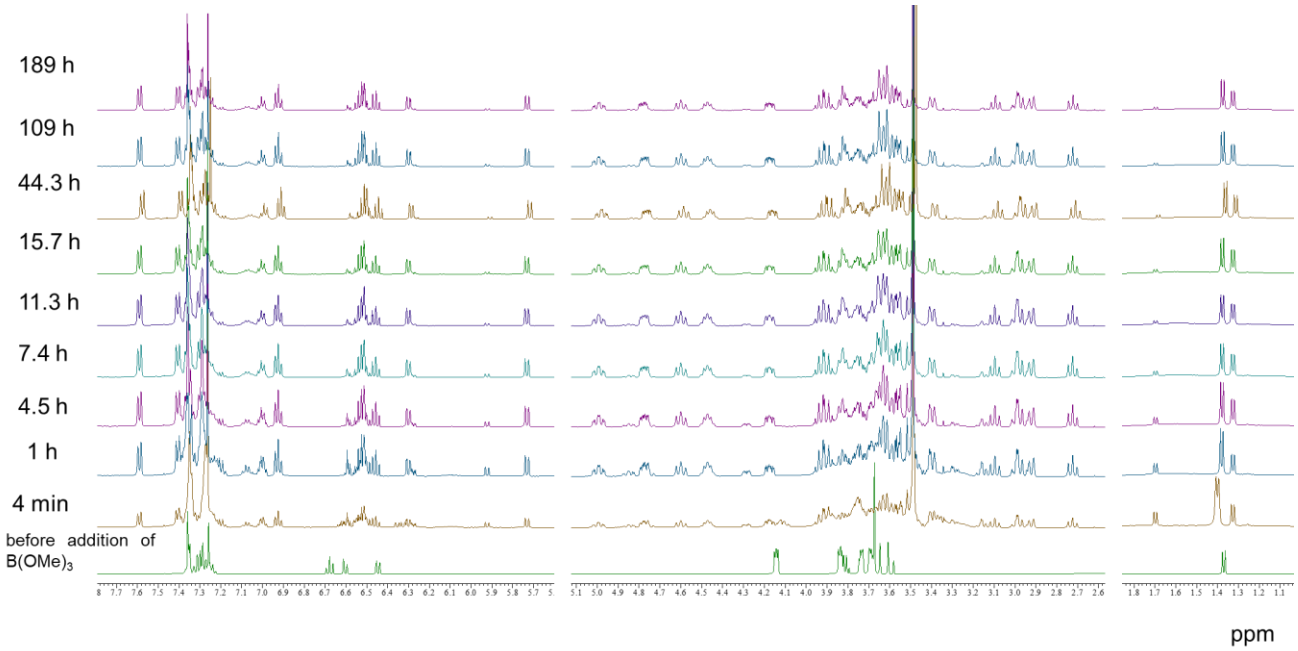

Figure S5. Time-dependent ^{1}H NMR spectra (500 MHz, $CDCl_3$) of a mixture of bis-catechol **1**, amine **2a** in the presence of trimethyl borate.

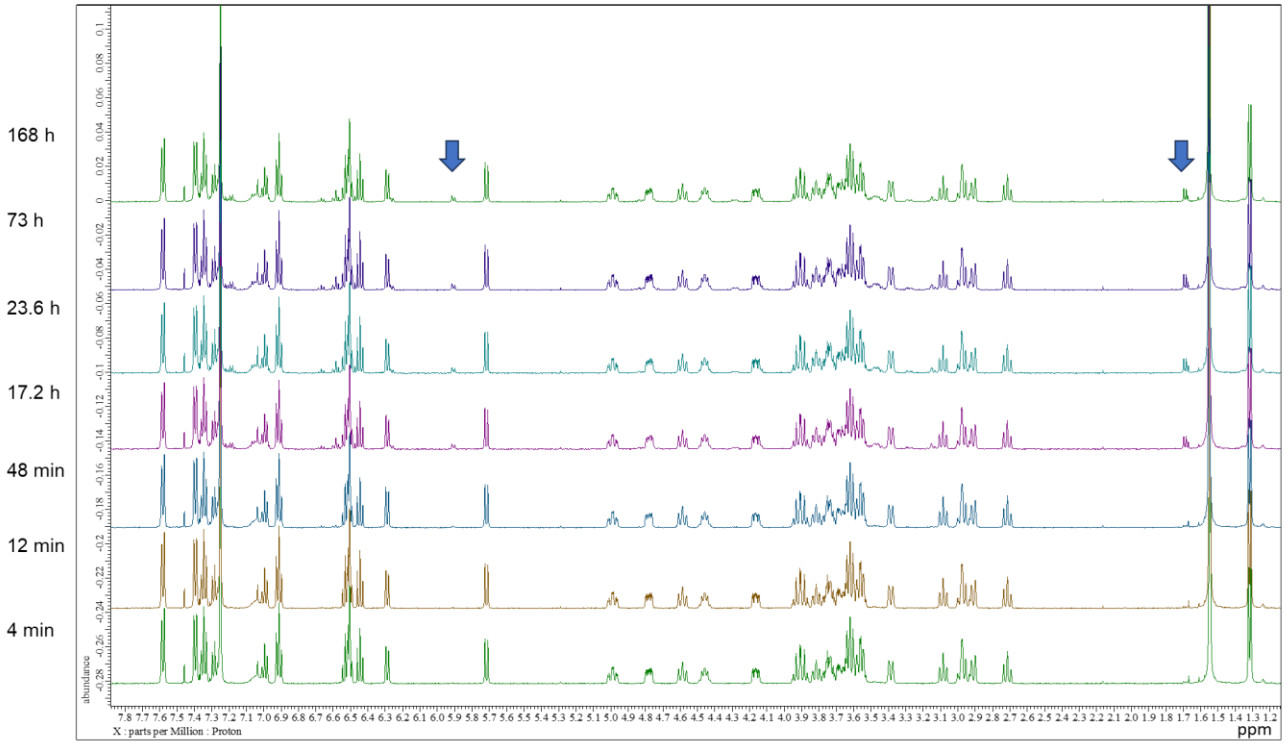

Figure S6a. Time-dependent ^{1}H NMR spectra of pseudo[2]rotaxane **3a** in $CDCl_3$.

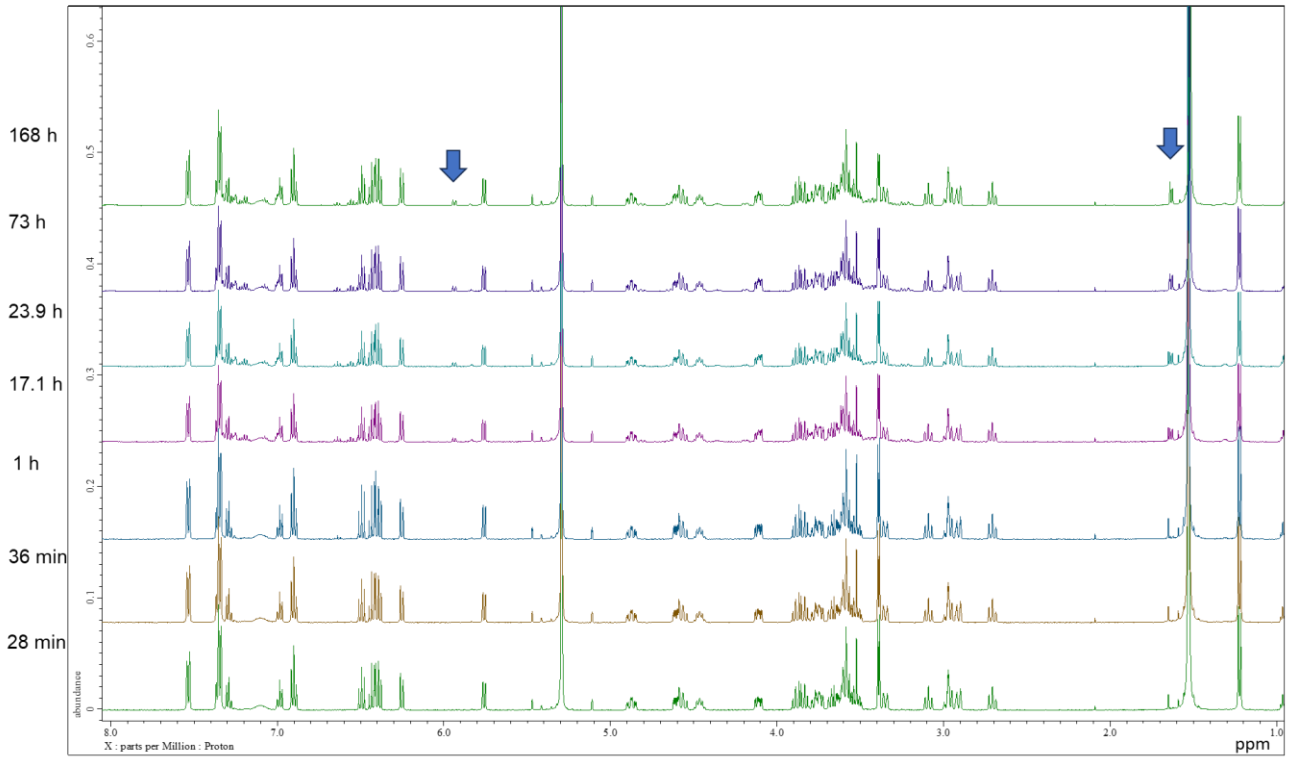

Figure S6b. Time-dependent ^{1}H NMR spectra of pseudo[2]rotaxane **3a** in CD_2Cl_2.

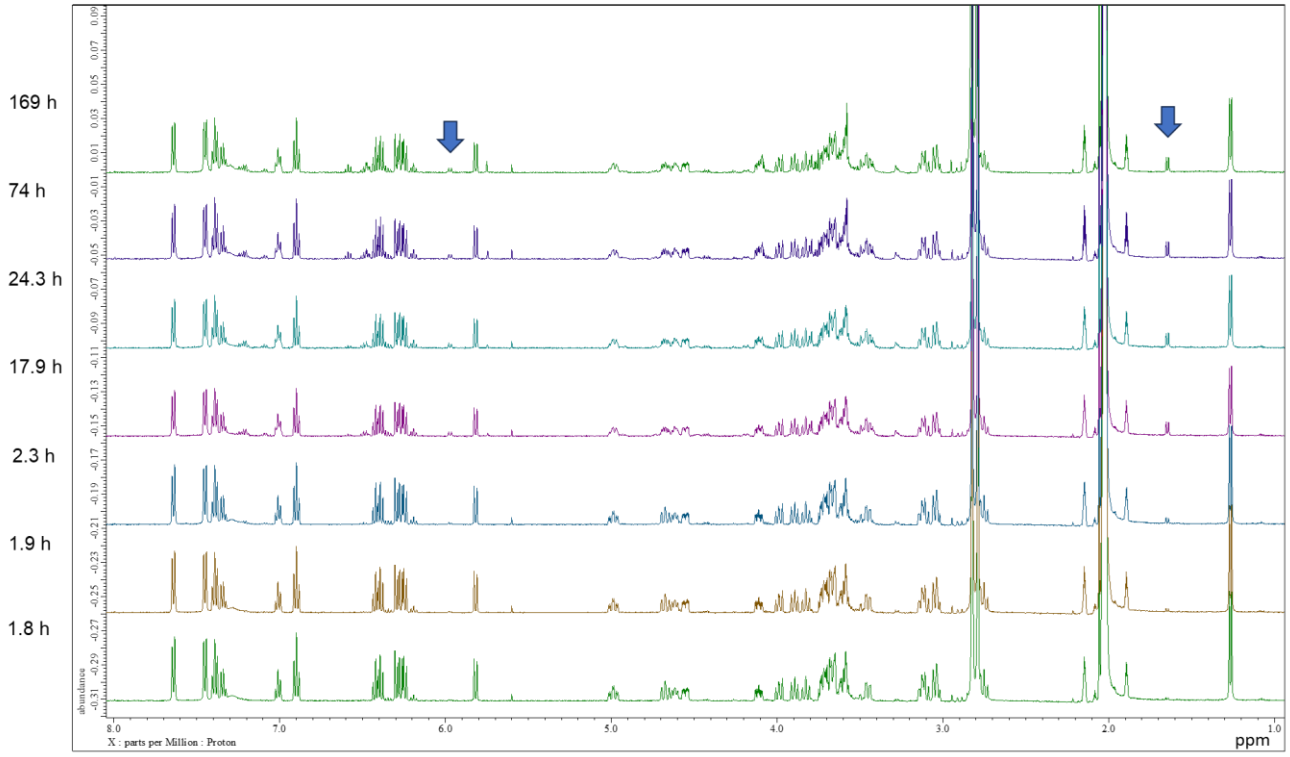

Figure S6c. Time-dependent ^{1}H NMR spectra of pseudo[2]rotaxane **3a** in acetone-d_6.

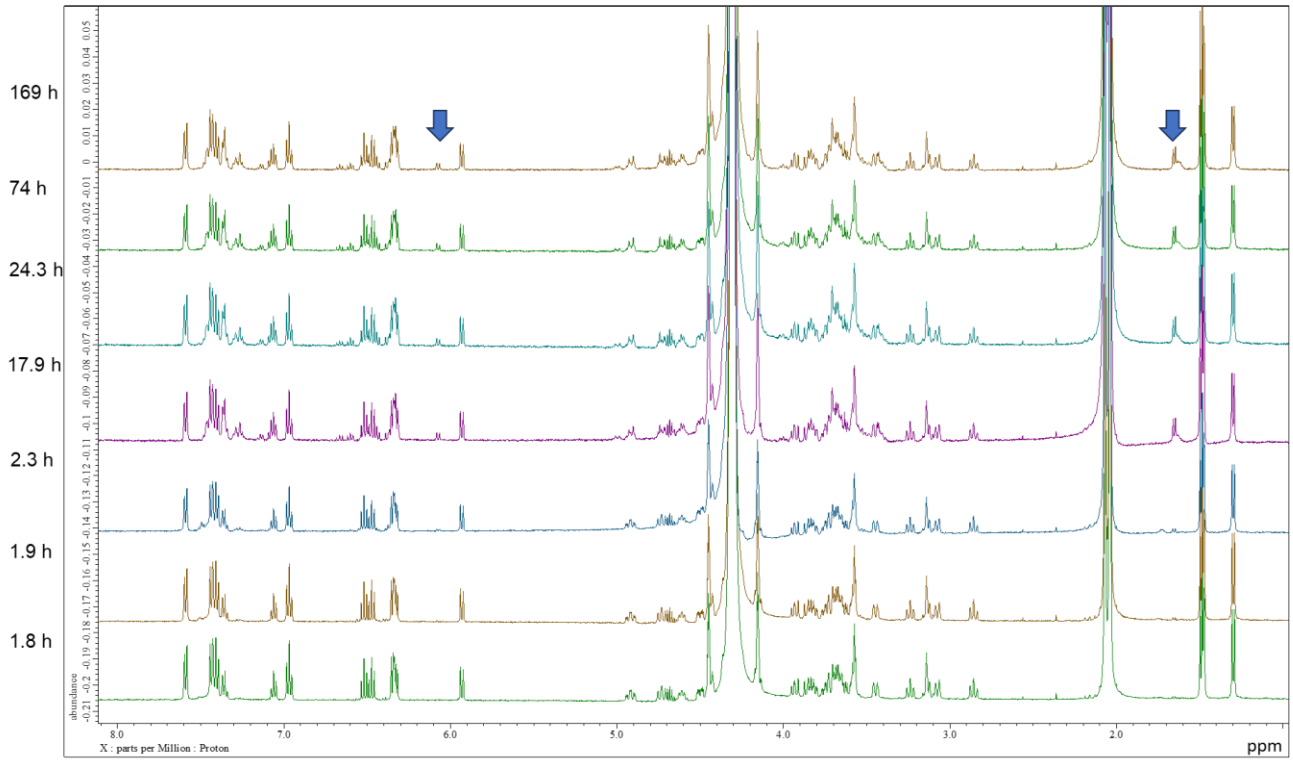

Figure S6d. Time-dependent ^{1}H NMR spectra of pseudo[2]rotaxane **3a** in CD_3NO_2.

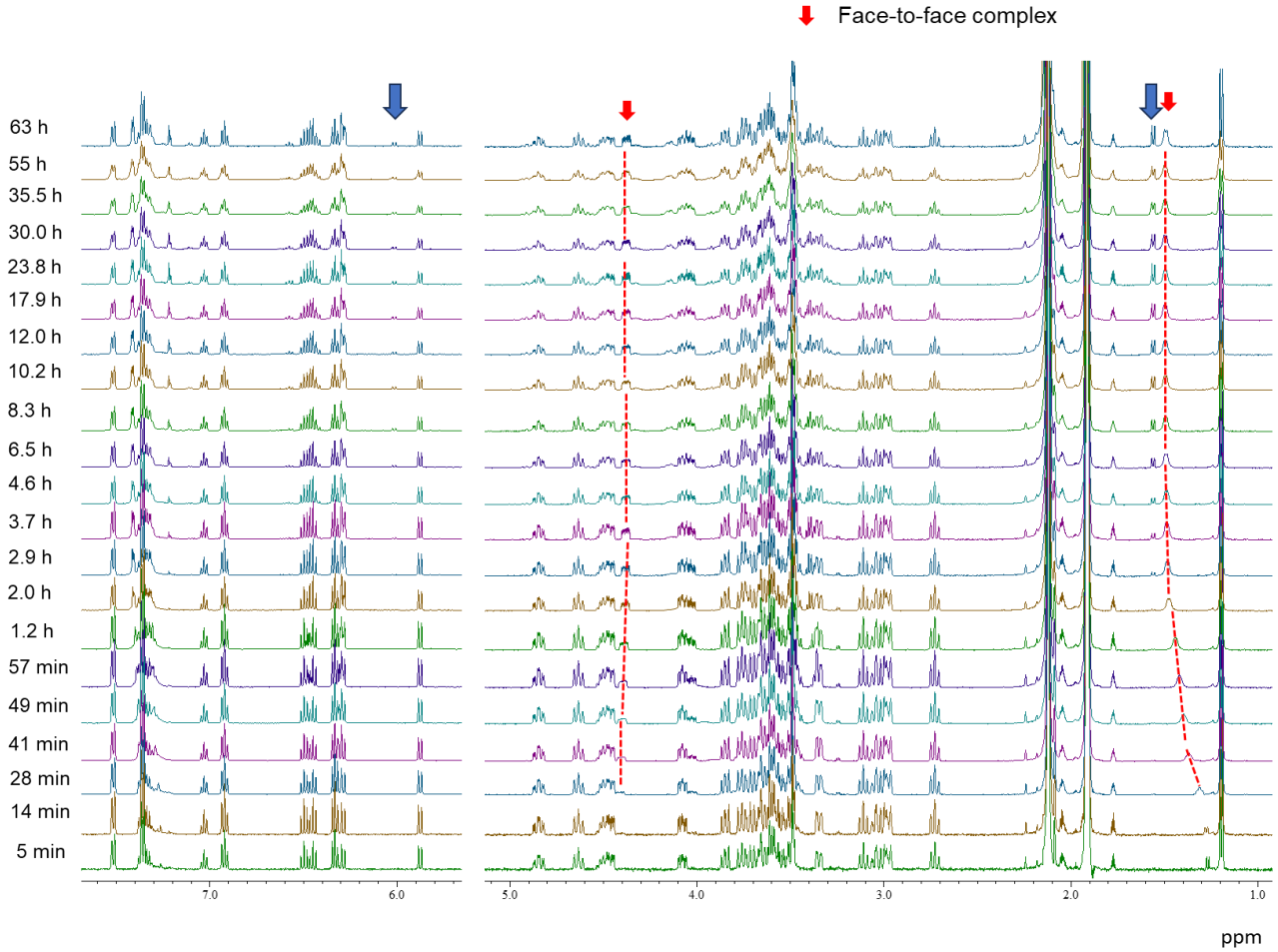

Figure S6e. Time-dependent ^{1}H NMR spectra of pseudo[2]rotaxane **3a** in CD_3CN.

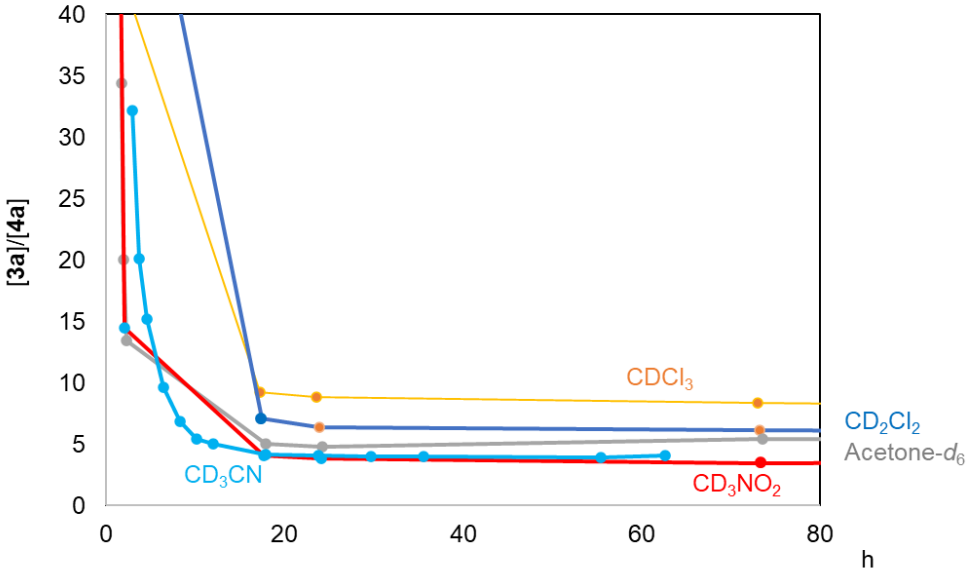

Figure S6f. Ratios of **3a** and **4a** after pseudo[2]rotaxane **3a** was dissolved in various solvents at room temperature.

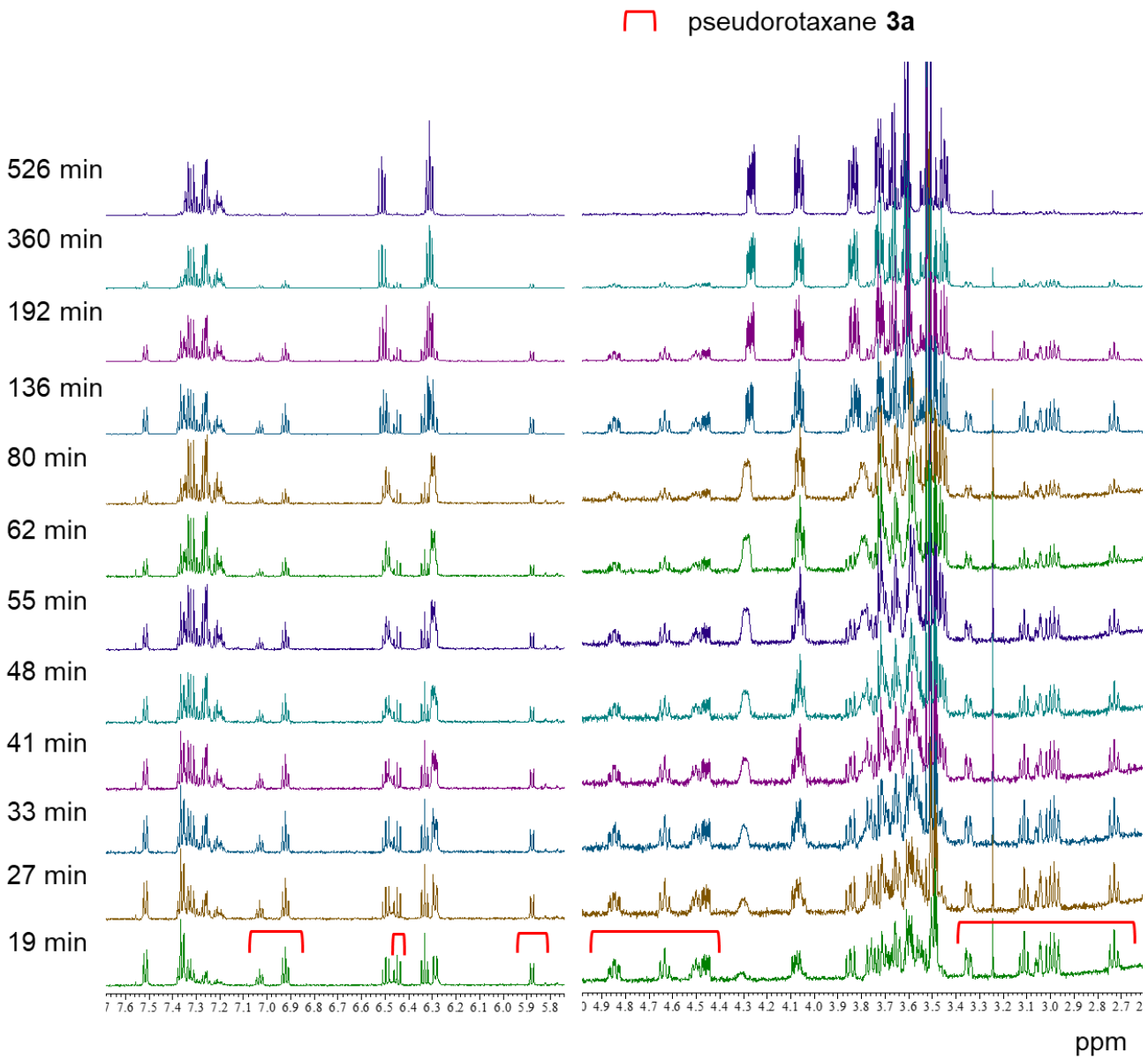

tert-Butylamine (40 equiv.) was added to a solution of (*P*,*S*)-pseudorotaxaxane **3a** (0.25 mM) in CD_3CN.

Figure S7a. Time-dependent ^1H NMR spectra of pseudo[2]rotaxane **3a** in the presence of excess amount of *tert*-butylamine in CD_3CN.

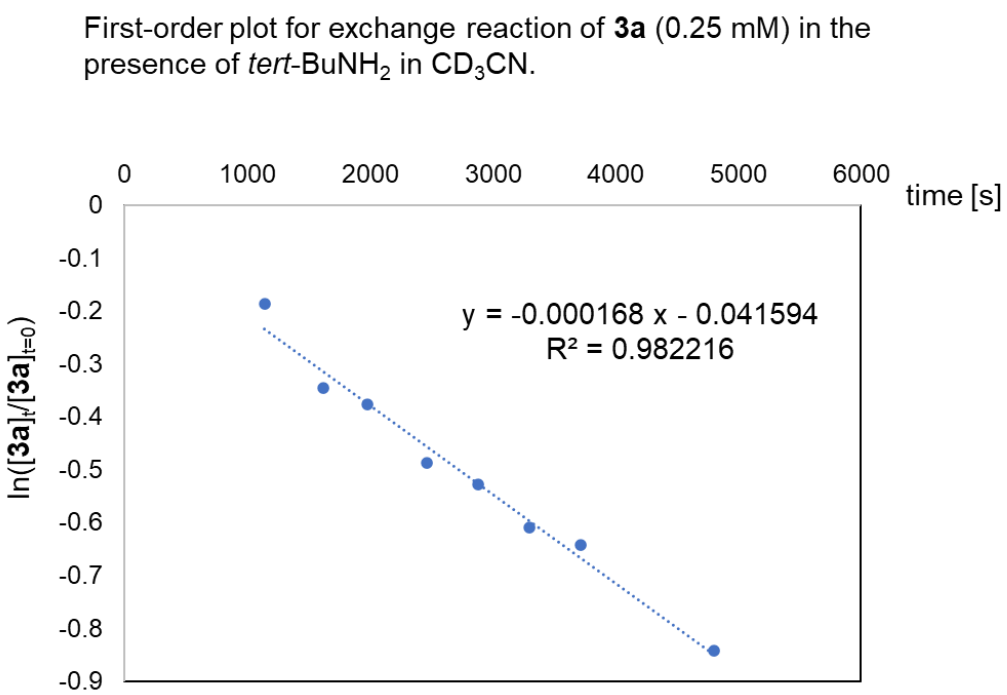

Figure S7b. First-order plot of the exchange reaction of the ammonium component of **3a**; *tert*-Butylamine (40 equiv.) was added to a solution of (*P*,*S*)-pseudorotaxaxane **3a** (0.25 mM) in CD_3CN.

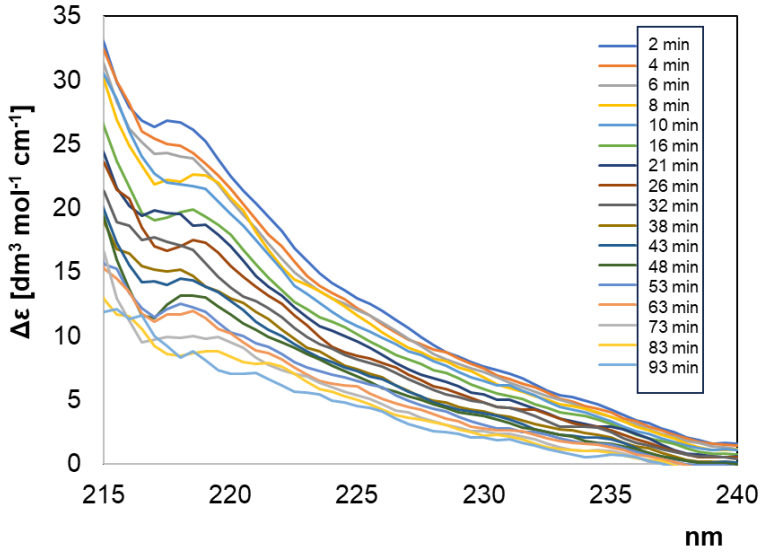

tert-Butylamine (40 equiv.) was added to a solution of (*P*,*S*)-pseudorotaxaxane **3a** (0.25 mM) in CH_3CN.

Figure S8a. Time-dependent CD spectra of pseudo[2]rotaxane **3a** in the presence of excess amount of *tert*-butylamine in CH_3CN.

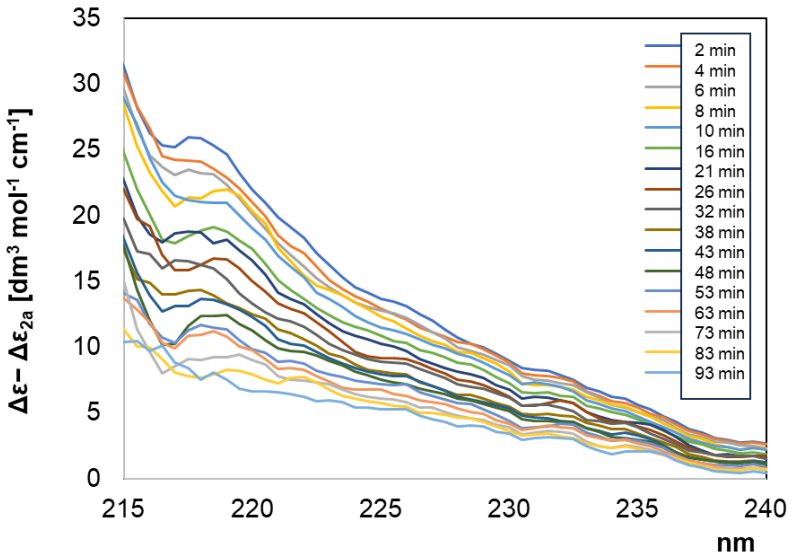

calculated time-dependent CD spectra = time-dependent CD spectra − CD spectra of **2a**

Figure S8b. Calculated time-dependent CD spectra of pseudo[2]rotaxane **3a** in the presence of excess amount of *tert*-butylamine in CH_3CN.

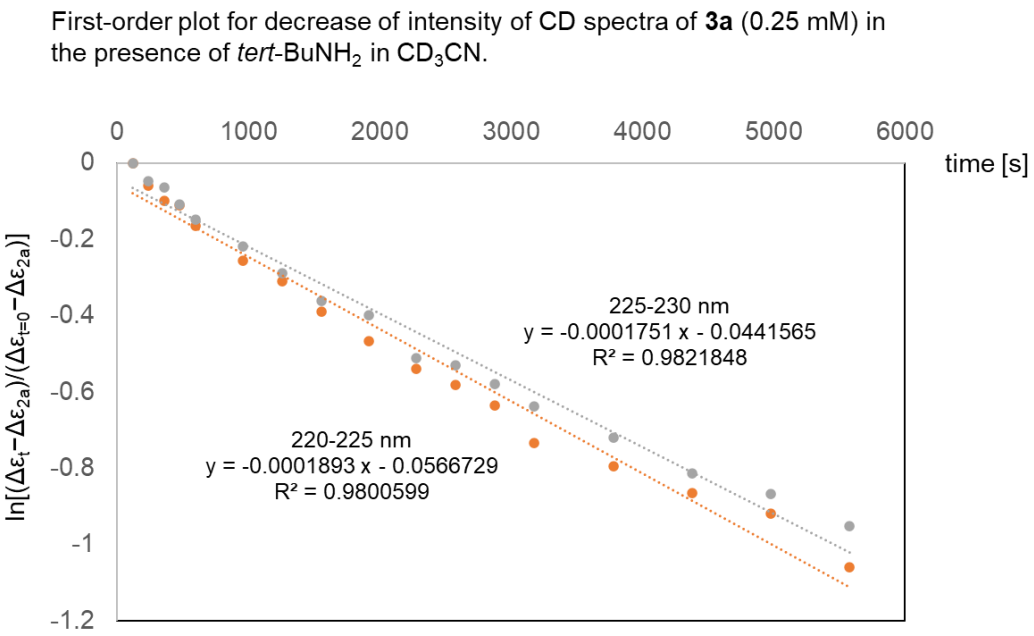

Figure S8c. The first-order plot obtained from the decrease in the intensity of the calculated time-dependent CD spectra (Figure S8b). The $\Delta\varepsilon_t - \Delta\varepsilon_{2a}$ and $\Delta\varepsilon_{t=0} - \Delta\varepsilon_{2a}$ values were used as the average intensities (220–225 and 225–230 nm, respectively) of the calculated time-dependent CD spectra (Figure S8b).

Selective formation of (*R*)-pseudo[2]rotaxane **3b** under thermodynamic conditions.

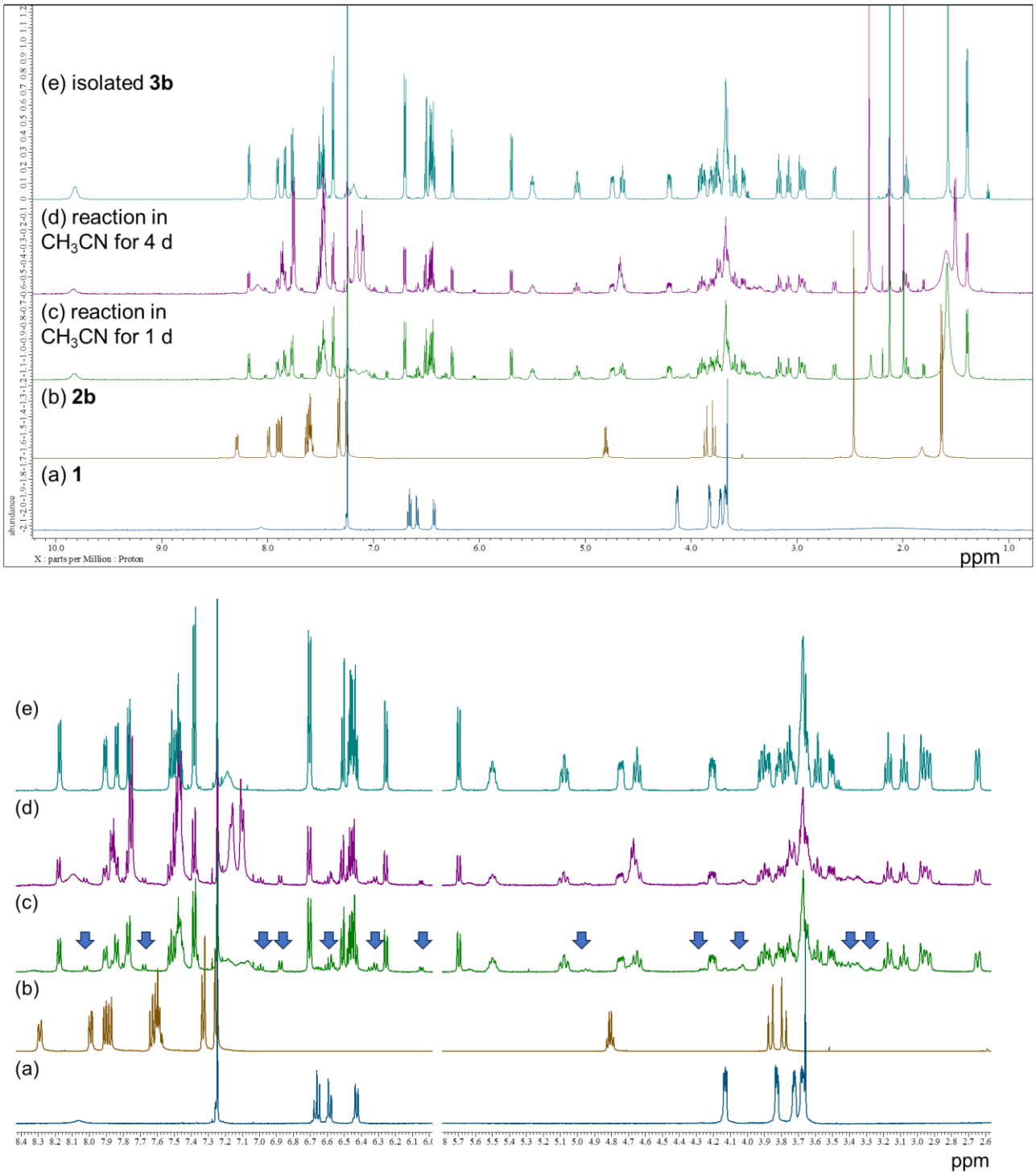

Figure S9a. ^{1}H NMR spectra (500 MHz, $CDCl_3$) of the reaction of **1**, **2b**, and boric acid in CH_3CN at 50 °C. (a) Bis-catechol **1**, (b) amine **2b**, (c) crude product of the reaction for 1 d, (d) for 4 d, (e) isolated pseudo[2]rotaxane **3b**.

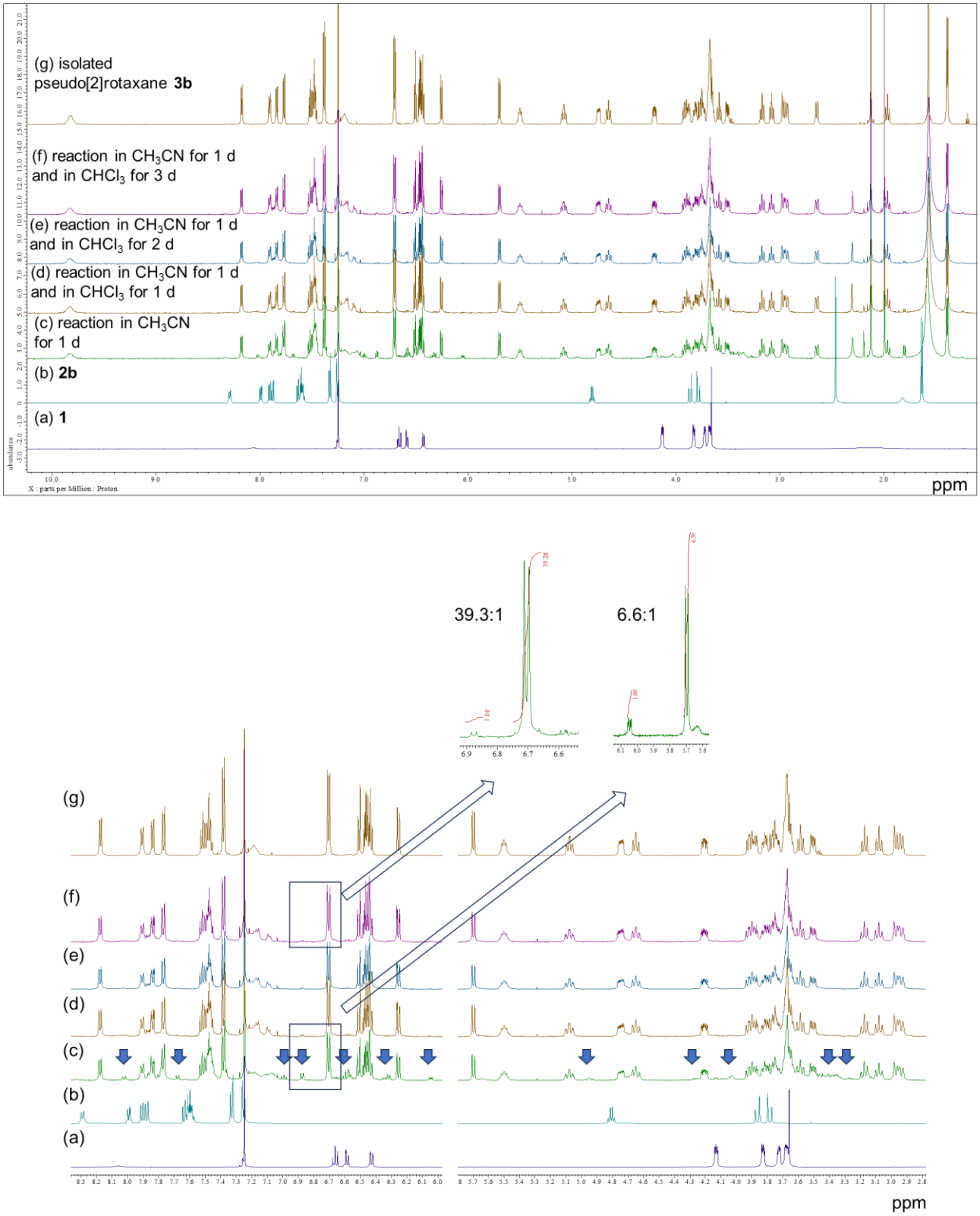

Figure S9b. ^{1}H NMR spectra (500 MHz, $CDCl_3$) of the reaction of bis-catechol **1**, amine **2b**, and boric acid in CH_3CN at 50 °C. (a) **1**, (b) **2b**, (c) crude product of the reaction in CH_3CN for 1 d, (d) the reaction in CH_3CN for 1 d and in $CHCl_3$ for 1 d, (e) the reaction in CH_3CN for 1 d and in $CHCl_3$ for 2 d, (f) the reaction in CH_3CN for 1 d and in $CHCl_3$ for 3 d, (g) isolated pseudo[2]rotaxane **3b**.

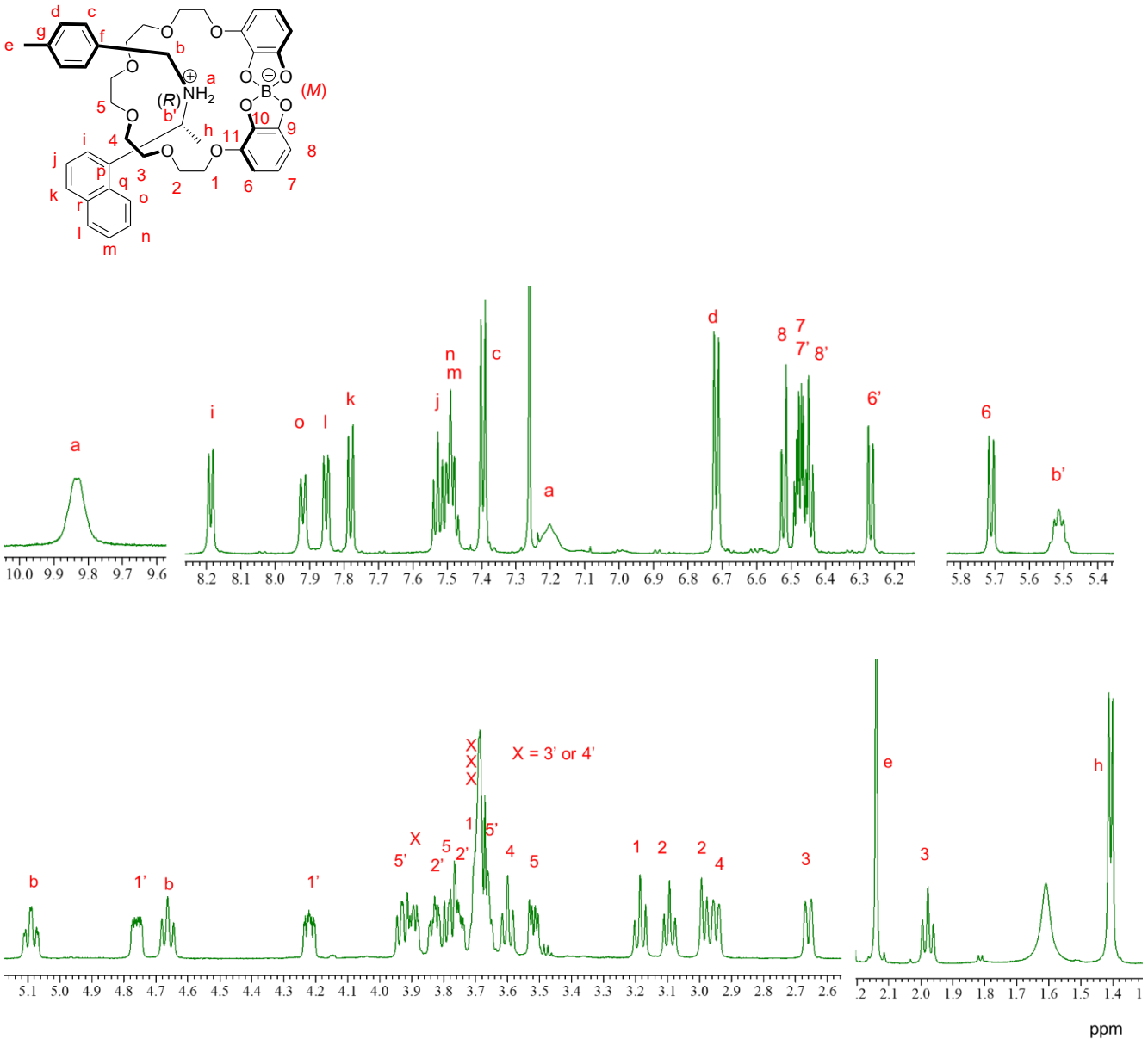

Figure S10a. ^{1}H NMR spectrum (600 MHz, $CDCl_3$) of (*R*)-pseudo[2]rotaxane **3b**.

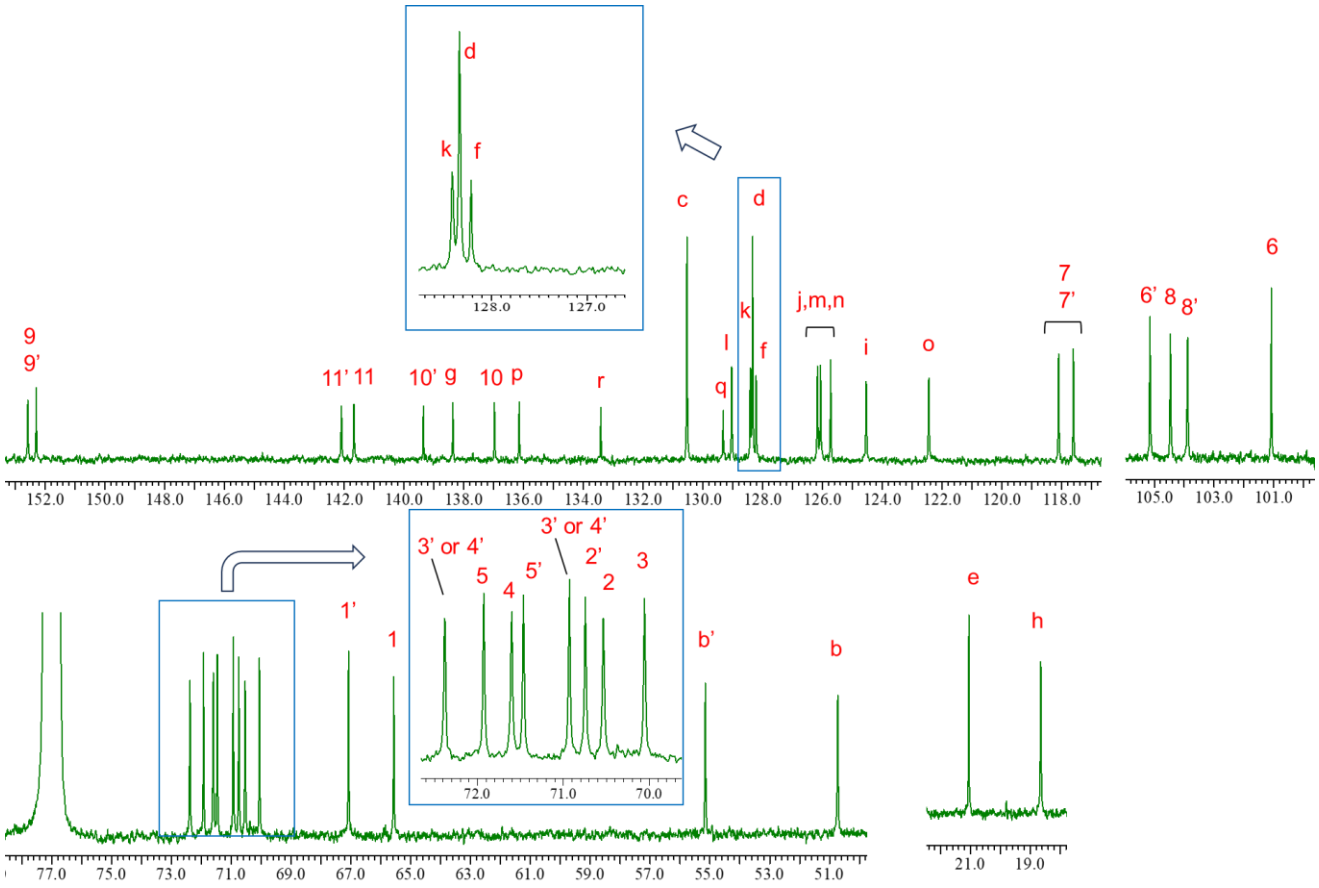

Figure S10b. ^{13}C NMR spectrum (150 MHz, $CDCl_3$) of (*R*)-pseudo[2]rotaxane **3b**.

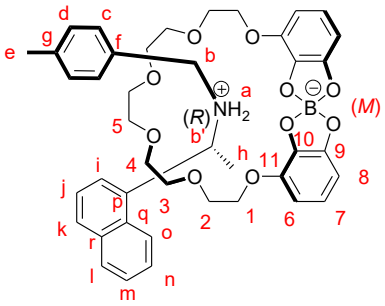
d
c
g
f
e
b
O
O
O
a
(R)NH2
O
B
O
(M)
5
O
b'
h
11
10
9
8
i
4
O
O
j
p
q
3
2
1
6
7
k
r
o
l
m
n

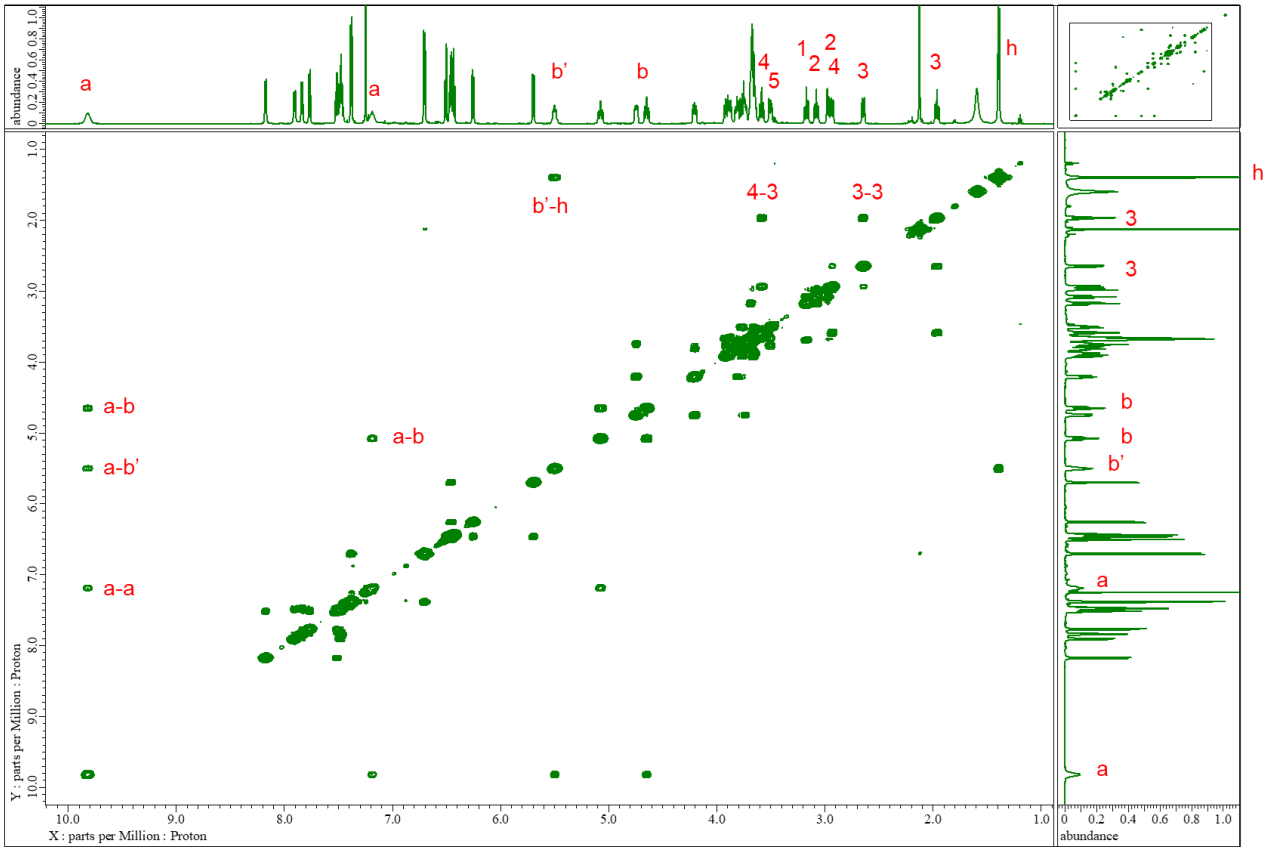
abundance
a
a
b'
b
4
5
1
2
2
4
3
3
h
b'-h
4-3
3-3
a-b
a-b'
a-a
a-b
h
3
3
b
b
b'
a
a
Y : parts per Million : Proton
X : parts per Million : Proton
abundance

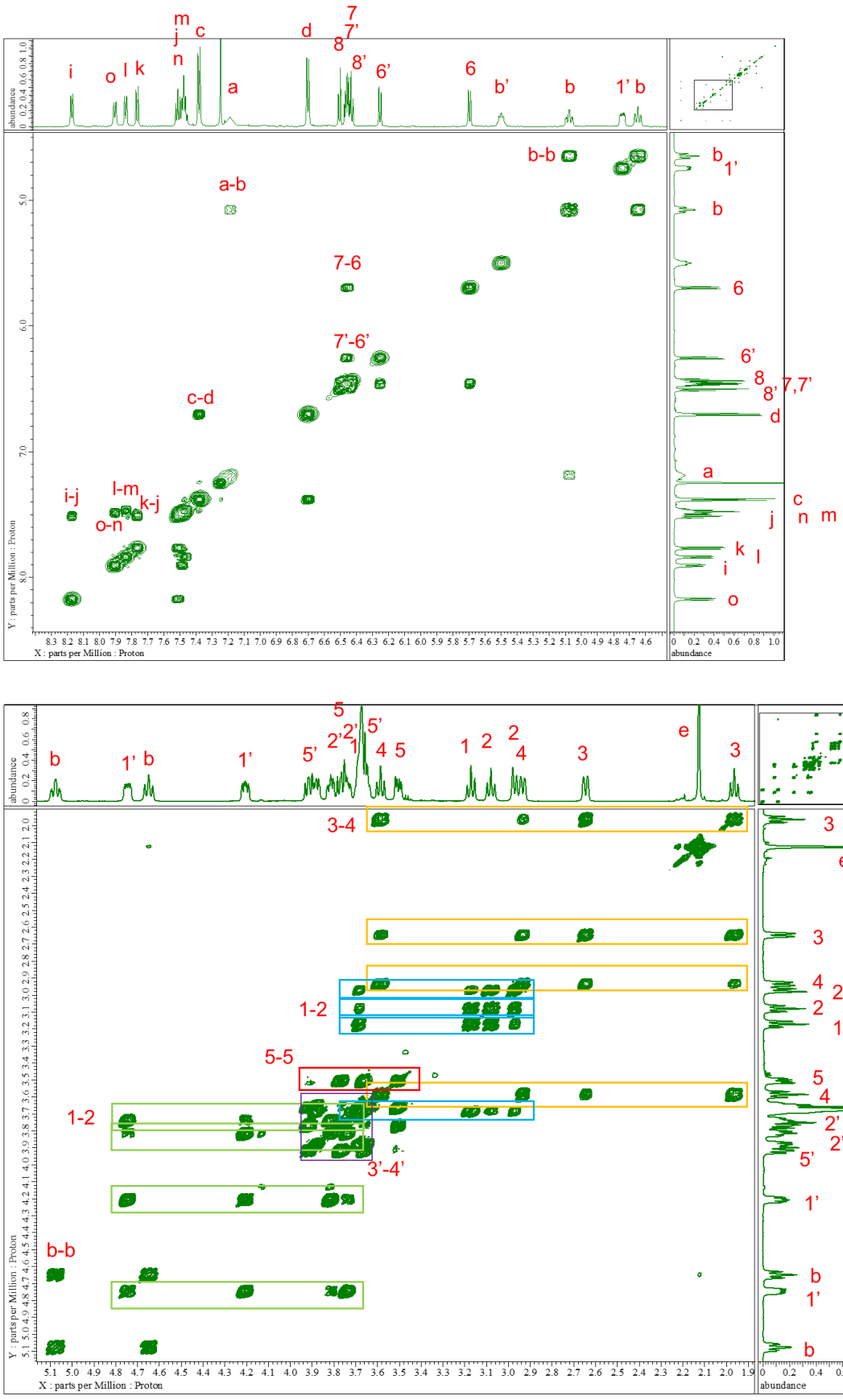

Figure S11a. COSY spectrum (600 MHz, $CDCl_3$) of (*R*)-pseudo[2]rotaxane **3b**.

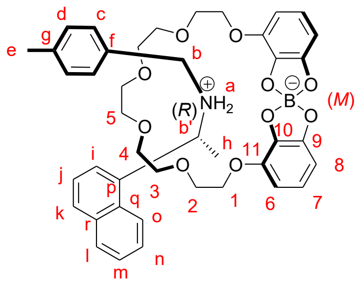

d
c
e
g
f
b
a
NH2
(R)
b'
h
(M)
B
11
10
9
8
4
5
3
2
1
6
7
i
j
p
q
k
r
o
l
m
n

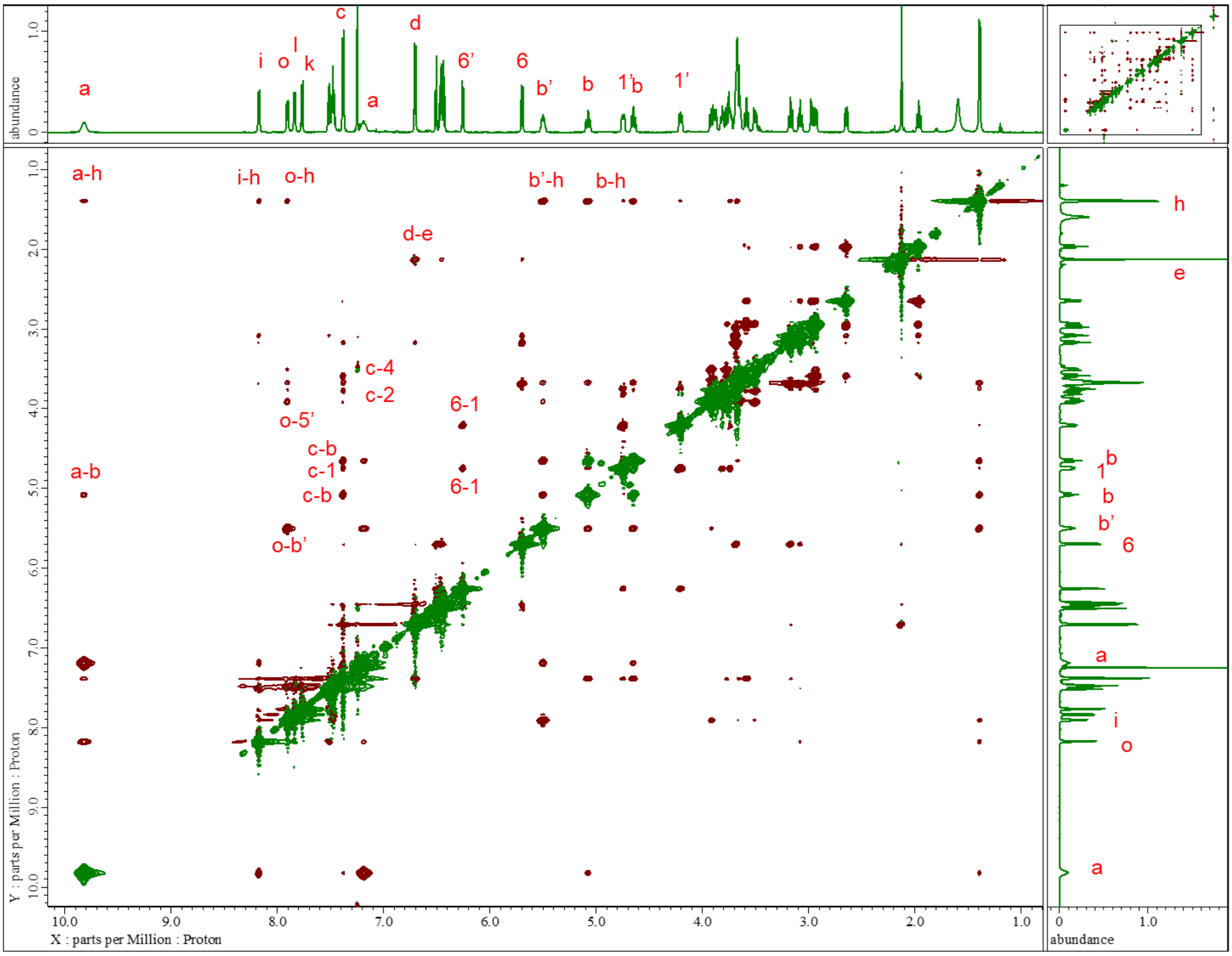

a-h
i-h
o-h
b'-h
b-h
d-e
c-4
c-2
6-1
o-5'
c-b
c-1
c-b
6-1
a-b
o-b'
X : parts per Million : Proton
Y : parts per Million : Proton
abundance

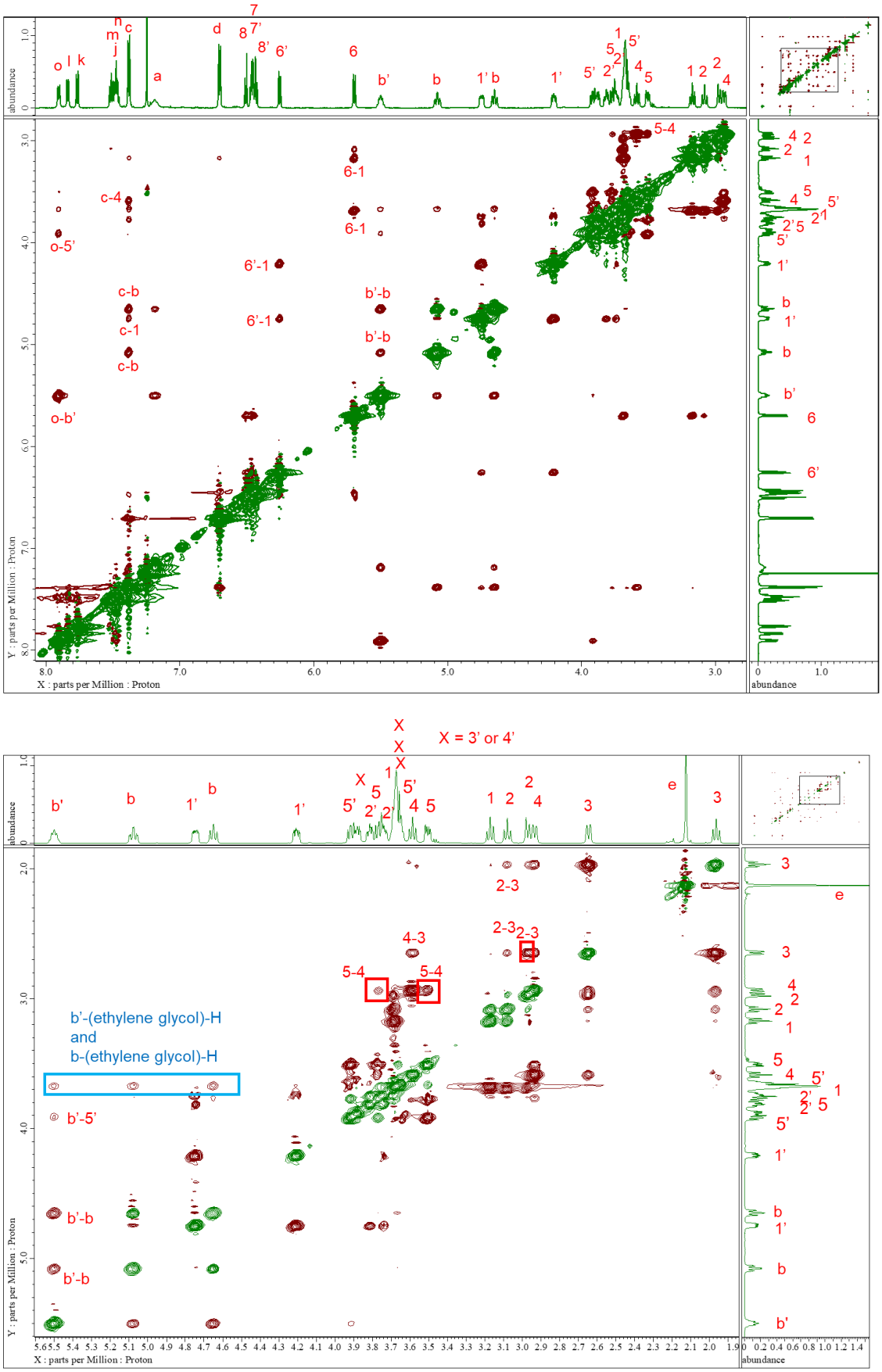

Figure S11b. ROESY spectrum (600 MHz, $CDCl_3$) of (*R*)-pseudo[2]rotaxane **3b**.

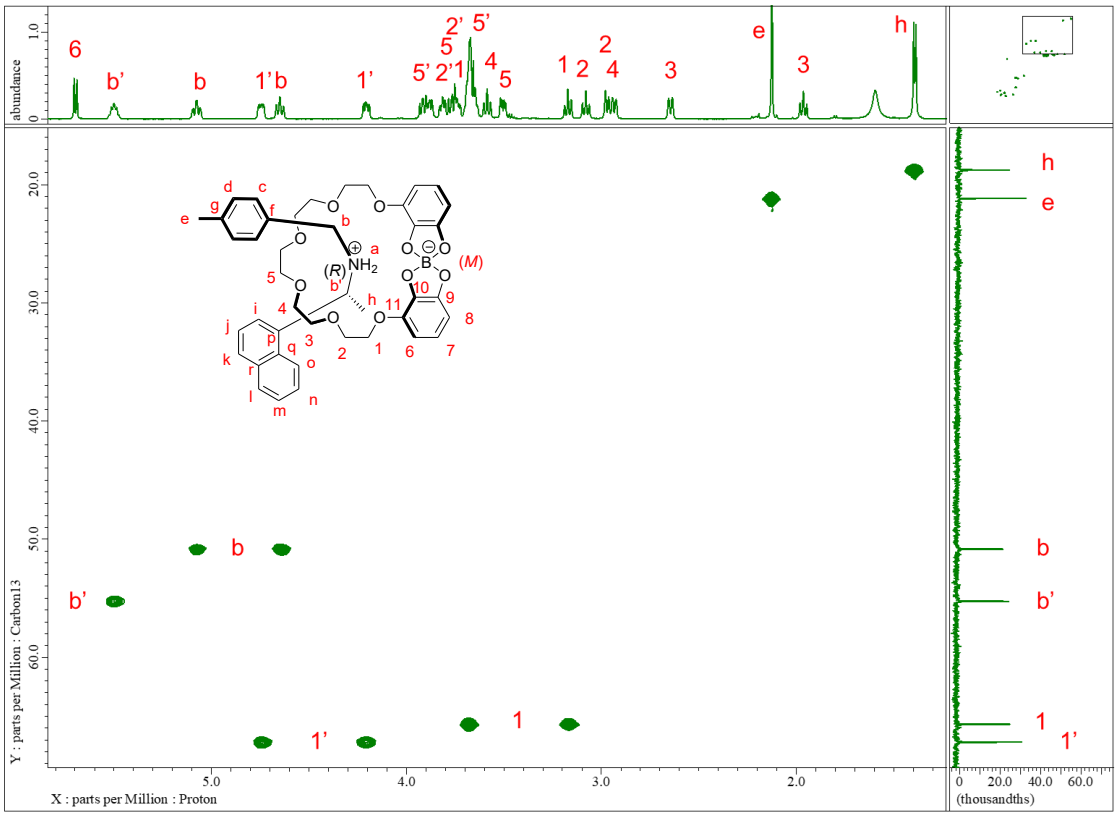
abundance
6
b'
b
1'b
1'
5' 2'1
5
2' 5'
4
5
1 2
2
4
3
e
3
h
(M)
(R)NH2
Y : parts per Million : Carbon13
X : parts per Million : Proton
5.0
4.0
3.0
2.0
(thousandths)

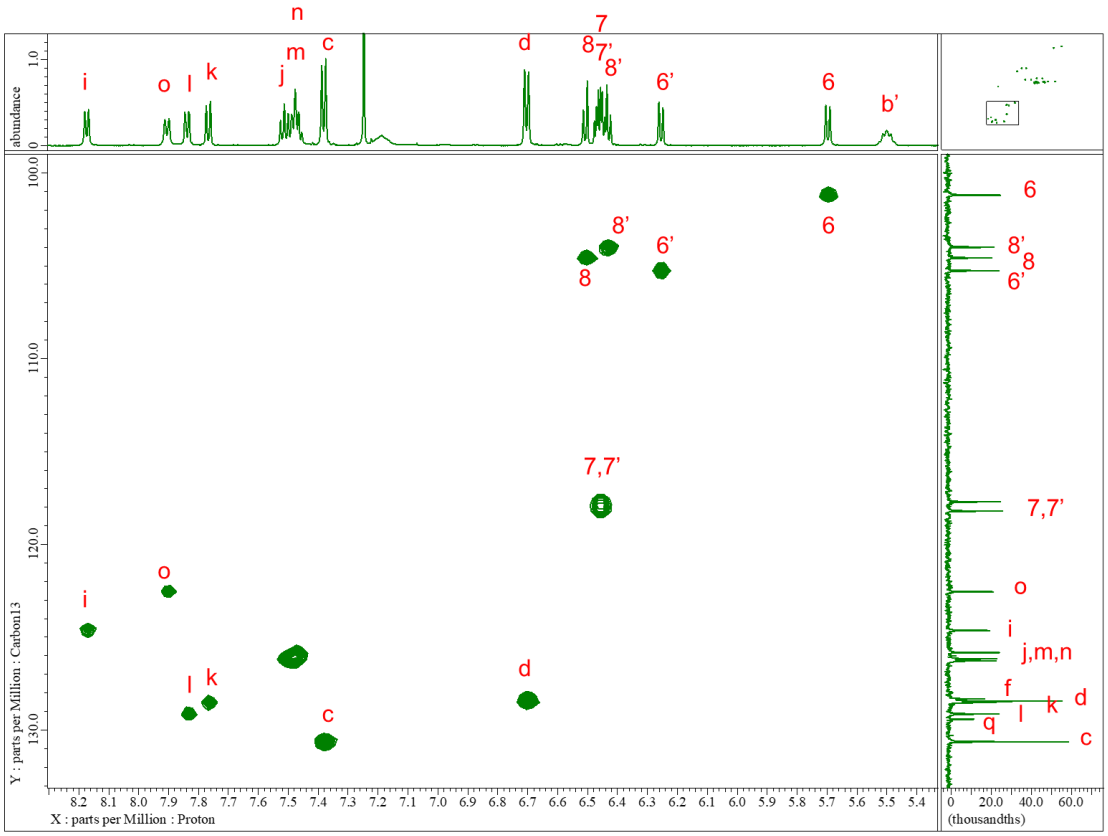
abundance
i
o
l
k
j
m
n
c
d
7
8
7'
8'
6'
6
b'
7,7'
Y : parts per Million : Carbon13
X : parts per Million : Proton
(thousandths)

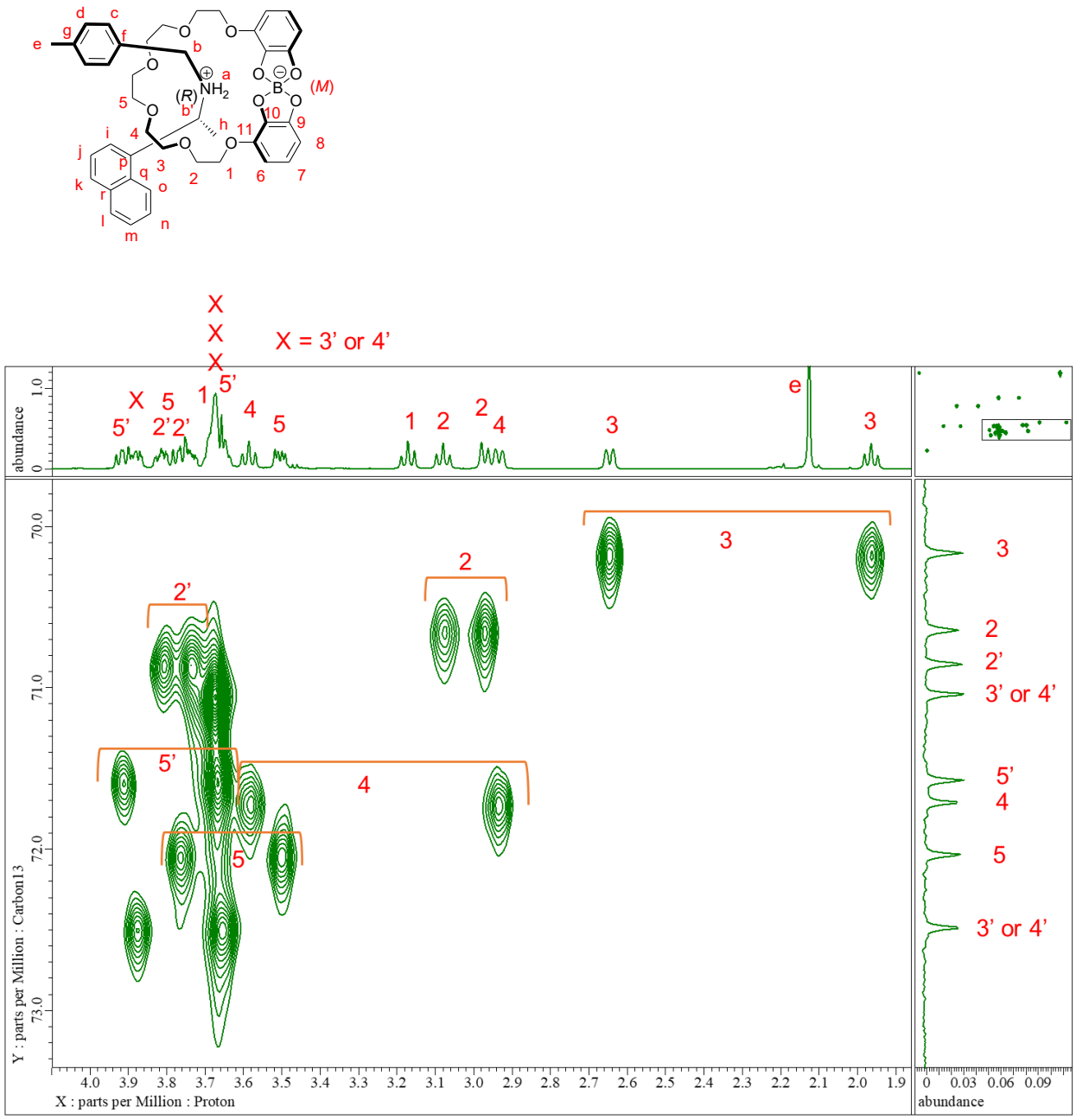

Figure S11c. HSQC spectrum (600 MHz, $CDCl_3$) of (*R*)-pseudo[2]rotaxane **3b**.

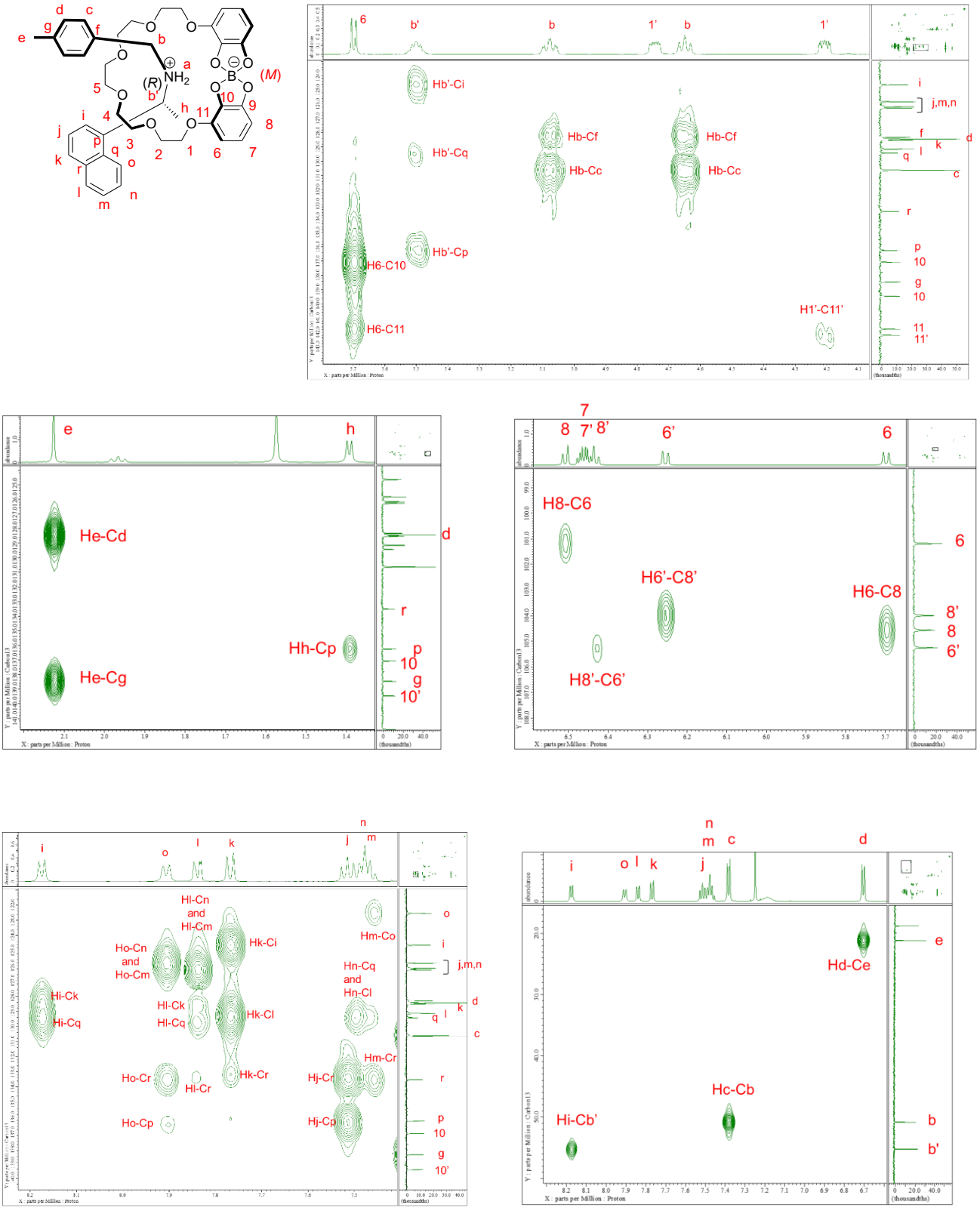

Figure S11d. HMBC spectrum (600 MHz, $CDCl_3$) of (*R*)-pseudo[2]rotaxane **3b**.

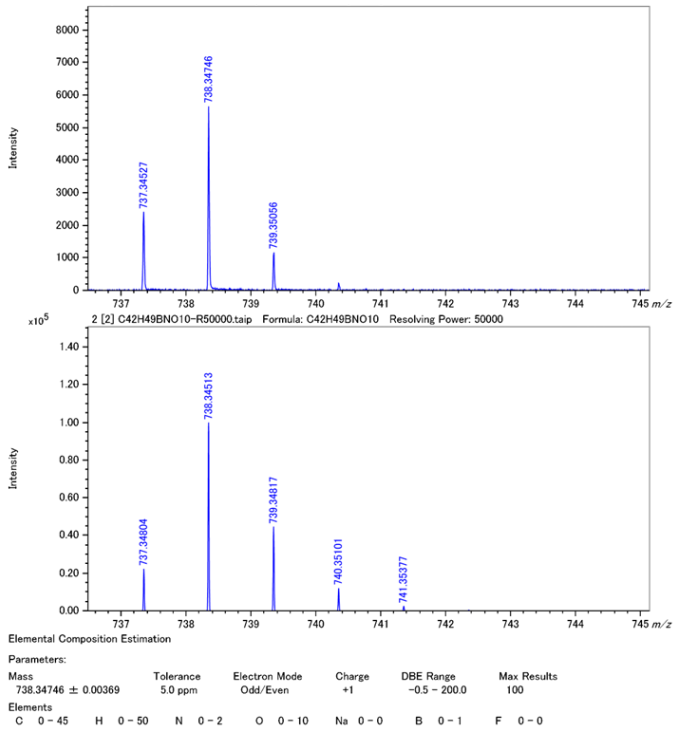

Figure S12a. Mass spectrum (MALDI-TOF) of (*S*)-pseudo[2]rotaxane **3b**: experimental (top) and calculated (bottom) isotopic patterns.

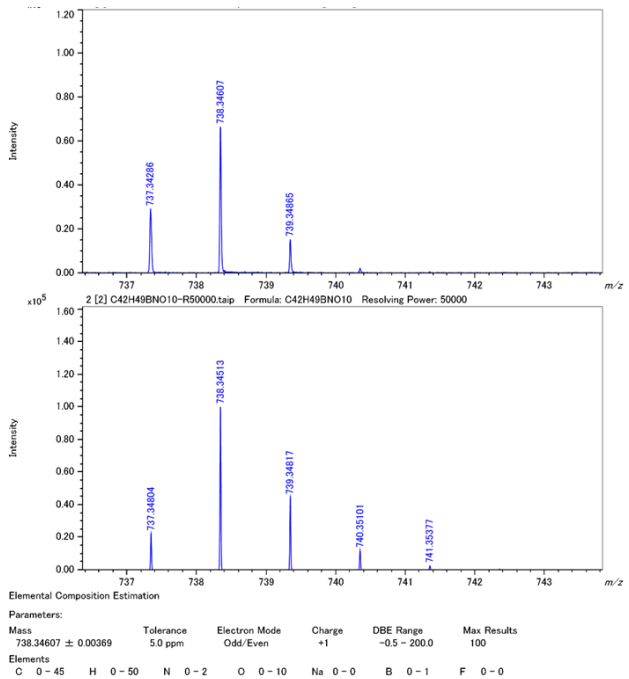

Figure S12b. Mass spectrum (MALDI-TOF) of (*R*)-pseudo[2]rotaxane **3b**: experimental (top) and calculated (bottom) isotopic patterns.

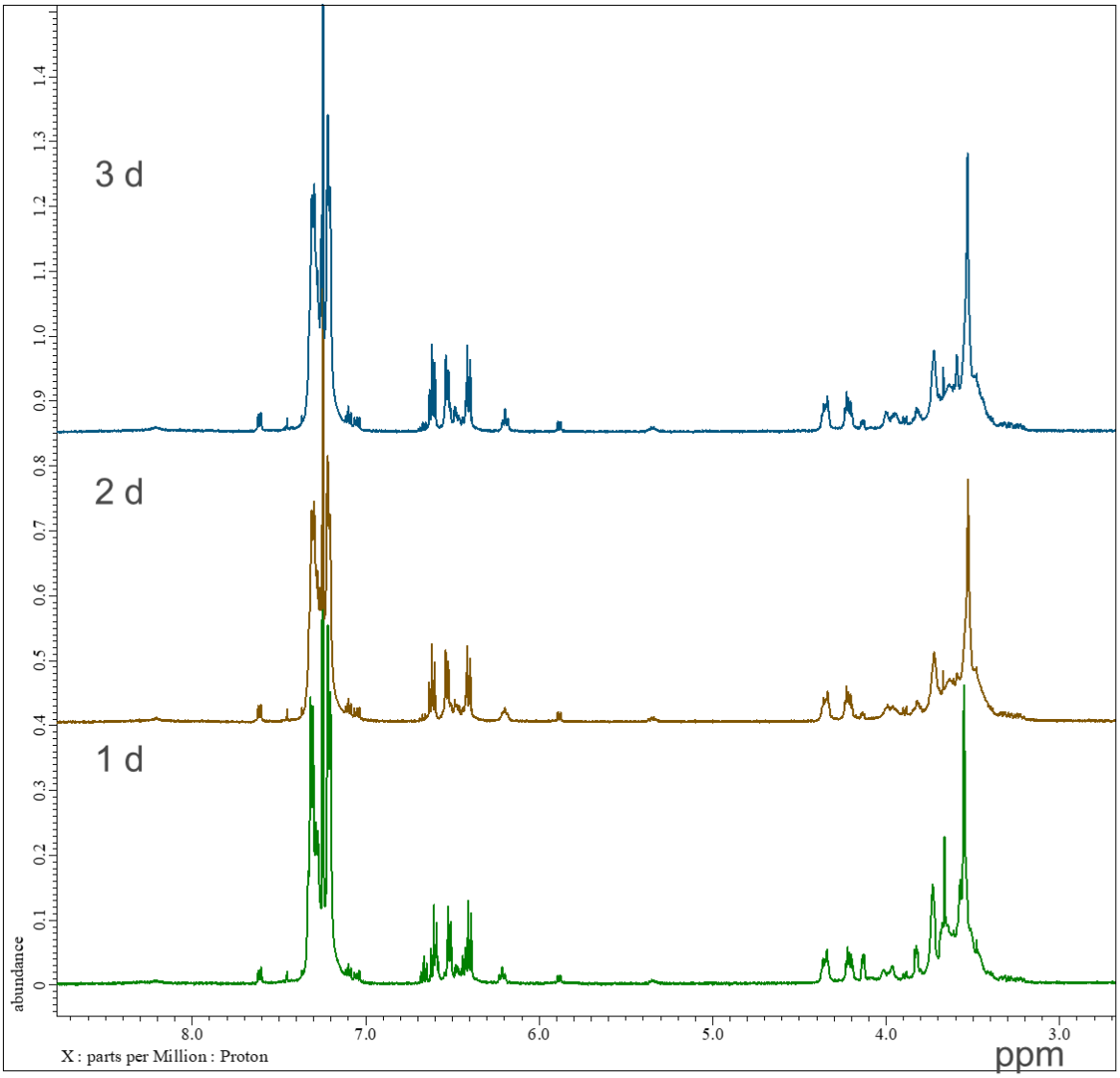

Figure S13. ^{1}H NMR spectra (500 MHz, $CDCl_3$) of crude products of a reaction mixture of **1** and (±)-**2c** in the presence of boric acid in CH_3CN at 50 °C.

(a) (b)

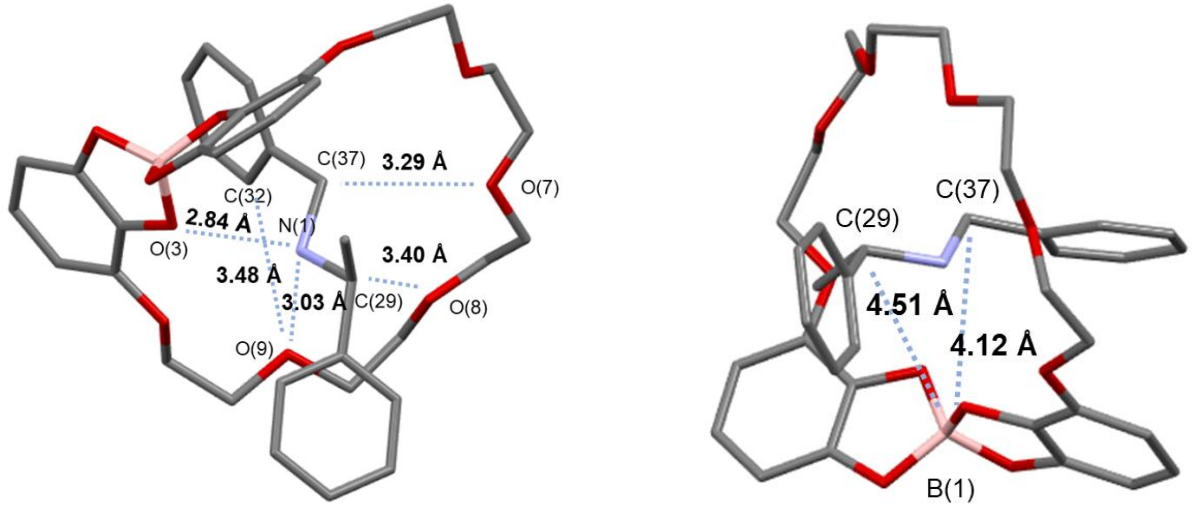

(c)

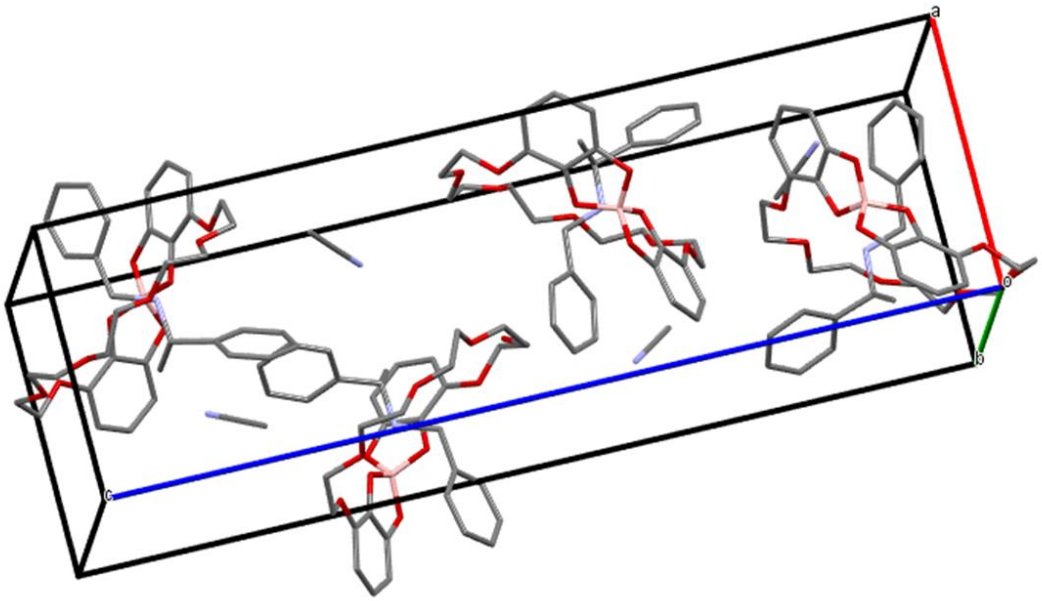

Figure S14. X-ray crystal structure of (*P,S*)-pseudo[2]rotaxane **3a**. (a) Distances of hydrogen-bonding atoms. (b) Distances between boron and benzylic carbon atoms. (c) The packing structure of pseudo[2]rotaxane **3a** in the crystalline state. Acetonitrile molecules located around the rotaxane structures. Gray: carbon; blue: nitrogen; red: oxygen; pale red: boron.

Table S1. Crystal data and structure refinement details for (*P*,*S*)-pseudo[2]rotaxane **3a**.

Parameter	(*P*,*S*)-pseudo[2]rotaxane **3a**
Formula	$C_{39}H_{47}BN_2O_{10}$
Formula weight	714.62
Temperature	–100 °C
Crystal color, habit	colorless, block
Crystal size / mm	0.740 × 0.200 × 0.170
Crystal system	orthorhombic
Space group	$P2_12_12_1$ (#19)
a / Å	9.5801(3)
b / Å	12.3377(4)
c / Å	31.1719(10)
α / deg	90
β / deg	90
γ / deg	90
V / Å^3	3684.4(2)
Z	4
D_{calcd} / g cm^{-3}	1.288
F(000)	1520.00
$2\theta_{max}$ / deg	55.0
No. of reflns meads	35638
No. of obsd reflns	8427
No. of variables	614
R_1 [$I > 2\sigma(I)$][a]	0.0656
wR_2 (all reflns)[b]	0.1431
Goodness of fit	1.146

[a] $R_1 = \Sigma(|F_o| - |F_c|)/\Sigma(|F_o|)$. [b] $wR_2 = \{\Sigma[w(F_o^2 - F_c^2)^2]/\Sigma w(F_o^2)^2\}^{1/2}$.

Table S2. Calculated transition energies, oscillator strength ***f***, rotational strength ***R***, and composition for pseudo[2]rotaxane **3** with the accommodated (*S*)-amine **2a** molecule.[a]

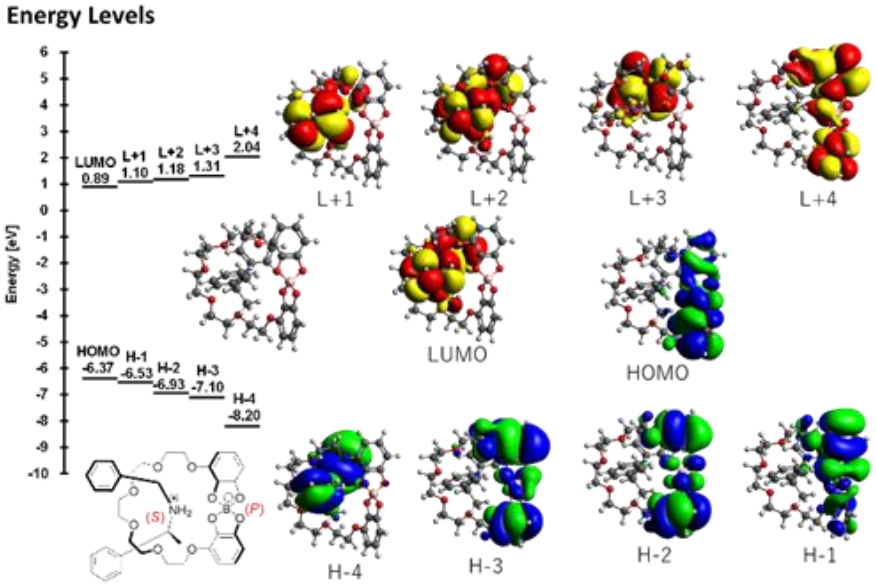

Energy/eV (nm)	***f***	***R***/10^{-38} cgs	Composition (weight %)
5.23 (236.9)	0.059	-0.13	H→L+6 (29), H→L+7 (15), H-2→L+5 (11), H-2→L+4 (10)
5.68 (218.3)	0.092	0.37	H→L+5 (34), H→L+4 (20), H→L+7 (15), H→L (10).
5.71 (217.3)	0.031	-0.40	H-1→L+3 (44), H-1→L+4 (17)
6.24 (198.8)	0.072	-0.22	H-4→L (35), H-5→L+3 (15), H-6→L+2 (12)
6.44 (192.6)	0.982	5.32	H-2→L+4 (25), H→L+6 (13), H-2→L+5 (12)
6.47 (191.6)	0.030	0.82	H-2→L (65)
6.54 (189.5)	0.650	-12.15	H-2→L+5 (25), H-3→L+4 (19)
6.58 (188.5)	0.153	1.37	H-3→L (37), H-2→L+1 (17), H-3→L+1 (10)
6.60 (187.8)	0.453	5.69	H-2→L+6 (26), H-3→L+7 (14), H-3→L+5 (11)
6.73 (184.3)	0.101	-0.46	H→L+4 (48), H→L+5 (29)
6.75 (183.8)	0.084	-0.91	H-2→L+7 (27), H-3→L+6 (16)
6.85 (180.9)	0.009	0.28	H→L+6 (45), H→L+7 (34)
7.00 (177.2)	1.412	-0.20	H-7→L+1 (34), H-5→L+3 (24), H-4→L (18)
7.06 (175.6)	0.024	0.69	H→L+11 (19), H→L+14 (19), H→L+9 (15), H→L+10 (10)
7.10 (174.6)	0.361	8.60	H-7→L (28), H-6→L+1 (25), H-7→L+2 (12), H-4→L+1 (12)
7.13 (173.9)	0.605	-5.29	H-4→L+3 (35), H-5→L (16), H-5→L+2 (14)
7.16 (173.1)	0.127	-2.20	H-1→L+10 (19), H-1→L+13 (17), H-1→L+12 (11)
7.20 (172.3)	0.535	-0.90	H-5→L+3 (29), H-7→L+1 (16), H-6→L (14), H-4→L+2 (14)

[a]Only contributions greater than 10% for transitions with either ***f*** > 0.02 or ***R*** > |0.20| x10^{-38} cgs are consistently included. In the energy column, brown letters and green letters indicate transitions in the borate-crown and chiral amine moieties, respectively. Letters in black mainly indicate CT transitions from the borate-crown to the chiral amine moieties.

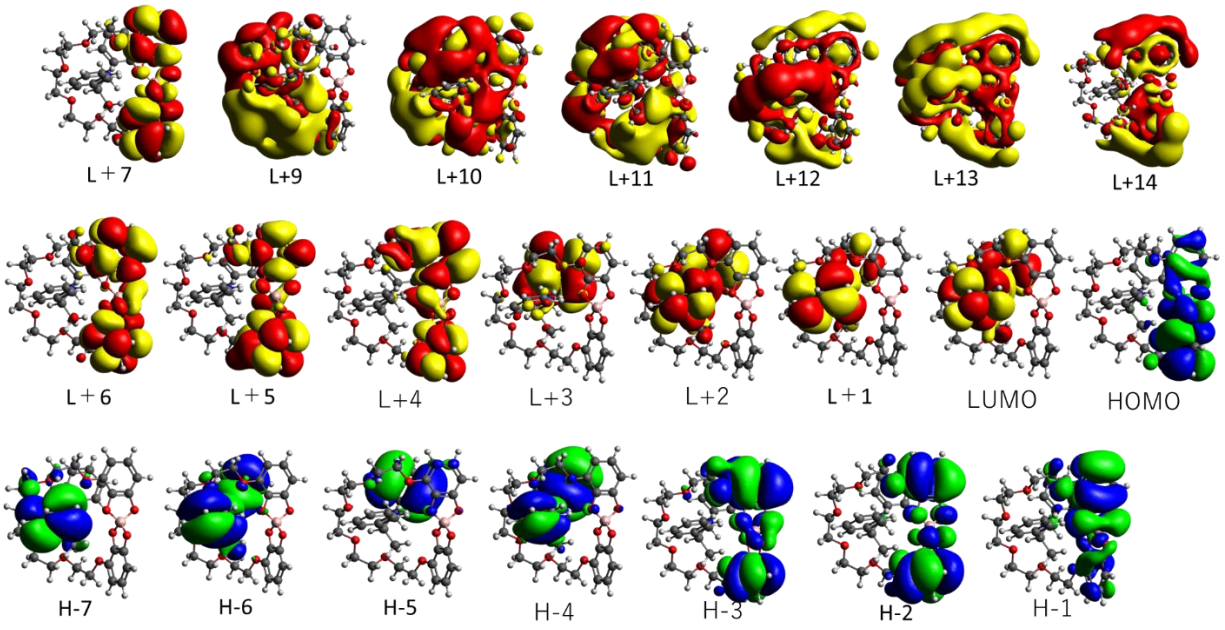

Figure S15. Some molecular orbitals of (*P*,*S*)-pseudo[2]rotaxane **3a**.

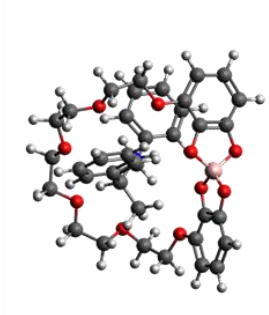

Table S3. The calculated transition energies, oscillator strength ***f***, rotational strength ***R***, and composition for pseudo[2]rotaxane **3a**.

No.	Energy[eV]	Wavelength[nm]	*f*	*R* /10^{-40}	Major contribs
1	5.23	236.9	0.0587	-13.07	H-2->L+4 (10%), H-2->L+5 (11%), HOMO->L+6 (29%), HOMO->L+7 (15%)
2	5.27	235.5	0.0058	-0.46	H-3->L+4 (18%), H-1->L+4 (13%), H-1->L+5 (13%), H-1->L+6 (18%)
3	5.44	228.1	0.0022	1.69	H-1->LUMO (40%), H-1->L+2 (22%)
4	5.57	222.8	0.0003	0.38	H-7->LUMO (34%), H-6->L+1 (29%)
5	5.59	221.8	0.0013	-0.70	H-5->LUMO (13%), H-5->L+2 (19%), H-4->L+3 (23%), H-1->LUMO (15%)
6	5.68	218.3	0.0923	36.66	HOMO->LUMO (10%), HOMO->L+4 (20%), HOMO->L+5 (34%), HOMO->L+7 (15%)
7	5.71	217.3	0.0309	-40.07	H-1->L+3 (44%), H-1->L+4 (17%)

8	5.75	215.5	0.0069	2.74	HOMO->LUMO (74%)
9	5.77	214.9	0.0160	-16.43	H-1->L+3 (31%), H-1->L+4 (33%)
10	5.92	209.6	0.0009	-0.61	H-1->LUMO (23%), H-1->L+1 (29%), H-1->L+2 (15%), HOMO->L+1 (15%)
11	6.01	206.2	0.0016	-1.36	H-1->L+2 (13%), HOMO->L+1 (35%), HOMO->L+2 (17%)
12	6.04	205.3	0.0004	-1.27	H-1->L+1 (27%), H-1->L+2 (14%), HOMO->L+1 (14%), HOMO->L+2 (34%)
13	6.07	204.4	0.0043	-14.01	H-3->LUMO (24%), H-3->L+2 (17%), H-2->LUMO (14%), HOMO->L+1 (16%)
14	6.13	202.4	0.0014	-1.77	H-1->L+1 (21%), H-1->L+2 (20%), HOMO->L+1 (19%), HOMO->L+2 (23%)
15	6.13	202.1	0.0006	0.39	HOMO->L+3 (76%)
16	6.24	198.8	0.0717	-22.49	H-6->L+2 (12%), H-5->L+3 (15%), H-4->LUMO (35%)
17	6.28	197.4	0.0058	11.92	H-6->LUMO (13%), H-3->L+3 (36%), H-2->L+3 (19%)
18	6.30	196.9	0.0186	3.16	H-7->L+1 (10%), H-6->LUMO (18%), H-5->L+3 (10%), H-4->L+2 (14%), H-3->L+3 (22%), H-2->L+3 (11%)
19	6.44	192.6	0.9816	531.78	H-2->L+4 (25%), H-2->L+5 (12%), HOMO->L+6 (13%)
20	6.47	191.6	0.0302	82.13	H-2->LUMO (65%)
21	6.54	189.5	0.6497	-1215.54	H-3->L+4 (19%), H-2->L+5 (25%)
22	6.58	188.5	0.1531	137.09	H-3->LUMO (37%), H-3->L+1 (10%), H-2->L+1 (17%)
23	6.60	187.8	0.4524	569.37	H-3->L+5 (11%), H-3->L+7 (14%), H-2->L+6 (26%)
24	6.66	186.3	0.0201	7.30	H-3->LUMO (11%), H-3->L+2 (14%), H-2->L+1 (39%), H-2->L+2 (22%)
25	6.73	184.3	0.1006	-45.81	HOMO->L+4 (48%), HOMO->L+5 (29%)
26	6.75	183.8	0.0843	-91.46	H-3->L+6 (16%), H-2->L+7 (27%)
27	6.78	183.0	0.0156	-14.02	H-3->L+1 (60%), H-2->L+1 (23%), H-2->L+2 (10%)
28	6.84	181.4	0.0019	2.72	H-3->L+1 (10%), H-3->L+2 (46%), H-2->L+2 (35%)
29	6.85	180.9	0.0090	27.72	HOMO->L+6 (45%), HOMO->L+7 (34%)
30	6.95	178.5	0.0016	4.12	H-1->L+4 (11%), H-1->L+5 (60%), H-1->L+6 (17%)
31	6.97	177.9	0.0006	-0.79	H-3->L+3 (34%), H-2->L+3 (62%)
32	7.00	177.2	1.4116	-20.19	H-7->L+1 (34%), H-5->L+3 (24%), H-4->LUMO (18%)
33	7.04	176.0	0.0154	12.00	H-1->L+6 (27%), H-1->L+7 (65%)
34	7.06	175.6	0.0237	69.19	HOMO->L+9 (15%), HOMO->L+10 (10%), HOMO->L+11 (19%), HOMO->L+14 (19%)

35	7.10	174.6	0.3613	859.88	H-7->LUMO (28%), H-7->L+2 (12%), H-6->L+1 (25%), H-4->L+1 (12%)
36	7.13	173.9	0.6049	-528.82	H-5->LUMO (16%), H-5->L+2 (14%), H-4->L+3 (35%)
37	7.16	173.1	0.1272	-219.82	H-1->L+10 (19%), H-1->L+12 (11%), H-1->L+13 (17%)
38	7.20	172.3	0.5352	-89.72	H-7->L+1 (16%), H-6->LUMO (14%), H-5->L+3 (29%), H-4->L+2 (14%)
39	7.61	162.9	0.0070	-8.54	H-2->L+4 (21%)
40	7.63	162.6	0.0021	4.24	H-3->L+4 (15%), H-2->L+4 (28%)
41	7.66	161.9	0.0032	-3.07	H-3->L+10 (16%), H-3->L+13 (15%)
42	7.75	160.0	0.0067	-4.74	H-6->LUMO (14%), H-4->LUMO (32%), H-4->L+2 (28%)
43	7.77	159.6	0.0011	0.69	H-2->L+6 (20%), H-2->L+7 (14%), HOMO->L+9 (13%)
44	7.78	159.4	0.0025	0.02	H-3->L+5 (12%), H-2->L+6 (16%), H-2->L+7 (11%), HOMO->L+9 (14%), HOMO->L+14 (10%)
45	7.79	159.1	0.0082	-22.06	H-11->LUMO (17%), H-10->LUMO (22%)
46	7.79	159.1	0.0024	2.63	H-3->L+5 (37%), H-3->L+6 (21%), H-2->L+5 (19%)
47	7.82	158.5	0.0042	-8.04	H-10->LUMO (11%), H-5->LUMO (11%)
48	7.90	157.0	0.0029	4.82	H-6->LUMO (12%), H-6->L+2 (40%)
49	7.90	156.9	0.0036	-1.36	H-3->L+6 (20%), H-3->L+7 (54%), H-2->L+7 (14%)
50	7.91	156.8	0.0015	-0.56	H-6->L+1 (10%), H-4->L+1 (25%)
51	7.93	156.3	0.0148	15.99	H-10->LUMO (21%), H-5->LUMO (33%), H-5->L+1 (11%), H-5->L+2 (17%)
52	7.95	156.0	0.0022	-0.23	H-29->LUMO (11%), H-4->L+1 (26%)
53	7.99	155.3	0.0018	-0.62	H-11->L+1 (28%), H-10->L+1 (26%), H-5->L+1 (25%)
54	8.01	154.8	0.0007	-0.63	H-1->L+8 (42%), HOMO->L+8 (16%)
55	8.06	153.9	0.0171	11.58	H-26->L+3 (10%), H-24->L+3 (10%)
56	8.06	153.9	0.0112	-17.72	H-26->L+3 (15%), H-24->L+3 (13%)
57	8.08	153.4	0.0146	6.26	HOMO->L+8 (26%)
58	8.09	153.3	0.0017	1.24	H-29->L+1 (22%), H-24->L+1 (11%), H-23->L+1 (12%)
59	8.10	153.1	0.0069	-4.80	H-11->LUMO (18%), H-10->LUMO (16%), H-7->LUMO (10%), H-7->L+2 (23%)
60	8.11	153.0	0.0058	0.22	H-21->L+2 (10%)
61	8.12	152.7	0.0032	2.66	H-11->L+1 (13%), H-10->L+1 (13%), H-5->L+1 (42%)

62	8.15	152.1	0.0025	-9.10	H-7->L+2 (20%), H-6->L+3 (10%)
63	8.15	152.1	0.0004	-0.40	H-21->L+3 (13%), H-6->L+3 (13%)
64	8.16	152.0	0.0025	0.44	HOMO->L+8 (38%)
65	8.17	151.8	0.0004	-2.05	H-8->LUMO (61%), H-8->L+2 (11%)
66	8.18	151.6	0.0011	1.26	H-30->L+1 (6%), H-26->L+1 (4%), H-25->L+1 (6%), H-24->L+1 (5%), H-23->L+1 (8%), H-23->L+2 (3%), H-21->L+1 (6%), H-20->L+1 (3%), H-8->LUMO (5%), H-7->L+2 (2%), H-4->L+1 (7%)
67	8.22	150.8	0.0030	-3.84	H-5->L+4 (76%), H-5->L+5 (15%)
68	8.23	150.6	0.0008	2.05	H-4->L+4 (71%), H-4->L+5 (13%)
69	8.25	150.3	0.0095	-1.03	H-1->L+8 (11%), H-1->L+11 (26%)
70	8.27	150.0	0.0005	0.45	H-9->LUMO (79%)
71	8.27	149.9	0.0024	5.52	H-2->L+9 (10%), HOMO->L+10 (15%), HOMO->L+12 (15%)
72	8.31	149.2	0.0023	-0.27	H-11->LUMO (15%), H-10->L+2 (52%)
73	8.32	149.0	0.0005	-0.57	H-1->L+9 (51%)
74	8.35	148.4	0.0022	1.85	H-10->L+2 (13%), H-6->L+3 (45%)
75	8.40	147.6	0.0005	0.16	H-5->L+5 (17%), H-5->L+6 (52%), H-5->L+7 (24%)
76	8.41	147.4	0.0018	3.77	H-11->L+1 (20%), H-11->L+2 (13%), H-10->L+1 (25%), H-10->L+8 (13%)
77	8.42	147.3	0.0052	2.27	H-4->L+5 (14%), H-4->L+6 (43%), H-4->L+7 (19%)
78	8.42	147.2	0.0006	0.71	H-3->L+8 (12%), H-1->L+11 (13%)
79	8.43	147.0	0.0002	-0.22	H-7->L+3 (72%)
80	8.45	146.7	0.0127	11.57	H-8->LUMO (12%), H-8->L+2 (44%), H-8->L+9 (14%)

[a]Only contributions greater than 10% for transitions with either $\boldsymbol{f} > 0.02$ or $\boldsymbol{R} > |0.20| \times 10^{-38}$ cgs are consistently included except for No. 66.

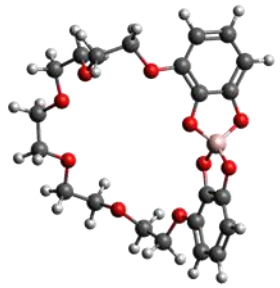

Table S4. The calculated transition energies, oscillator strength ***f***, rotational strength ***R***, and composition for pseudo[2]rotaxane **3a** after the removal of the accommodated (*S*)-amine **2a** from (*P*,*S*)-rotaxane **3a** (macrocyclic component of pseudo[2]rotaxane **3**).[a]

No.	Energy[eV]	Wavelength[nm]	*f*	*R* /10^{-40}	Major contribs
1	5.18	239.3	0.1068	4.87	H-2->LUMO (13%), H-1->L+1 (19%), HOMO->L+2 (27%)
2	5.22	237.6	0.0141	-11.31	H-3->LUMO (15%), H-2->L+1 (10%), H-1->L+2 (26%), HOMO->L+1 (11%), HOMO->L+3 (22%)
3	5.58	222.3	0.1589	90.79	H-1->LUMO (10%), H-1->L+3 (10%), HOMO->LUMO (39%), HOMO->L+1 (12%)
4	5.61	220.8	0.0261	-109.40	H-1->LUMO (46%), HOMO->L+1 (21%), HOMO->L+3 (12%)
5	6.40	193.6	1.1415	873.07	H-3->L+1 (14%), H-2->LUMO (38%), HOMO->L+2 (15%)
6	6.50	190.8	0.7204	-1446.94	H-3->LUMO (23%), H-2->L+1 (32%)
7	6.57	188.7	0.6719	391.62	H-3->L+1 (10%), H-3->L+3 (15%), H-2->L+2 (31%), HOMO->LUMO (27%)
8	6.62	187.3	0.2175	73.79	H-1->LUMO (12%), HOMO->LUMO (22%), HOMO->L+1 (26%)
9	6.71	184.8	0.0223	33.29	HOMO->L+2 (43%), HOMO->L+3 (27%)
10	6.73	184.2	0.0397	-8.19	H-1->L+1 (46%), H-1->L+2 (21%), HOMO->L+1 (12%)
11	6.79	182.7	0.0120	-7.81	H-3->L+2 (24%), H-2->L+3 (37%)
12	6.82	181.8	0.0208	51.30	H-1->L+2 (11%), H-1->L+3 (68%)
13	7.14	173.6	0.0005	3.83	H-1->L+9 (11%), HOMO->L+7 (21%), HOMO->L+8 (20%), HOMO->L+9 (23%)
14	7.16	173.2	0.0027	9.48	H-1->L+7 (45%), H-1->L+9 (14%), HOMO->L+9 (12%)
15	7.66	162.0	0.0048	0.08	H-3->LUMO (24%), H-3->L+1 (10%), H-2->LUMO (33%), H-2->L+1 (18%)
16	7.69	161.2	0.0031	-5.56	H-3->L+7 (12%), H-3->L+9 (20%), H-2->L+7 (21%)
17	7.70	160.9	0.0035	-3.15	H-3->L+7 (15%), H-2->L+9 (30%)
18	7.77	159.6	0.0035	12.42	H-3->LUMO (12%), H-3->L+1 (45%), H-2->L+2 (22%)
19	7.78	159.4	0.0061	-11.29	H-3->L+2 (37%), H-2->L+1 (15%), H-2->L+2 (16%), H-2->L+3 (11%)

20	7.80	159.0	0.0070	-0.56	H-3->L+7 (15%), H-1->L+5 (23%)
21	7.86	157.7	0.0042	-2.79	HOMO->L+4 (22%), HOMO->L+5 (12%), HOMO->L+6 (13%), HOMO->L+8 (10%)
22	7.88	157.3	0.0046	-2.21	H-3->L+2 (11%), H-3->L+3 (55%), H-2->L+3 (20%)
23	8.33	148.9	0.0104	-9.54	H-3->L+5 (10%), H-1->L+4 (19%), HOMO->L+4 (25%)
24	8.36	148.3	0.0057	14.91	H-2->L+5 (10%), HOMO->L+4 (33%)
25	8.40	147.6	0.0029	-6.06	H-1->L+4 (48%)
26	8.43	147.1	0.0101	-10.23	H-4->L+4 (19%)
27	8.47	146.5	0.0029	-4.65	HOMO->L+5 (10%)
28	8.50	145.9	0.0036	-1.83	H-1->L+14 (11%)
29	8.51	145.7	0.0115	-33.56	H-4->L+4 (23%)
30	8.51	145.7	0.0033	0.76	H-12->L+1 (10%), H-11->L+1 (10%)
31	8.55	145.0	0.0064	7.25	HOMO->L+5 (28%)
32	8.55	145.0	0.0278	22.58	H-6->L+4 (25%), H-5->L+4 (14%)
33	8.56	144.9	0.0161	-29.89	H-13->LUMO (12%), H-6->L+4 (11%)
34	8.60	144.2	0.0555	51.91	H-7->L+4 (34%), H-7->L+5 (12%), H-4->L+6 (14%)
35	8.64	143.5	0.0030	5.70	H-1->L+5 (31%), H-1->L+6 (11%)
36	8.65	143.4	0.0186	-15.72	H-6->L+5 (10%), H-5->L+5 (25%)
37	8.65	143.4	0.0073	22.42	H-13->L+3 (19%), H-12->L+3 (15%)
38	8.66	143.1	0.0020	3.93	H-15->L+2 (28%), H-13->L+2 (17%)
39	8.69	142.6	0.0782	40.42	H-9->L+1 (23%), H-8->LUMO (30%), H-8->L+2 (11%)
40	8.70	142.5	0.0582	-18.57	H-9->LUMO (14%), H-8->L+1 (37%)
41	8.74	141.8	0.0031	5.89	HOMO->L+6 (19%), HOMO->L+7 (11%), HOMO->L+10 (10%)
42	8.79	141.1	0.0872	-31.70	H-9->L+3 (11%), H-8->LUMO (11%), H-8->L+2 (21%)
43	8.80	140.9	0.0218	0.11	HOMO->L+6 (11%), HOMO->L+7 (19%), HOMO->L+9 (19%)
44	8.84	140.3	0.0111	-12.86	H-9->LUMO (15%), H-9->L+2 (11%), H-8->L+3 (34%)
45	8.86	139.9	0.0012	3.46	H-1->L+8 (10%), H-1->L+9 (33%)
46	8.92	139.1	0.0040	0.31	H-3->L+13 (3%), H-3->L+15 (2%), H-3->L+17 (2%), H-3->L+19 (3%), H-2->L+4 (5%), H-2->L+8 (2%), H-2->L+11 (3%), H-2->L+13 (5%), H-2->L+14 (4%), H-2->L+15 (5%), H-2->L+17 (4%), H-2->L+18 (3%),

					H-2->L+19 (7%), H-2->L+22 (3%), HOMO->L+19 (4%), HOMO->L+22 (2%)
47	8.93	138.8	0.0107	8.39	H-10->L+3 (4%), H-9->L+2 (2%), H-9->L+3 (3%), H-3->L+13 (2%), H-3->L+14 (6%), H-3->L+16 (6%), H-3->L+17 (4%), H-3->L+20 (7%), H-2->L+13 (2%), H-2->L+14 (3%), H-2->L+16 (4%), H-2->L+17 (3%), H-2->L+20 (4%), H-1->L+6 (2%), H-1->L+16 (3%), H-1->L+20 (7%)
48	8.94	138.6	0.0119	-4.77	H-10->L+3 (10%), H-9->L+3 (15%)
49	8.95	138.6	0.0041	4.11	H-21->LUMO (5%), H-21->L+1 (3%), H-15->LUMO (3%), H-14->LUMO (9%), H-14->L+1 (5%), H-11->LUMO (7%), H-10->LUMO (3%), H-10->L+1 (2%), H-10->L+3 (3%), H-6->LUMO (3%), H-5->LUMO (9%), H-5->L+1 (5%)
50	8.97	138.2	0.0016	1.35	H-13->L+1 (11%)
51	8.98	138.0	0.0016	-2.18	H-1->L+6 (30%)
52	9.02	137.5	0.0024	5.34	H-12->L+2 (15%), H-11->L+2 (15%)
53	9.06	136.9	0.0007	0.05	HOMO->L+7 (16%), HOMO->L+8 (35%), HOMO->L+9 (10%)
54	9.08	136.6	0.0048	-2.55	H-2->L+4 (28%)
55	9.08	136.5	0.0007	9.09	H-21->L+2 (4%), H-15->LUMO (4%), H-15->L+1 (5%), H-15->L+2 (4%), H-14->L+2 (8%), H-12->L+1 (3%), H-12->L+2 (5%), H-11->LUMO (5%), H-11->L+1 (3%), H-10->LUMO (5%), H-6->L+2 (3%), H-5->L+1 (3%), H-5->L+2 (7%), H-2->L+4 (2%)
56	9.10	136.3	0.0038	-4.97	H-2->L+4 (12%)
57	9.10	136.3	0.0008	-3.19	H-16->L+1 (10%)
58	9.12	135.9	0.0088	-11.17	H-15->LUMO (14%), H-5->LUMO (20%)
59	9.15	135.5	0.0066	-6.62	H-3->L+4 (29%)
60	9.16	135.4	0.0055	24.40	H-16->L+3 (23%)
61	9.19	134.9	0.0138	-4.43	H-5->LUMO (10%)
62	9.21	134.6	0.1104	86.76	H-10->L+2 (18%), H-10->L+3 (16%)
63	9.24	134.3	0.0692	-52.86	H-10->L+1 (18%)
64	9.25	134.0	0.0195	-4.67	H-10->LUMO (15%)
65	9.28	133.6	0.0066	-3.75	H-1->L+8 (21%), H-1->L+20 (16%)
66	9.29	133.4	0.0015	12.46	HOMO->L+12 (12%), HOMO->L+13 (10%)
67	9.32	133.0	0.0024	1.09	H-3->L+4 (14%), H-2->L+5 (14%)
68	9.33	132.9	0.0031	12.55	H-5->L+2 (21%)

69	9.37	132.3	0.0335	-22.05	H-10->L+3 (11%)
70	9.38	132.2	0.0108	10.74	H-4->L+1 (18%)
71	9.39	132.1	0.0019	-1.79	H-3->L+4 (11%), H-3->L+5 (10%), H-2->L+5 (15%)
72	9.44	131.3	0.0004	2.48	H-2->L+5 (12%), H-1->L+11 (11%)
73	9.44	131.3	0.0016	0.13	H-3->L+5 (26%)
74	9.51	130.4	0.0025	-0.45	H-7->L+3 (10%), H-4->LUMO (15%), H-4->L+2 (10%), H-4->L+3 (33%)
75	9.51	130.4	0.0025	2.87	H-2->L+6 (13%), HOMO->L+10 (18%), HOMO->L+11 (22%)
76	9.52	130.2	0.0192	14.71	H-6->L+5 (31%), H-6->L+6 (11%), H-5->L+5 (12%)
77	9.54	130.0	0.0003	-2.76	H-1->L+10 (17%), H-1->L+11 (11%)
78	9.55	129.8	0.0038	2.78	HOMO->L+10 (22%)
79	9.58	129.5	0.0011	2.72	H-1->L+10 (21%), H-1->L+11 (19%)
80	9.59	129.3	0.0506	12.15	H-5->LUMO (11%), H-5->L+6 (11%), H-5->L+11 (12%)

[a]Only contributions greater than 10% for transitions with either $\boldsymbol{f} > 0.02$ or $\boldsymbol{R} > |0.20| \times 10^{-38}$ cgs are consistently included except for No. 46, 47, 49, and 55.

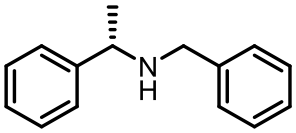

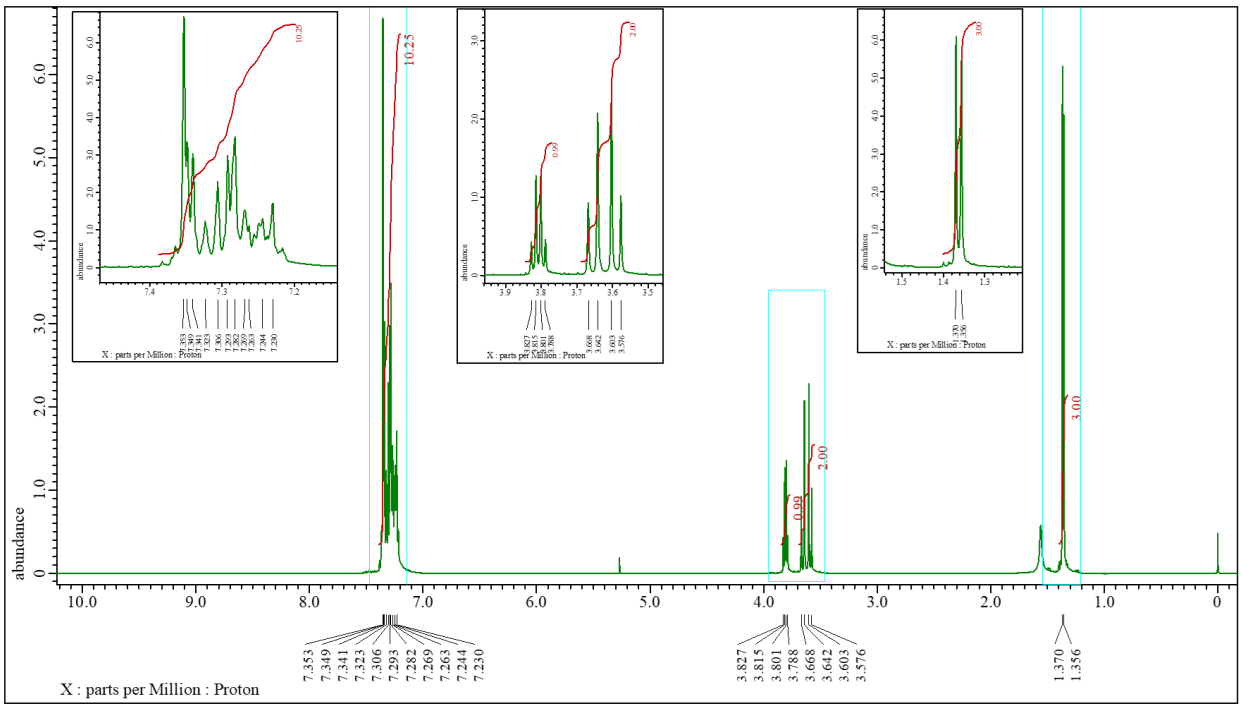

Figure. ^{1}H NMR spectrum (500 MHz, $CDCl_3$) of **2a**.

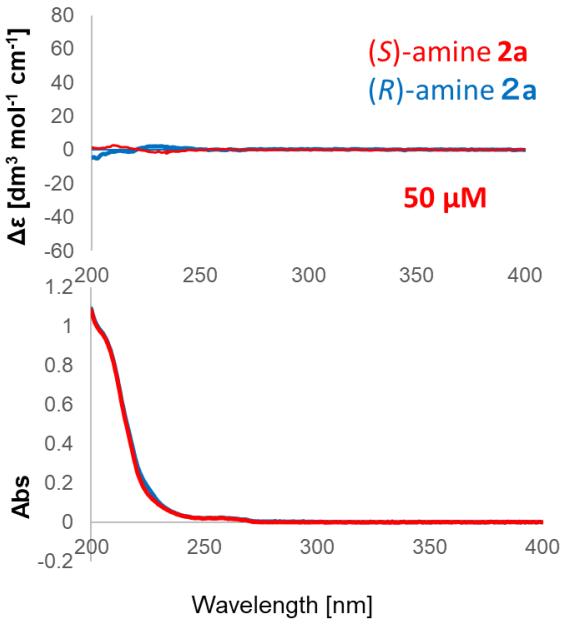

Figure. (a) Electronic absorption (bottom) and CD (top) spectra of amine **2a** in CH_3CN.

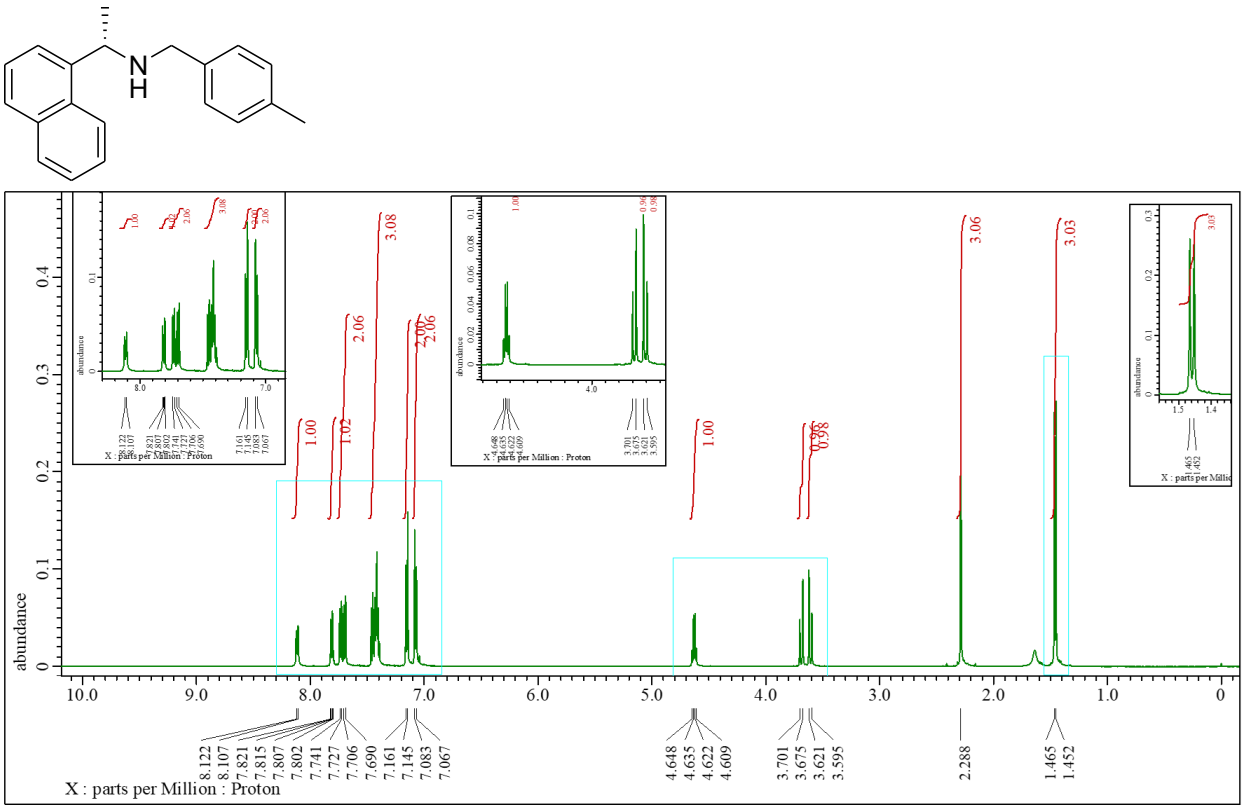

Figure. ^{1}H NMR spectrum (500 MHz, $CDCl_3$) of **2b**.

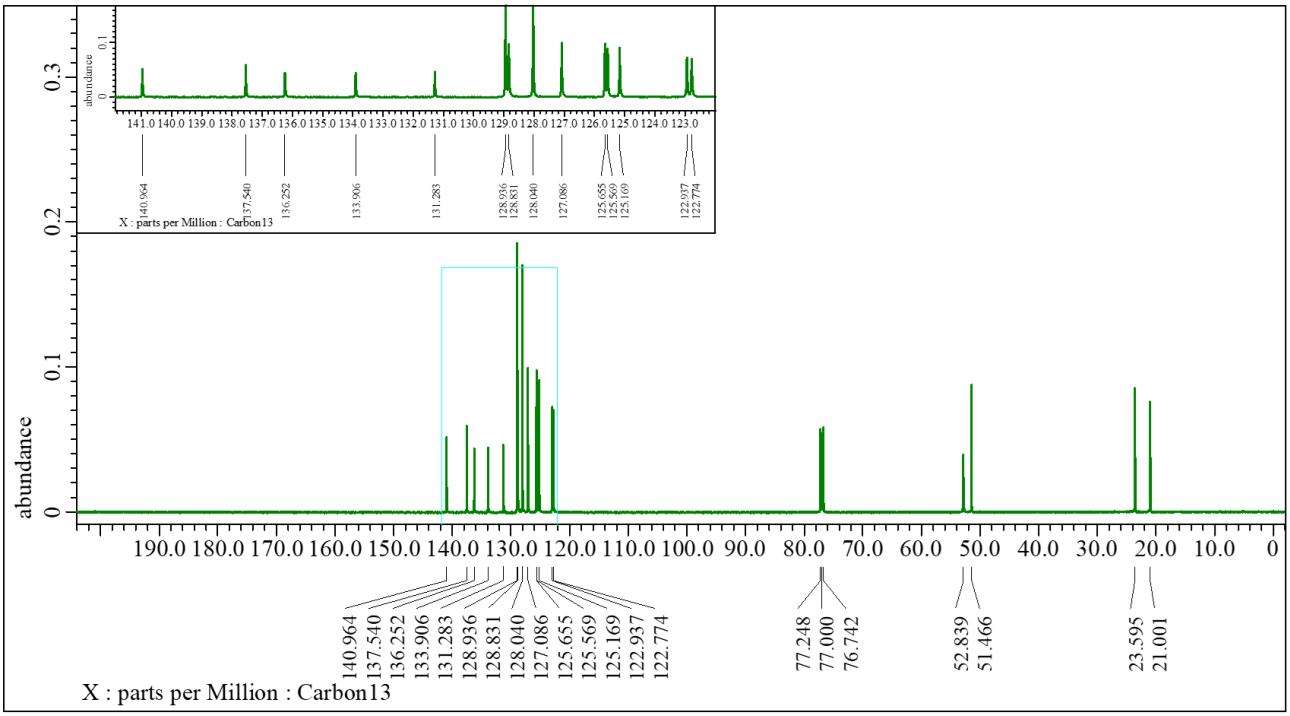

Figure. ^{13}C NMR spectrum (125 MHz, $CDCl_3$) of **2b**.

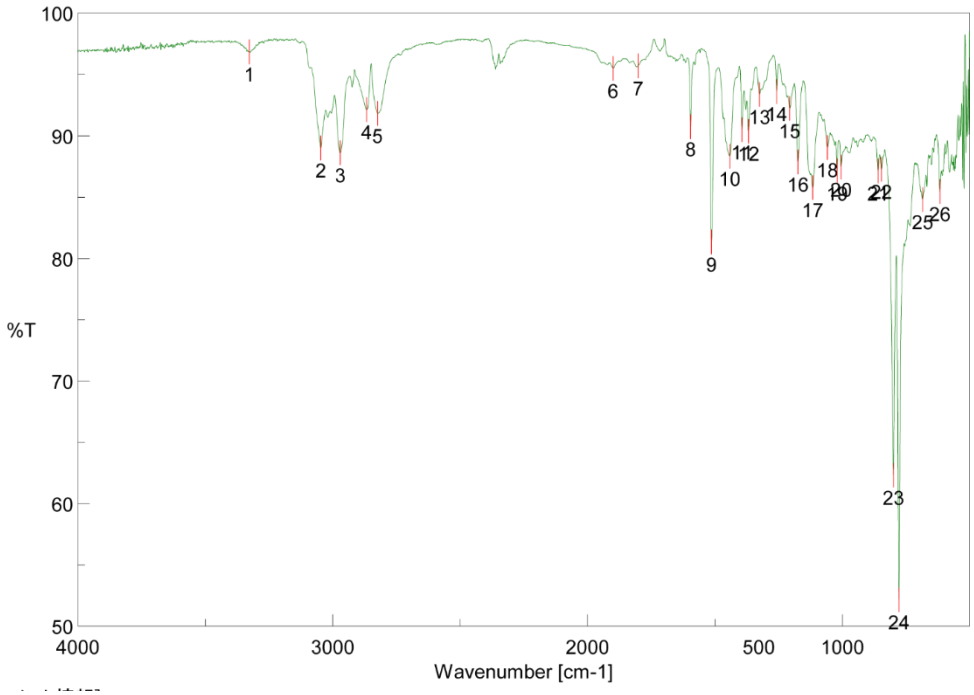

Figure. IR spectrum (NaCl) of **2b**.

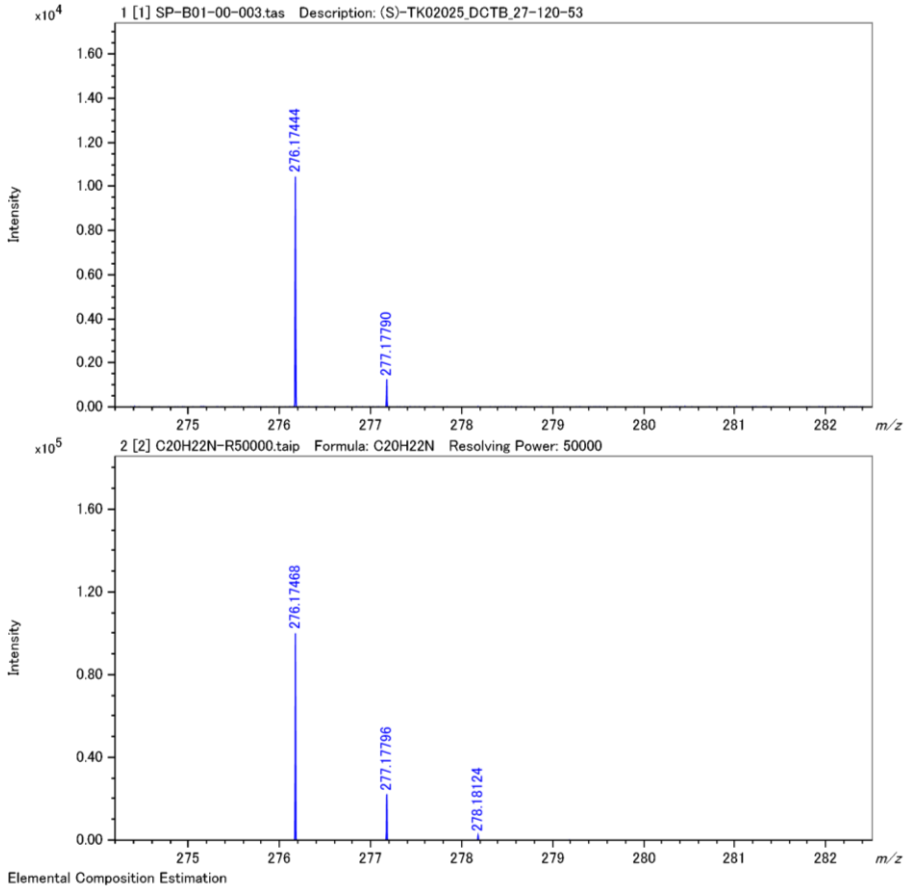

Figure. Mass spectrum (MALDI-TOF) of **2b**: experimental (top) and calculated (bottom) isotopic patterns.

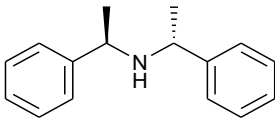

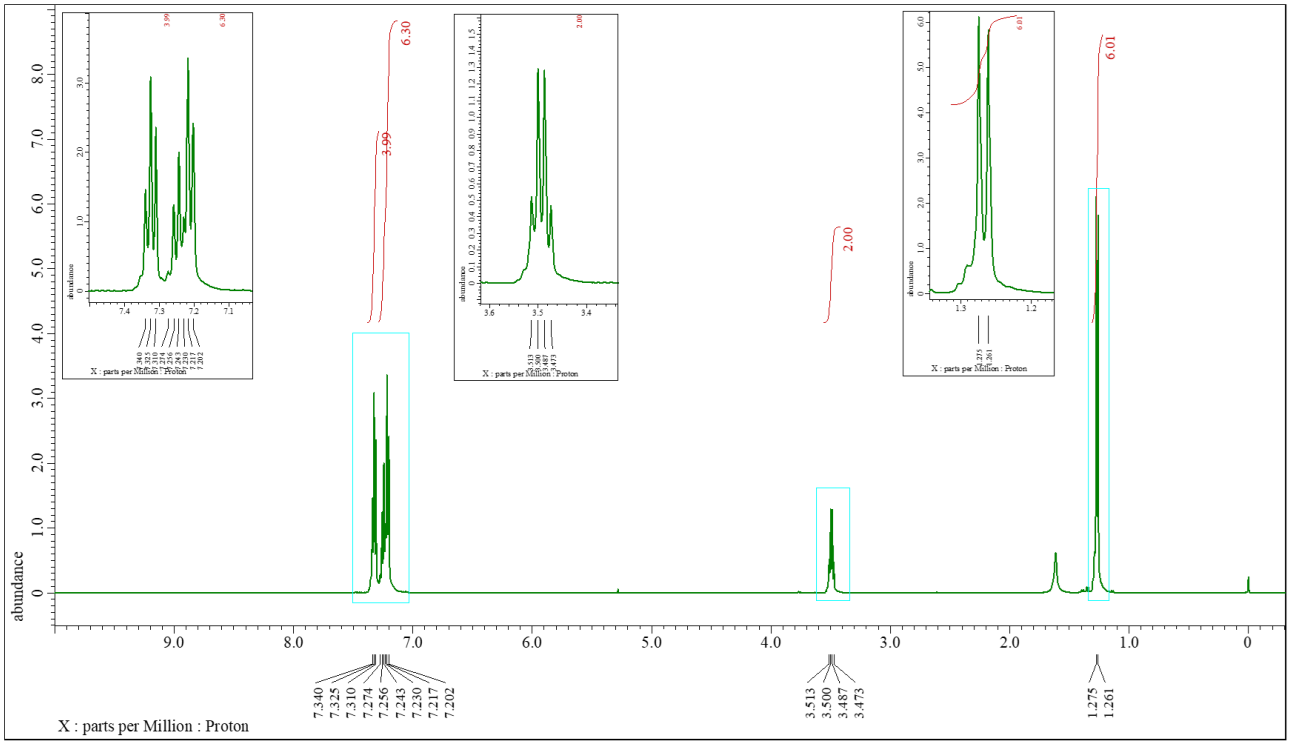

Figure. ^{1}H NMR spectrum (500 MHz, $CDCl_3$) of **2c**.

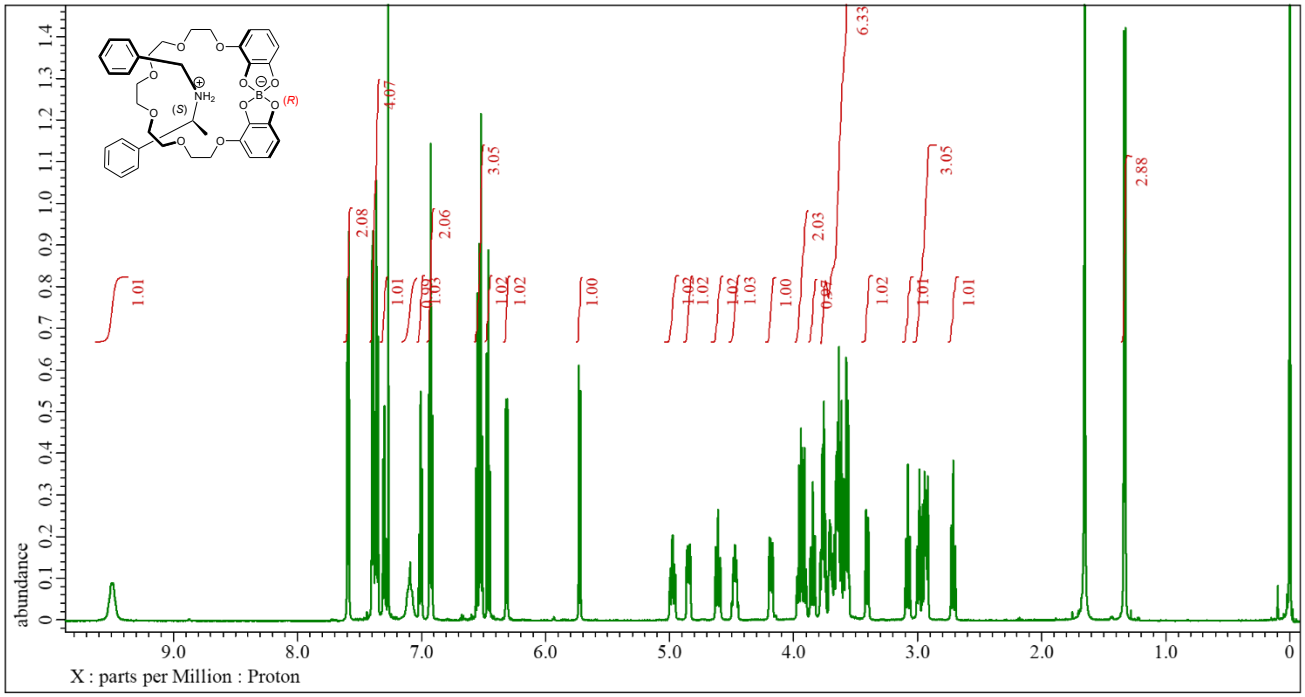

Figure. ^{1}H NMR spectrum (600 MHz, $CDCl_3$, 5 °C) of **3a**.

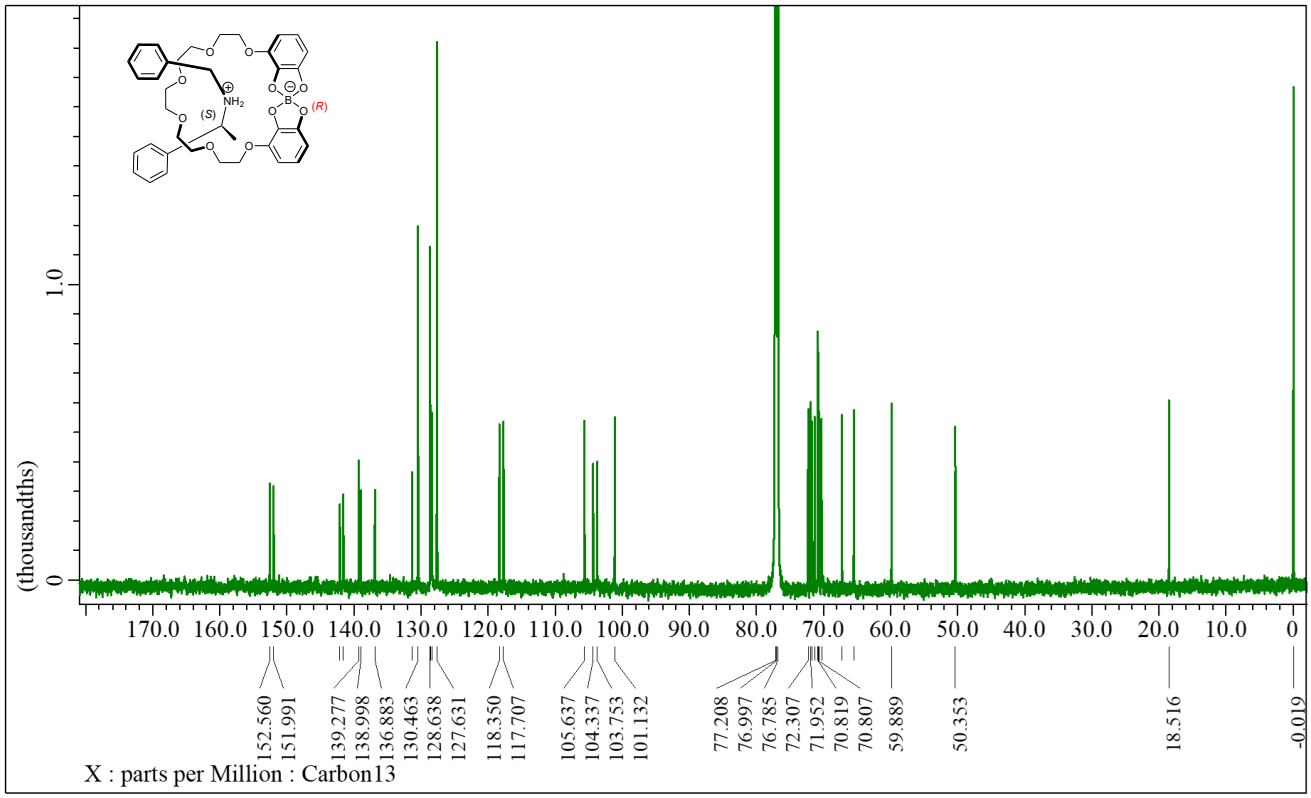

Figure. ^{13}C NMR spectrum (150 MHz, $CDCl_3$, 5 °C) of **3a**.

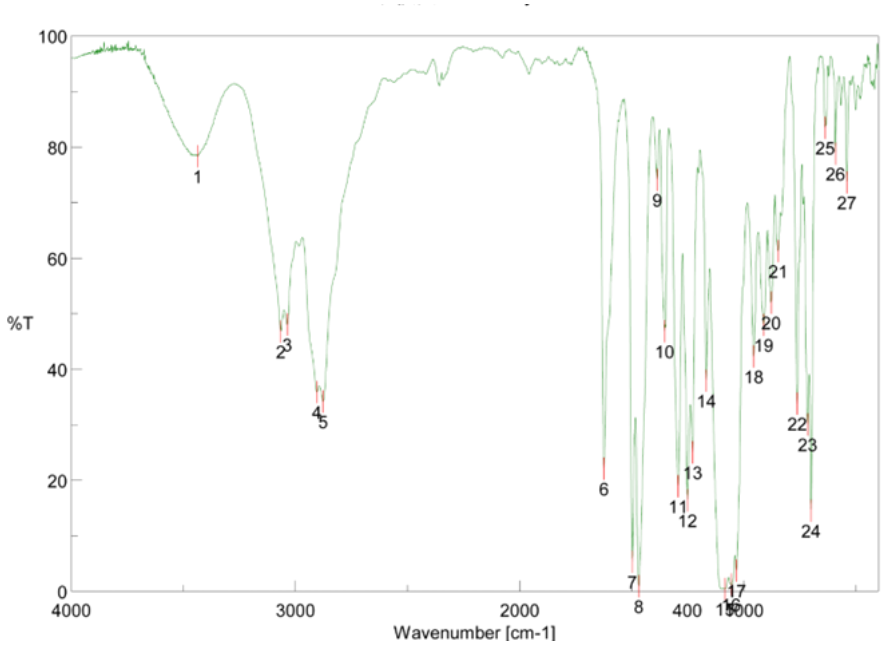

Figure. IR spectrum (KBr) of **3a**.

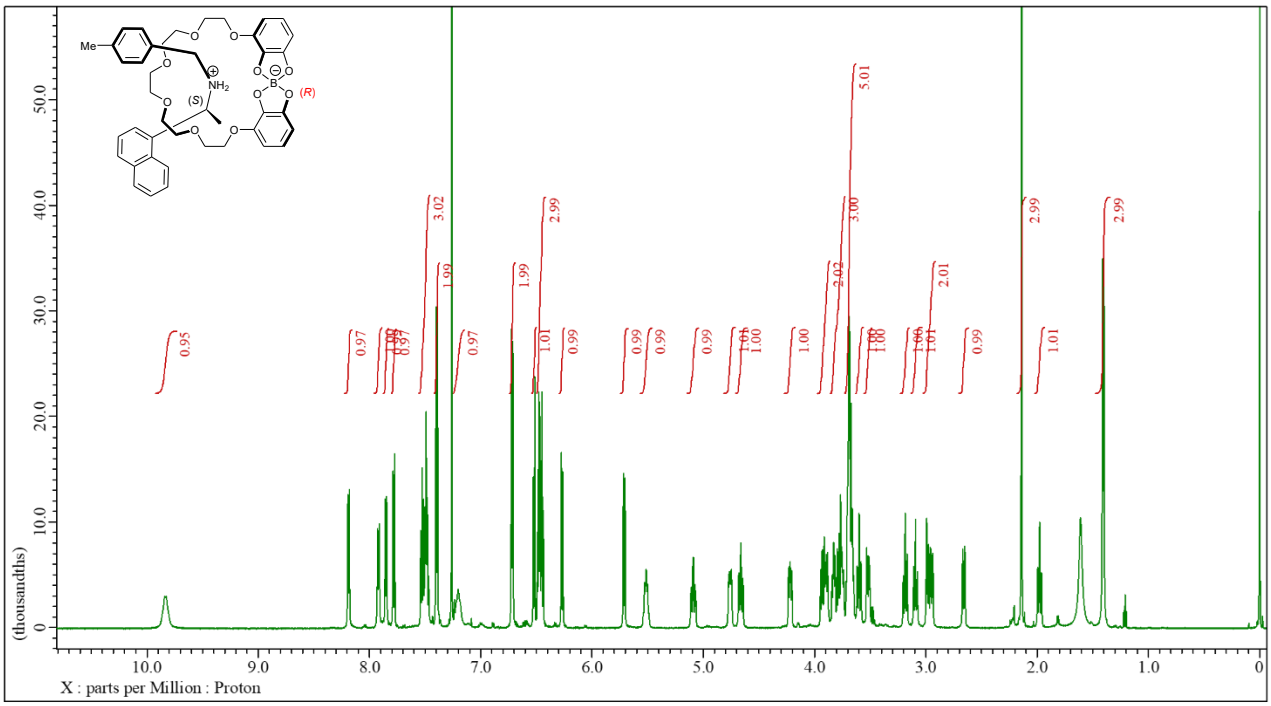

Figure. ^{1}H NMR spectrum (600 MHz, $CDCl_3$) of **3b**.

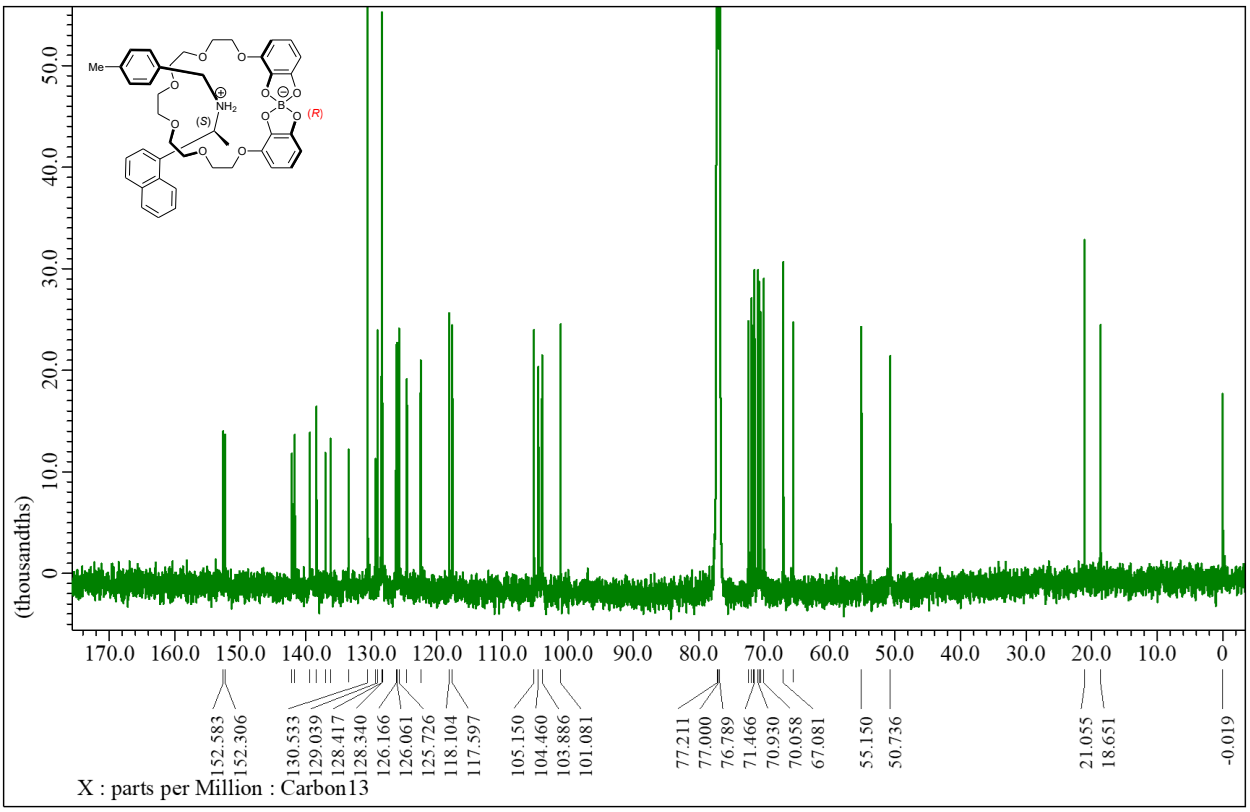

Figure. ^{13}C NMR spectrum (600 MHz, $CDCl_3$) of **3b**.

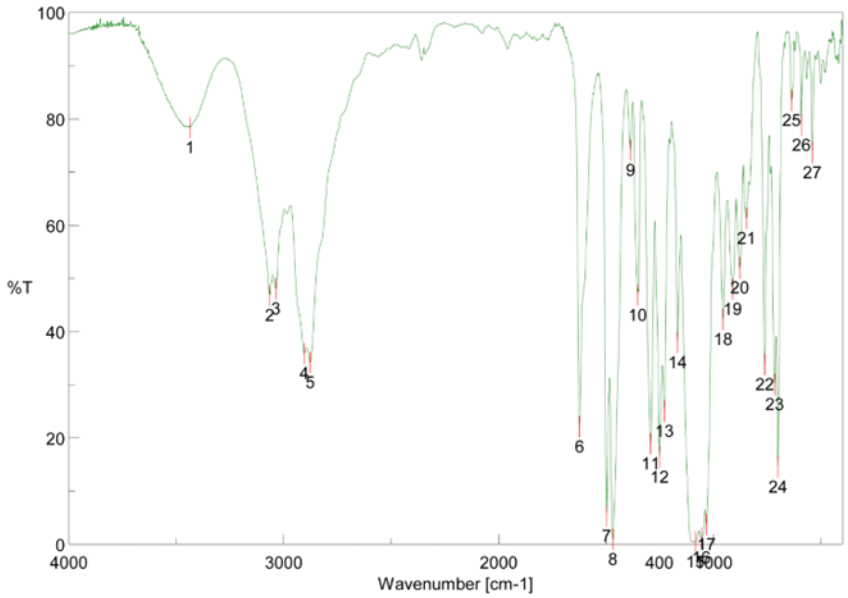

Figure. IR spectrum (KBr) of **3b**.